Selective Polymeric Membranes for Ion Specific Separation

A Dissertation

Presented to the Faculty of the School of Engineering and Applied Science at the

University of Virginia

In Partial Fulfillment of the Requirements for the Degree of

Doctor of Philosophy in Chemical Engineering

By

Yuanyuan Ji

December 2019

The Dissertation Committee for Yuanyuan Ji Certifies that this is the Approved Version of the Following Dissertation:

Selective Polymeric Membranes for Ion Specific Separation

Committee:

Geoffrey M. Geise, Dissertation Advisor

Gary Koenig, Chairperson

David L. Green

Roseanne M. Ford

Rachel Letteri

Dedication

To those who have supported me tremendously in this long journey of pursuing a Ph.D.

Acknowledgements

Throughout the process of earning a Ph.D. and writing this dissertation, I have received a great deal of guidance and support. The journey to get to this final point is full of challenges and earnings. I was lucky enough to receive guidance from great mentors, help from incredible colleagues, and unconditional company from family and friends. I want to sincerely thank every one of you for helping me reach this milestone of my life.

I would like to first express tremendous gratefulness to my dissertation advisor, Dr. Geoffrey M. Geise, for his dedication to the profession and willingness to influence me positively with his knowledge and experience. Dr. Geise always sets and maintains high academic standards for himself and the rest of the group. Such high standards have always challenged me to become the best researcher and professional I could ever be, and I definitely benefited tremendously. I am sincerely grateful to everything you have done and taught me, as well as the influence you had on me.

I also enjoyed interacting with every colleague in the group including Tianyi Xue, Huan Zhang, Dr. Bill Morris, Hongxi Luo, Kevin Chang, Saringi Agata and Patrick McCormack, on a daily basis. I am specifically thankful to Hongxi for the fruitful discussion on research as well as the efforts he put in assisting me to make the membrane materials for my research. I really enjoyed every moment in the lab with you all. I would also like to thank you my fellow students who have been with me through graduate school. They are too many to name individually, but thank you all, for making the time I have spent in Charlottesville so colorful and remarkable. I am also grateful to the rest of my committee members, Dr. Gary Koenig, Dr. David L. Green, Dr. Roseanne M. Ford and Dr. Rachel Letteri, for serving as my defense committee and provide advice on my Ph.D. work.

Finally, I would like to thank my grandparents, for raising me up with instilling in me the curiosity and courage to pursue science. I am also forever grateful to the love and unconditional support from the rest of my family and friends. Words cannot express my gratefulness to all of you.

Abstract

Providing sustainable supply of clean water and energy is critical for the survival and development of human kind. Membrane-based electrochemical technologies are widely applied for water purification (e.g., electrodialysis (ED) and membrane capacitive deionization (MCDI)), energy generation (e.g., reverse electrodialysis (RED)) and storage (e.g., redox flow batteries (RFB)). To achieve maximum water and energy generation efficiency, those technologies all rely on ion exchange membranes (IEMs) to selectively transport certain ions of interest. Moreover, those technologies expose IEMs to a wide variety of ions, which are typically different from the commonly studied sodium and chloride. Fundamental knowledge of the interactions between polymeric IEMs and diverse ions to guide membrane permselectivity optimization remains insufficient. Therefore, this work is aimed at closing this knowledge gap by understanding how the experimental, ion and polymer chemistry specific factors affect the ion-membrane interaction as well as membrane separation performance.

The influence of experimental factors on membrane apparent permselectivity measurement inaccuracy was examined, and experimental factors were demonstrated to introduce no-larger-than 2% uncertainty to permselectivity. Ion-specific factors such as bare and hydrated ion radii, ion geometry and complexation-forming nature were demonstrated to affect membrane permselectivity via thermodynamic sorption or kinetic diffusion effects. The membrane fixed charge group chemistry was demonstrated to introduce up to 6% permselectivity enhancement. Results from this research addressed knowledge gaps from the experimental, ion and polymeric chemistry specific perspectives and can be applied to guide the design, engineering and optimization of ion specific selective membranes, which can facilitate the sustainable supply of clean water and energy.

Table of Contents

List of Tables

List of Figures

Chapter 1: Introduction

1.1. Water-Energy Nexus

As the global population expands,[1,2] so does the demand for fresh water and energy. However, with the increasing water pollution and decreasing reserves of traditional fossil fuels, it becomes more and more challenging to satisfy such demands. Solutions to alleviate the global freshwater and energy shortage problems including relying on water pacification technologies to generate clean water,[3,4] and increasing utilization of sustainable energy sources.[5,6] Moreover, water and energy, the two fundamental resources for the survival of mankind, are inherently interdependent.[7] Substantial amount of water is required to produce energy, and substantial amount of energy is required to purify water.[4]

Membrane technologies play a crucially intermediate role in such water-energy nexus. Various membrane-based processes are widely used, or being considered for water purification (e.g., reverse osmosis (RO), electrodialysis (ED) and capacitive deionization (CDI)),[7–9] energy generation (reverse electrodialysis (RED) and pressure retarded osmosis (PRO)) and storage (e.g., redox flow batteries (RFB)) applications.[5,10] RO, as the current dominant membrane-based seawater desalination technologies, are utilized to produce 44% of global desalinated water. ED has been utilized for over 50 years to produce potable water from industrial waste water.[11] The membrane-based renewable energy generation technologies, such as RED and PRO generate electricity by harnessing the salinity gradient energy (i.e., energy from the concentration difference between salt streams, e.g., sea water and river water).[7,12] Although neither of them has been industrialized yet, predictions show that the total potential energy that can be harnessed by RED and PRO is 2.6TW,[12] larger than the current global electricity consumption (i.e., 2.0TW).[9] Additionally, membrane-based energy storage technology such as RFB advances large-scale utilization of wind and solar energy, total of which provide 4% of current electricity production but the penetration is still growing at 25% per year.[13]

All of those applications reply on selective ion exchange membranes (IEMs) to control the transport of different ions. The permselectivity of an IEM describes the extent to which a membrane exclusively transports one ion over another, and is critical to the efficiency of a membrane process.[14–21] It has always been a major challenge as to optimize membrane permselectivity for a wide range of different ions in the membrane field.[21] Therefore, this research study focuses on developing the fundamental knowledge to guide the characterization, design and optimization of ion specific selective membrane.

1.2. Goals and Organization of the Dissertation

The primary goal of this research was to develop fundamental understanding on ion specific transport behavior in IEMs and its effect on the permselectivity of IEMs. IEMs have been studied mostly using sodium and chloride in this field. However emerging membrane separation challenges expose IEMs to a wider range of ions different from sodium and chloride. An understanding of the interactions between IEMs and diverse ions could lead to the rational design and optimization of highly selective IEMs for the water purification and energy applications. To accomplish this goal, a combination of experimental and theoretical work was conducted in this research. The experimental method used to characterize membrane permselectivity was examined. The permselectivity, ion sorption and diffusion properties of commercially-available and lab-synthesized cation exchange membranes (CEMs) and anion exchange membranes (AEMs) were experimentally measured and modeled, and the measured and modeled results were compared to understand the mechanism behind the ion-membrane specific interactions.

This dissertation is composed of eight total chapters. Chapter 1 emphasizes the importance of this work within the scope of addressing the global water and energy shortage problems. Chapter 2 provides the background information of ion exchange membrane and theoretical understanding on the correlation between membrane permselectivity and ion transport. Chapter 3 contains detailed information about all theoretical models used in this work to predict ion sorption coefficients and diffusivities. Chapter 4 gives information about the polymeric membrane materials used in this study and the experimental and calculation techniques used to characterize the membrane materials.

Understanding the ion specific effects on membrane permselectivity requires accurate measurements of permselectivity. Chapter 5 evaluates the accuracy of membrane apparent permselectivity measurement using a widely applied static method. Such method requires accurate control or measurement of experimental factors such as temperature, concentration of electrolyte solutions used and electrical potential across the membrane. Deviation of any experimental factors might introduce unexpected errors to measured permselectivity and disturb the understanding of ion specific effects on membrane permselectivity. The deviations introduced by three experimental factors, i.e., temperature variation, concentration deviation and electrical potential fluctuation were quantified either through experimental measurements or theoretical calculations using error propagation.

In chapter 6, the apparent permselectivity, ion sorption and diffusion properties of three CEMs were measured using four monovalent strong electrolytes and modeled using different models. The apparent permselectivity was linked with ion sorption and diffusion properties. The ion sorption was linked with ion properties such as polarizability and bare radius and a phenomenon observed as ion-polymer complexation. The ion diffusion was linked with ion properties such as geometry and hydrated radius. Results demonstrated that ion specific factors such as size, geometry and complexation-forming nature influence ion specific behaviors within polymeric membranes.

In chapter 7, two AEMs with similar polymer backbone structure and different fixed charge groups were synthesized. The permselectivity, ion sorption and diffusion properties of two AEMs were measured using five monovalent electrolytes. The permselectivity, ion sorption and diffusion properties of the two AEMs were compared with the values from each other. The permselectivity, ion sorption and diffusion of the two AEMs were linked with the physiochemistry properties, i.e., Van der Waals volume and hydrophilicity, of the polymer fixed charged groups.

Lastly, chapter 8 contains conclusions and future recommendations for extending the work initiated in this dissertation. Following chapter 8, Appendix A lists the nomenclature used throughout the dissertation. Appendix B, C and D provide all the supplementary discussions for chapter 5, 6 and 7, respectively.

1.3. References

(1) Schwarzenbach, R. P.; Egli, T.; Hofstetter, T. B.; Von Gunten, U.; Wehrli, B. Global Water Pollution and Human Health. *Annu. Rev. Environ. Resour.* **2010**, *35*, 109–136.

(2) Shafiee, S.; Topal, E. When Will Fossil Fuel Reserves Be Diminished? *Energy Policy* **2009**, *37* (1), 181–189.

(3) Elimelech, M.; Phillip, W. A. The Future of Seawater Desalination: Energy, Technology, and the Environment. *science* **2011**, *333* (6043), 712–717.

(4) Geise, G. M.; Paul, D. R.; Freeman, B. D. Fundamental Water and Salt Transport Properties of Polymeric Materials. *Prog. Polym. Sci.* **2014**, *39* (1), 1–42.

(5) Logan, B. E.; Elimelech, M. Membrane-Based Processes for Sustainable Power Generation Using Water. *Nature* **2012**, *488* (7411), 313.

(6) Dincer, I. Renewable Energy and Sustainable Development: A Crucial Review. *Renew. Sustain. Energy Rev.* **2000**, *4* (2), 157–175.

(7) Kamcev, J.; Freeman, B. D. Charged Polymer Membranes for Environmental/Energy Applications. *Annu. Rev. Chem. Biomol. Eng.* **2016**, *7*, 111–133.

(8) Nicolaisen, B. Developments in Membrane Technology for Water Treatment. *Desalination* **2003**, *153* (1–3), 355–360.

(9) Długołęcki, P.; van der Wal, A. Energy Recovery in Membrane Capacitive Deionization. *Environ. Sci. Technol.* **2013**, *47* (9), 4904–4910.

(10) Geise, G. M.; Lee, H.; Miller, D. J.; Freeman, B. D.; McGrath, J. E.; Paul, D. R. Water Purification by Membranes: The Role of Polymer Science. *J. Polym. Sci. Part B Polym. Phys.* **2010**, *48* (15), 1685–1718.

(11) Greenlee, L. F.; Lawler, D. F.; Freeman, B. D.; Marrot, B.; Moulin, P. Reverse Osmosis Desalination: Water Sources, Technology, and Today's Challenges. *Water Res.* **2009**, *43* (9), 2317–2348.

(12) Post, J. W.; Veerman, J.; Hamelers, H. V.; Euverink, G. J.; Metz, S. J.; Nymeijer, K.; Buisman, C. J. Salinity-Gradient Power: Evaluation of Pressure-Retarded Osmosis and Reverse Electrodialysis. *J. Membr. Sci.* **2007**, *288* (1–2), 218–230.

(13) Alotto, P.; Guarnieri, M.; Moro, F. Redox Flow Batteries for the Storage of Renewable Energy: A Review. *Renew. Sustain. Energy Rev.* **2014**, *29*, 325–335.

(14) McGovern, R. K.; Zubair, S. M. The Cost Effectiveness of Electrodialysis for Diverse Salinity Applications. *Desalination* **2014**, *348*, 57–65.

(15) Strathmann, H. Electrodialysis, a Mature Technology with a Multitude of New Applications. *Desalination* **2010**, *264* (3), 268–288.

(16) Güler, E.; Elizen, R.; Vermaas, D. A.; Saakes, M.; Nijmeijer, K. Performance-Determining Membrane Properties in Reverse Electrodialysis. *J. Membr. Sci.* **2013**, *446*, 266–276.

(17) Hong, J. G.; Zhang, B.; Glabman, S.; Uzal, N.; Dou, X.; Zhang, H.; Wei, X.; Chen, Y. Potential Ion Exchange Membranes and System Performance in Reverse Electrodialysis for Power Generation: A Review. *J. Membr. Sci.* **2015**, *486*, 71–88.

(18) Yip, N. Y.; Elimelech, M. Comparison of Energy Efficiency and Power Density in Pressure Retarded Osmosis and Reverse Electrodialysis. *Environ. Sci. Technol.* **2014**, *48* (18), 11002–11012.

(19) Darling, R.; Gallagher, K.; Xie, W.; Su, L.; Brushett, F. Transport Property Requirements for Flow Battery Separators. *J. Electrochem. Soc.* **2016**, *163* (1), A5029–A5040.

(20) Perry, M. L.; Weber, A. Z. Advanced Redox-Flow Batteries: A Perspective. *J. Electrochem. Soc.* **2016**, *163* (1), A5064–A5067.

(21) Luo, T.; Abdu, S.; Wessling, M. Selectivity of Ion Exchange Membranes: A Review. *J. Membr. Sci.* **2018**, *555*, 429–454.

Chapter 2: Background

2.1. Ion Exchange Membranes

Ion exchange membranes (IEMs) often are prepared using charged polymers, and such polymers have ionizable fixed charge groups incorporated into the polymer matrix.[1–10] The concentration of fixed charge groups on the polymer is often quantified by the ion exchange capacity (*IEC*) defined as milliequivalents of charge per gram of dry polymer. Anion exchange membranes (AEMs) contain positively charged groups and preferentially transport anions (i.e., counter-ions) while excluding cations (i.e., co-ions).[10,11] In contrast, cation exchange membranes (CEMs) contain negatively charged groups and preferentially transport cations (i.e., counter-ions) while excluding anions (i.e., co-ions).[12] The ability of these IEMs to selectively transport counter-ions over co-ions is defined as membrane permselectivity and it is critical to their function in electromembrane processes.[13]

The permselectivity of an IEM describes the extent to which a membrane selectively transports counter-ions and excludes co-ions,[2,3] and it is linked to the efficiency of many electromembrane-based separation (e.g., electrodialysis (ED)[6,8,14] and capacitive deionization (CDI)[15,16]), energy generation (e.g., reverse electrodialysis (RED)[17–23]) and energy storage (e.g., redox flow batteries (RFB)[24–28]) technologies. Highly permselective IEMs enable efficient ED and CDI separation processes, efficient energy recovery in RED, and high coulombic efficiency of and low capacity fade in redox flow batteries.[9,14,22,28] Therefore, it is critical to maximize the permselectivity of ion exchange membranes for those applications.

2.2. Knowledge Gaps in Optimizing Membrane Permselectivity

Several challenges exist in the endeavors to maximize the permselectivity for ion exchange membranes. The first one arises from the question of whether we are able to correctly measure the permselectivity. Membrane permselectivity was typically measured as apparent permselectivity, as defined by Strathmann,[2,5] using a static method that is not affected by boundary layers and solution – membrane interfaces, and neglects osmotic water transport through the membrane.[2,5] According to the permselectivity definition (Equation 2.1), permselectivity should not exceed unity. However, apparent permselectivity values that exceed unity have be reported.[29,13,30] In these cases, the values are typically close to unity (e.g., typical values are reported up to an apparent permselectivity of 1.04).[29,13,30] These nonphysical results, in some cases, have been attributed to fluctuations in room temperature.[12,13] Presumably these room-temperature variations are relatively small (i.e., likely no more than a few degrees Celsius). Such reports, though, reveal the first knowledge gap about the sensitivity of the apparent permselectivity to temperature and other experimental parameters. Experimental measurements of apparent permselectivity as a function of experimental parameters would help to inform this issue and close this first knowledge gap.

The second knowledge gap of optimizing membrane permselectivity for electromembrane applications is the lack of understanding on ion specific behaviors within membranes. Traditionally, ion exchange membrane permselectivity has been characterized and studied only using sodium and chloride. Emerging separation challenges and electro-membrane applications, however, require membrane optimized for solutions containing ions that are different from sodium and chloride.[8,10,13,19,24,25,27,31–36] Perhaps one of the most pronounced examples of this situation is the application of membranes as separators in RFB applications. The development of flow batteries has involved the identification of a wide range of battery chemistry options, and vanadium-based ions, bromide, zinc ions, cerium, or organic redox shuttles are a few examples of the types of molecules that could be exposed to the membrane separator in RFB systems.[24,25,27,33] Additionally, many membrane-based energy recovery technologies can expose ion exchange membranes to complex ionic solutions, such as ammonium bicarbonate,[37] lithium chlorate,[19] or copper and ammonia-based solutions.[34,35] Furthermore, deionization via ED or CDI could be challenged with increasingly contaminated waters containing, for example, chromium,[38] cadmium,[39,40] fluoride,[41] nitrate,[9] perchlorate,[42–44] and sulfate.[9] Since IEMs are required in these technologies, membrane permselectivity properties must be understood for ions other than sodium and chloride. Experimental and theoretical studies to correlate ion specific factors with membrane performance will address this issue and close this second knowledge gap.

The third knowledge gap is the lack of understanding on how the polymer chemical structure of membranes can be modified to enhance the ion specific permselectivity. Efforts have been made in this field to tune the membrane specific selectivity towards certain ions and most of those falls into two categories. The first category covers all kinds of surface modifications including increasing the surface degree of crosslinking of membrane,[12,45] creating an oppositely charged surface layer,[46] or creating a layer-by-layer structure.[47–52] Surface modifications have been demonstrated to be effective in selectively separating ions having different valence, e.g., monovalent ions and divalent ions. For example, Sata et al. demonstrated that CEMs based on styrene and divinyl benzene copolymers exhibited slightly increase in sodium/calcium selectivity with increasing surface degree of crosslinking.[12] Firdaous et al. demonstrated that a thin positively charged surface layer on a commercially available cation exchange membrane (Neosepta CMX-S, Tokuyama Soda Co. Ltd., Japan) enhanced the sodium permeation as compared to that of calcium and magnesium.[46] White et al. coated a cation exchange Nafion™ 115 membrane with 5.5 bilayers of poly(4-styrenesulfonate) (PSS)/protonated poly(allylamine) (PAH), and the modified lay-by-layer membrane exhibited remarkable permeation selectivity to potassium over magnesium.[51] The second category includes modifying the polymer fixed charge group chemistry,[12,53] and such method have been demonstrated to be effective in enhancing membrane selectivity among ions with the same valence. For CEMs, cation exchange group options include sulfonic acid, phosphoric acid, carboxylic acid, boric acid, and phenolic acid.[54] Sata et al. concluded that CEM having boric acid groups did not remarkably enhance the selectivity between alkaline earth metal cations and sodium ions, as compared to CEMs having sulfonic acid groups.[12] The study by Nagarale et al. suggested that CEMs with phosphoric acid groups were more effective in separating cations with identical charges as compared with CEMs with sulfonic acid groups.[53] A larger library of anion exchange groups exist for AEMs, e.g., quaternary ammonium, quaternary phosphonium, quinuclidinium-based quaternary ammonium, imidazolium, pyridinium, and pentamethylguanidinium groups.[10,11] The effects of anion exchange group on the performance of AEMs have been investigated in the field of fuel cells,[10,11,55–60] yet little discussions exist in aqueous based electro-membrane systems. Therefore, a study aimed at understanding the effects of different fixed charge group on the performance of AEMs in aqueous separation system will help closing this third knowledge gap.

2.3. Influence of Ion Transport on Permselectivity

Membrane permselectivity, α, is defined using cation and anion transport number:

$$\alpha = \frac{t_M^m - t_M^s}{t_X^s} = 1 - \frac{t_X^m}{t_X^s} \tag{2.1}$$

where t_i^j is the transport number of an ion *i* in phase *j*.[2,5] Superscripts m and s represent the membrane and solution phase, respectively, and subscript *M* and *X* represent counter-ion and co-ion species, respectively. The ion transport number is defined as the fraction of current that is carries by ion *i* relative to the other charge carries, *k*:

$$t_i^j = \frac{|z_i| c_i^j D_i^j}{\sum_k |z_k| c_k^j D_k^j} \tag{2.2}$$

where z_i the ion valence, c_i^j is the concentration of ion *i* in phase *j*, and D_i^j is the diffusion coefficient of ion *i* in phase *j*.

Increase in the membrane-phase co-ion transport number drive a decrease in permselectivity (Equation 2.1).[13,36,59] A perfectly permselective membrane (α = 1) passes current via only counter-ions and completely prevents co-ion transport (i.e., t_X^m = 0).[13,36,59,61] In the other limiting case, in a non-permselective membrane, relative rates of ion transport will not be affected by the membrane (i.e., $t_X^m = t_X^s$ and α = 0).[13,36,59,61] The permselectivity, therefore, varies between zero and unity as the co-ion transport number varies between zero and the value in bulk solution.

The definition of the membrane phase transport numbers, t_i^m, include both the ion concentration and diffusivity in the membrane phase. As a result, permselectivity is expected to increase as either the co-ion concentration or mobility in the membrane phase is suppressed, or either the counter-ion concentration or mobility is enhanced. Therefore, attempts to understand or model membrane permselectivity properties should recognize the contribution of counter-ion or co-ion specific sorption (or partitioning) and diffusion effects. In this study, the ion transport and its effect on membrane permselectivity was studied via understanding the ion sorption (or partitioning) and diffusion effects.

2.4. References

(1) Helfferich, F. G. *Ion Exchange*; Courier Corporation, 1995.

(2) Strathmann, H.; Giorno, L.; Drioli, E. *Introduction to Membrane Science and Technology*; Wiley-VCH Weinheim, 2011; Vol. 544.

(3) Długołęcki, P.; Nymeijer, K.; Metz, S.; Wessling, M. Current Status of Ion Exchange Membranes for Power Generation from Salinity Gradients. *J. Membr. Sci.* **2008**, *319* (1–2), 214–222.

(4) Geise, G. M.; Paul, D. R.; Freeman, B. D. Fundamental Water and Salt Transport Properties of Polymeric Materials. *Prog. Polym. Sci.* **2014**, *39* (1), 1–42.

(5) Strathmann, H.; Grabowski, A.; Eigenberger, G. Ion-Exchange Membranes in the Chemical Process Industry. *Ind. Eng. Chem. Res.* **2013**, *52* (31), 10364–10379.

(6) Geise, G. M.; Lee, H.; Miller, D. J.; Freeman, B. D.; McGrath, J. E.; Paul, D. R. Water Purification by Membranes: The Role of Polymer Science. *J. Polym. Sci. Part B Polym. Phys.* **2010**, *48* (15), 1685–1718.

(7) Nunes, S. P.; Peinemann, K.-V. *Membrane Technology*; Wiley Online Library, 2001.

(8) Kamcev, J.; Freeman, B. D. Charged Polymer Membranes for Environmental/Energy Applications. *Annu. Rev. Chem. Biomol. Eng.* **2016**, *7*, 111–133.

(9) Strathmann, H. Electrodialysis, a Mature Technology with a Multitude of New Applications. *Desalination* **2010**, *264* (3), 268–288.

(10) Varcoe, J. R.; Atanassov, P.; Dekel, D. R.; Herring, A. M.; Hickner, M. A.; Kohl, P. A.; Kucernak, A. R.; Mustain, W. E.; Nijmeijer, K.; Scott, K. Anion-Exchange Membranes in Electrochemical Energy Systems. *Energy Environ. Sci.* **2014**, *7* (10), 3135–3191.

(11) Merle, G.; Wessling, M.; Nijmeijer, K. Anion Exchange Membranes for Alkaline Fuel Cells: A Review. *J. Membr. Sci.* **2011**, *377* (1–2), 1–35.

(12) Sata, T.; Sata, T.; Yang, W. Studies on Cation-Exchange Membranes Having Permselectivity between Cations in Electrodialysis. *J. Membr. Sci.* **2002**, *206* (1), 31–60.

(13) Cassady, H. J.; Cimino, E. C.; Kumar, M.; Hickner, M. A. Specific Ion Effects on the Permselectivity of Sulfonated Poly(Ether Sulfone) Cation Exchange Membranes. *J. Membr. Sci.* **2016**, *508*, 146–152.

(14) McGovern, R. K.; Zubair, S. M. The Cost Effectiveness of Electrodialysis for Diverse Salinity Applications. *Desalination* **2014**, *348*, 57–65.

(15) Lee, J.-B.; Park, K.-K.; Eum, H.-M.; Lee, C.-W. Desalination of a Thermal Power Plant Wastewater by Membrane Capacitive Deionization. *Desalination* **2006**, *196* (1), 125–134.

(16) Welgemoed, T. J.; Schutte, C. F. Capacitive Deionization Technology^{TM}: An Alternative Desalination Solution. *Desalination* **2005**, *183* (1), 327–340.

(17) Długołęcki, P.; Gambier, A.; Nijmeijer, K.; Wessling, M. Practical Potential of Reverse Electrodialysis As Process for Sustainable Energy Generation. *Environ. Sci. Technol.* **2009**, *43* (17), 6888–6894.

(18) Post, J. W.; Veerman, J.; Hamelers, H. V. M.; Euverink, G. J. W.; Metz, S. J.; Nymeijer, K.; Buisman, C. J. N. Salinity-Gradient Power: Evaluation of Pressure-Retarded Osmosis and Reverse Electrodialysis. *J. Membr. Sci.* **2007**, *288* (1), 218–230.

(19) Tamburini, A.; Tedesco, M.; Cipollina, A.; Micale, G.; Ciofalo, M.; Papapetrou, M.; Van Baak, W.; Piacentino, A. Reverse Electrodialysis Heat Engine for Sustainable Power Production. *Appl. Energy* **2017**, *206*, 1334–1353.

(20) Kim, D.-K.; Duan, C.; Chen, Y.-F.; Majumdar, A. Power Generation from Concentration Gradient by Reverse Electrodialysis in Ion-Selective Nanochannels. *Microfluid. Nanofluidics* **2010**, *9* (6), 1215–1224.

(21) Veerman, J.; Saakes, M.; Metz, S. J.; Harmsen, G. J. Reverse Electrodialysis: A Validated Process Model for Design and Optimization. *Chem. Eng. J.* **2011**, *166* (1), 256–268.

(22) Güler, E.; Elizen, R.; Vermaas, D. A.; Saakes, M.; Nijmeijer, K. Performance-Determining Membrane Properties in Reverse Electrodialysis. *J. Membr. Sci.* **2013**, *446*, 266–276.

(23) Vermaas, D. A.; Veerman, J.; Yip, N. Y.; Elimelech, M.; Saakes, M.; Nijmeijer, K. High Efficiency in Energy Generation from Salinity Gradients with Reverse Electrodialysis. *ACS Sustain. Chem. Eng.* **2013**, *1* (10), 1295–1302.

(24) Weber, A. Z.; Mench, M. M.; Meyers, J. P.; Ross, P. N.; Gostick, J. T.; Liu, Q. Redox Flow Batteries: A Review. *J. Appl. Electrochem.* **2011**, *41* (10), 1137.

(25) Li, X.; Zhang, H.; Mai, Z.; Zhang, H.; Vankelecom, I. Ion Exchange Membranes for Vanadium Redox Flow Battery (VRB) Applications. *Energy Env. Sci* **2011**, *4* (4), 1147–1160.

(26) Yang, Z.; Zhang, J.; Kintner-Meyer, M. C. W.; Lu, X.; Choi, D.; Lemmon, J. P.; Liu, J. Electrochemical Energy Storage for Green Grid. *Chem. Rev.* **2011**, *111* (5), 3577–3613.

(27) Prifti, H.; Parasuraman, A.; Winardi, S.; Lim, T. M.; Skyllas-Kazacos, M. Membranes for Redox Flow Battery Applications. *Membranes* **2012**, *2* (2), 275–306.

(28) Darling, R.; Gallagher, K.; Xie, W.; Su, L.; Brushett, F. Transport Property Requirements for Flow Battery Separators. *J. Electrochem. Soc.* **2016**, *163* (1), a5029–a5040.

(29) Fontananova, E.; Messana, D.; Tufa, R. A.; Nicotera, I.; Kosma, V.; Curcio, E.; Baak, W. van; Drioli, E.; Profio, G. D. Effect of Solution Concentration and Composition on the Electrochemical Properties of Ion Exchange Membranes for Energy Conversion. *J. Power Sources* **2017**, *340*, 282–293.

(30) Le, X. T. Permselectivity and Microstructure of Anion Exchange Membranes. *J. Colloid Interface Sci.* **2008**, *325* (1), 215–222.

(31) Richardson, S. D.; Ternes, T. A. Water Analysis: Emerging Contaminants and Current Issues. *Anal. Chem.* **2005**, *77* (12), 3807–3838.

(32) Brookes, J. D.; Carey, C. C.; Hamilton, D. P.; Ho, L.; van der Linden, L.; Renner, R.; Rigosi, A. Emerging Challenges for the Drinking Water Industry. *Environ. Sci. Technol.* **2014**, *48* (4), 2099–2101.

(33) Alotto, P.; Guarnieri, M.; Moro, F. Redox Flow Batteries for the Storage of Renewable Energy: A Review. *Renew. Sustain. Energy Rev.* **2014**, *29*, 325–335.

(34) Zhang, F.; LaBarge, N.; Yang, W.; Liu, J.; Logan, B. E. Enhancing Low-Grade Thermal Energy Recovery in a Thermally Regenerative Ammonia Battery Using Elevated Temperatures. *ChemSusChem* **2015**, *8* (6), 1043–1048.

(35) Zhang, F.; Liu, J.; Yang, W.; Logan, B. E. A Thermally Regenerative Ammonia-Based Battery for Efficient Harvesting of Low-Grade Thermal Energy as Electrical Power. *Energy Env. Sci* **2015**, *8* (1), 343–349.

(36) Geise, G. M.; Cassady, H. J.; Paul, D. R.; Logan, B. E.; Hickner, M. A. Specific Ion Effects on Membrane Potential and the Permselectivity of Ion Exchange Membranes. *Phys Chem Chem Phys* **2014**, *16* (39), 21673–21681.

(37) Logan, B. E.; Elimelech, M. Membrane-Based Processes for Sustainable Power Generation Using Water. *Nature* **2012**, *488*, 313–319.

(38) Nataraj, S. K.; Hosamani, K. M.; Aminabhavi, T. M. Potential Application of an Electrodialysis Pilot Plant Containing Ion-Exchange Membranes in Chromium Removal. *Desalination* **2007**, *217* (1), 181–190.

(39) Marder, L.; Bernardes, A. M.; Zoppas Ferreira, J. Cadmium Electroplating Wastewater Treatment Using a Laboratory-Scale Electrodialysis System. *Sep. Purif. Technol.* **2004**, *37* (3), 247–255.

(40) Marder, L.; Sulzbach, G. O.; Bernardes, A. M.; Ferreira, J. Z. Removal of Cadmium and Cyanide from Aqueous Solutions through Electrodialysis. *J. Braz. Chem. Soc.* **2003**, *14*, 610–615.

(41) Amor, Z.; Bariou, B.; Mameri, N.; Taky, M.; Nicolas, S.; Elmidaoui, A. Fluoride Removal from Brackish Water by Electrodialysis. *Desalination* **2001**, *133* (3), 215–223.

(42) Urbansky, E. T.; Schock, M. R. Issues in Managing the Risks Associated with Perchlorate in Drinking Water. *J. Environ. Manage.* **1999**, *56* (2), 79–95.

(43) Wang, P.-Y.; Shah, I.; Huang, C. P. Preparation and Characterization of Functionalized Poly(Vinyl Chloride) Membranes for Selective Separation of Perchlorate from Water. *J. Membr. Sci.* **2015**, *476*, 561–570.

(44) Srinivasan, R.; Sorial, G. A. Treatment of Perchlorate in Drinking Water: A Critical Review. *Sep. Purif. Technol.* **2009**, *69* (1), 7–21.

(45) Saracco, G.; Zanetti, M. C. Ion Transport through Monovalent-Anion-Permselective Membranes. *Ind. Eng. Chem. Res.* **1994**, *33* (1), 96–101.

(46) Firdaous, L.; Malériat, J.-P.; Schlumpf, J.-P.; Quéméneur, F. Transfer of Monovalent and Divalent Cations in Salt Solutions by Electrodialysis. *Sep. Sci. Technol.* **2007**, *42* (5), 931–948.

(47) Cheng, C.; White, N.; Shi, H.; Robson, M.; Bruening, M. L. Cation Separations in Electrodialysis through Membranes Coated with Polyelectrolyte Multilayers. *Polymer* **2014**, *55* (6), 1397–1403.

(48) Farhat, T. R.; Schlenoff, J. B. Ion Transport and Equilibria in Polyelectrolyte Multilayers. *Langmuir* **2001**, *17* (4), 1184–1192.

(49) Cheng, C.; Yaroshchuk, A.; Bruening, M. L. Fundamentals of Selective Ion Transport through Multilayer Polyelectrolyte Membranes. *Langmuir* **2013**, *29* (6), 1885–1892.

(50) Bruening, M. L.; Sullivan, D. M. Enhancing the Ion-transport Selectivity of Multilayer Polyelectrolyte Membranes. *Chem. Eur. J.* **2002**, *8* (17), 3832–3837.

(51) White, N.; Misovich, M.; Yaroshchuk, A.; Bruening, M. L. Coating of Nafion Membranes with Polyelectrolyte Multilayers to Achieve High Monovalent/Divalent Cation Electrodialysis Selectivities. *ACS Appl. Mater. Interfaces* **2015**, *7* (12), 6620–6628.

(52) Stair, J. L.; Harris, J. J.; Bruening, M. L. Enhancement of the Ion-Transport Selectivity of Layered Polyelectrolyte Membranes through Cross-Linking and Hybridization. *Chem. Mater.* **2001**, *13* (8), 2641–2648.

(53) Nagarale, R.; Gohil, G.; Shahi, V. K.; Rangarajan, R. Preparation and Electrochemical Characterizations of Cation-Exchange Membranes with Different Functional Groups. *Colloids Surf. Physicochem. Eng. Asp.* **2004**, *251* (1–3), 133–140.

(54) Luo, T.; Abdu, S.; Wessling, M. Selectivity of Ion Exchange Membranes: A Review. *J. Membr. Sci.* **2018**, *555*, 429–454.

(55) Yang, C.; Wang, S.; Jiang, L.; Hu, J.; Ma, W.; Sun, G. 1, 2-Dimethylimidazolium-Functionalized Cross-Linked Alkaline Anion Exchange Membranes for Alkaline Direct Methanol Fuel Cells. *Int. J. Hydrog. Energy* **2015**, *40* (5), 2363–2370.

(56) Qiu, B.; Lin, B.; Si, Z.; Qiu, L.; Chu, F.; Zhao, J.; Yan, F. Bis-Imidazolium-Based Anion-Exchange Membranes for Alkaline Fuel Cells. *J. Power Sources* **2012**, *217*, 329–335.

(57) Yan, X.; Gu, S.; He, G.; Wu, X.; Zheng, W.; Ruan, X. Quaternary Phosphonium-Functionalized Poly (Ether Ketone) as Highly Conductive and Alkali-Stable Hydroxide Exchange Membrane for Fuel Cells. *J. Membr. Sci.* **2014**, *466*, 220–228.

(58) Noonan, K. J.; Hugar, K. M.; Kostalik IV, H. A.; Lobkovsky, E. B.; Abruña, H. D.; Coates, G. W. Phosphonium-Functionalized Polyethylene: A New Class of Base-Stable Alkaline Anion Exchange Membranes. *J. Am. Chem. Soc.* **2012**, *134* (44), 18161–18164.

(59) Choi, J.-H.; Kim, S.-H.; Moon, S.-H. Heterogeneity of Ion-Exchange Membranes: The Effects of Membrane Heterogeneity on Transport Properties. *J. Colloid Interface Sci.* **2001**, *241* (1), 120–126.

(60) Kreuer, K.-D. Ion Conducting Membranes for Fuel Cells and Other Electrochemical Devices. *Chem. Mater.* **2013**, *26* (1), 361–380.

(61) Ji, Y.; Geise, G. M. The Role of Experimental Factors in Membrane Permselectivity Measurements. *Ind. Eng. Chem. Res.* **2017**, *56* (26), 7559–7566.

Chapter 3: Theoretical Models*

In this research, the ion transport was studied in terms of ion concentration within, and ion diffusion across the membrane phase. Both counter-ion and co-ion transport occur in the membrane phase. The co-ion concentration in the membrane phase, governed by the partitioning effects across the membrane-solution phase boundary, is more difficult to understand. The counter-ions enter the membrane phase and balance both the fixed charge groups having opposite charge and the co-ions. Once the co-ion concentration and membrane *IEC* are known, the counter-ion concentration can be calculated using electroneutrality conditions. Therefore, the ion concentration modeling part of this work will mainly focus on modeling the co-ion sorption and concentration in the membrane phase.

3.1. Equilibrium Co-Ion Sorption

The starting point for modeling co-ion sorption in charged polymers is to use Donnan exclusion theory to describe co-ion exclusion from the polymer that results from the combination of the thermodynamic equilibrium criterion and electroneutrality. Donnan theory, however, includes mean ionic activity coefficient terms for the membrane and solution phases that must be evaluated.[1–5] The solution phase mean ionic activity coefficients were evaluated using the Pitzer model.[6,7] The mean ionic activity coefficients in the membrane phase, however, are more difficult to model. The Manning counter-ion condensation model[8] does not consider ion specific properties that make a given ion different from another ion of the same valence. As such, we have also considered electrostatic and dispersion force-based approaches to calculate the mean ionic activity coefficients. The co-ion sorption coefficients, calculated using these models, are discussed and compared to experimentally measured co-ion sorption coefficients.

3.1.1. Donnan Theory

---

* This chapter has been adapted with permission from: Ji, Y.; Luo, H.; Geise, G.M. Specific Co-Ion Sorption and Diffusion Properties Influence Membrane Permselectivity. *J. Membr. Sci*. **2018**, *563*(1), 492 – 504

The co-ion sorption coefficient, k_X^m, is defined as the ratio of the concentration of co-ions in the membrane phase, c_X^m, relative to that in the external solution, c_X^s:[9]

$$k_X^m \equiv \frac{c_X^m}{c_X^s} \tag{3.1}$$

In IEMs, the co-ion sorption coefficient is equivalent to the mobile salt sorption coefficient, k_s^m, that is widely used to quantify the partitioning of mobile salt into polymers for membrane applications.[9–11] The co-ion sorption coefficient is a thermodynamic property that describes the equilibrium partitioning of co-ions from external solution into the membrane phase, so modeling approaches for the co-ion sorption coefficient begin from the definition of thermodynamic equilibrium (i.e., the thermodynamic activity of ions must be equivalent in the membrane phase and in the solution phase).[12] For unchanged polymers, the co-ion sorption coefficient, k_X^m, is equivalent to the ratio of the mean ionic activity coefficient in the solution phase, $\gamma_\pm^s$, to the mean ionic activity coefficient in the membrane phase, $\gamma_\pm^m$:[9]

$$k_X^m = \frac{\gamma_\pm^s}{\gamma_\pm^m} \tag{3.2}$$

For changed polymers, an electroneutrality condition must be included to account for the fact that some of the charges in the membrane are fixed to the polymer backbone. The Donnan exclusion model combines the thermodynamic equilibrium criterion with a change balance to describe co-ion sorption in charged materials.[2,12] The Donnan exclusion model describes the dependence of co-ion sorption on the concentration of fixed charges in the polymer, c_A^m, salt concentration in the external solution, c_s^s, mean ionic activity coefficient in the solution phase, $\gamma_\pm^s$, and mean ionic activity coefficient in the membrane phase, $\gamma_\pm^m$:

$$k_X^m = \left[\frac{1}{4}\left(\frac{c_A^m}{c_s^s}\right)^2 + \left(\frac{\gamma_\pm^s}{\gamma_\pm^m}\right)^2\right]^{\frac{1}{2}} - \frac{1}{2}\left(\frac{c_A^m}{c_s^s}\right) \tag{3.3}$$

In many studies, the ratio of the mean ionic activity coefficients in Equation 3.3 has been taken as unity, but recent reports have shown this assumption of solution ideality to be inappropriate, for example, for a series of highly-charged CEMs.[3,8] In this study, we consider three approaches for calculating the ratio of the mean ionic activity coefficients, $\gamma_\pm^s/\gamma_\pm^m$, to gain insight into the fundamental physics that governs observed co-ion specific sorption properties. In all cases, the mean ionic activity coefficient in the solution phase was calculated using the Pitzer model.

3.1.2. Counter-Ion Condensation Theory

The mean ionic activity coefficient in the membrane phase can be calculated using the Manning's counter-ion condensation theory, which treats polymer chains as infinite line charges with charged groups evenly spaced along the chain. A dimensionless parameter, ξ, compares the length scale of the electrostatic forces to the physical spacing of charge groups along the polymer chain:[3,8]

$$\xi = \frac{\lambda_B}{b} = \frac{e^2}{4\pi\varepsilon_0\varepsilon_m(0)k_BTb} \tag{3.4}$$

where λ_B is the Bjerrum length, e is the elementary charge, ε_0 is the vacuum permittivity, $\varepsilon_m(0)$ is the constant relative permittivity (i.e., the static dielectric constant) of the hydrated membrane, k_B is the Boltzmann's constant, T is the absolute temperature, and b is the distance between fixed charge groups on the polymer chain. The static dielectric constant of the hydrated membrane was estimated using an empirical relationship based on membrane water content.[13] The value of ξ can be related to the counter-ion condensation in highly charged ion exchange materials.[3,4,8]

For monovalent electrolytes, a critical value of $\xi = 1$ can be defined.[8] If $\xi > 1$, counter-ions condense on (or neutralize) polymer fixed charges to reduce ξ to unity.[3,4,8] The remaining uncondensed counter-ions are treated thermodynamically using the Debye-Huckel approximation. When $\xi > 1$, the mean ionic activity coefficient in the membrane phase can be calculated as:[3,4,8]

$$\gamma_\pm^m = \left[\left(\frac{X/\xi+1}{X+1}\right)\exp\left(-\frac{X}{X+2\xi}\right)\right]^{\frac{1}{2}} \tag{3.5}$$

where $X = c_A^m / c_s^m$, i.e., the ratio of fixed charge group concentration to mobile salt concentration in the membrane phase. When $\xi < 1$, counter-ion condensation does not occur, and the mean activity coefficient in the membrane is calculated directly using the Debye-Huckel approximation:

$$\ln \gamma_\pm^m = -\frac{\xi X}{2(X+2)} \tag{3.6}$$

3.1.3. Continuum Electrostatic Theory

Electrostatic theory can be used to describe the ratio of the mean ionic activity coefficients in the solution and membrane phases by considering the definition of the co-ion sorption coefficient for an uncharged polymer (Equation 3.2), and the free energy change, ΔG_i, associated with moving an ion from the solution to the membrane phase:

$$\frac{\gamma_\pm^s}{\gamma_\pm^m} = \frac{c_i^m}{c_i^s} = \exp\left[-\frac{\Delta Gi}{k_B T}\right] \tag{3.7}$$

Zhang et al. considered a simple case where ΔG_i was taken as the electrostatic solvation energy barrier, ΔW_i, calculated using the Born model.[13] The Born model treats the swollen polymer and the external solution phases as dielectric continua and the ions as charged, non-polarizable spheres.[14,15] Under these assumptions, the sorption free energy is the solvation energy change associated with transferring a charged, non-polarizable sphere from one dielectric continuum to another.[16] The Born model describes the free energy change associated with moving ion *i* from solution into the membrane as:[13]

$$\Delta W_i = \frac{z_i^2 e^2}{8\pi\varepsilon_0 a_i}\left(\frac{1}{\varepsilon_m(0)} - \frac{1}{\varepsilon_{sol}(0)}\right) \tag{3.8}$$

where z_i is the valence, a_i is the bare ionic radius, and $\varepsilon_{sol}(0)$ is the static dielectric constant of the solution.

Combining Equation 3.3, 3.7 and 3.8, the co-ion sorption coefficient can be described using a combination of Donnan theory and Born model as:

$$K_X^m = \sqrt{\frac{1}{4}\left(\frac{c_A^m}{c_s^s}\right)^2 + \left\{\exp\left[-\frac{z_i^2 e^2}{8\pi k_B T \varepsilon_0 a_i}\left(\frac{1}{\varepsilon_m(0)} - \frac{1}{\varepsilon_{sol}(0)}\right)\right]\right\}^2} - \frac{1}{2}\left(\frac{c_A^m}{c_s^s}\right) \tag{3.9}$$

3.1.4. Continuum Electrostatic and Dispersion-Based Theory

The electrostatic model described above can be modified to include dispersion energy forces.[17] Dispersion forces exist between molecules and have been suggested to be related to ion specific effects that have been observed in other systems.[17–23] Coupling dispersion forces with electrostatic forces attempts to account for the influence of ion polarizability on ion sorption. The electrostatic and dispersion force theory proposed by Boström and Ninham[17,24] requires many of the same assumptions as the Born model in that both the swollen polymer and external solution phases are treated as dielectric continua.[25] The difference, however, is that incorporating dispersion forces into the model enables the model to treat ions as polarizable charged spheres.[26] The dispersion energy reflects the fact that ions have different polarizability properties compared to the surrounding medium.

Ninham et al. developed a relationship that describes the difference in the dispersion energy between the membrane and solution phases, ΔD_i:[17]

$$\Delta D_i = \frac{4k_B T}{a_i^3\sqrt{\pi}} \sum_{n=0}^{\infty}\left[\frac{\alpha_m^*(i\omega_n)}{\varepsilon_m(i\omega_n)} - \frac{\alpha_{sol}^*(i\omega_n)}{\varepsilon_{sol}(i\omega_n)}\right] \tag{3.10}$$

where $\alpha_m^*(i\omega_n)$ and $\alpha_{sol}^*(i\omega_n)$ are the excess polarizability (i.e., the excess polarizability of an ion compared to the solvent of equivalent volume) in the membrane and the solution, respectively $\varepsilon_m(i\omega_n)$ and $\varepsilon_{sol}(i\omega_n)$ are the frequency-dependent relative permittivity functions for the membrane and solution phases, respectively. Equation 3.10 requires evaluation of the excess polarizability and relative permittivity terms at discrete frequencies, ω_n ($\omega_n = 2\pi k_B T\left(n + \frac{1}{2}\right)/\hbar$). The first frequency ($n$ = 0) is 1.23×10^{14} Hz and is in the ultraviolet frequency range. The summation over discrete energy levels, in Equation 3.10, originates from a quantum mechanical approach, take by London, that accounts for the contributions of different interaction states to the dispersion energy.[26] The co-ion sorption coefficient can be described using Donnan theory and the electrostatic-dispersion energy model by combining Equation 3.3, 3.7 and 3.10:

$$K_X^m = \sqrt{\frac{1}{4}\left(\frac{c_A^m}{c_S^s}\right)^2 + \left\{\exp\left[-\frac{z_i^2 e^2}{8\pi k_B T \varepsilon_0 a_i}\left(\frac{1}{\varepsilon_m(0)} - \frac{1}{\varepsilon_{sol}(0)}\right) - \frac{4}{a_i^3\sqrt{\pi}}\sum_{n=0}^{\infty}\left(\frac{\alpha_m^*(i\omega_n)}{\varepsilon_m(i\omega_n)} - \frac{\alpha_{sol}^*(i\omega_n)}{\varepsilon_{sol}(i\omega_n)}\right)\right]\right\}^2} - \frac{1}{2}\left(\frac{c_A^m}{c_S^s}\right) \tag{3.11}$$

The values of terms $\alpha_m^*(i\omega_n)$, $\alpha_{sol}^*(i\omega_n)$, $\varepsilon_m(i\omega_n)$ and $\varepsilon_{sol}(i\omega_n)$ for different ions are presented and discussed in further detail in Section 4.2.

3.2. Ion Diffusion

Ion diffusion in charged, hydrated polymer membranes can be influenced by tortuosity that created by the polymer chains of the membrane and electrostatic interactions between the fixed charge groups and counter-ions or co-ions. The Mackie and Meares model was used to describe the hindered diffusion of ions[13,27,28] and the counter-ion condensation model was combined to understand the electrostatic effects.[29,30]

3.2.1. Mackie and Meares Theory

The Mackie and Meares model was used to describe the influence of tortuosity on diffusion:[27]

$$\frac{D_i^m}{D_i^s} = \left(\frac{k_w}{2-k_w}\right)^2 \tag{3.12}$$

where k_w is the water sorption coefficient (i.e., the volume fraction of water sorbed by the membrane), and D_i^m and D_i^s are the diffusion coefficients of ion *i* in the membrane and solution phases, respectively. Thus, increasing the water content of the polymer results in a diffusion coefficient in the membrane phase that approaches the diffusion coefficient in bulk solution.

3.2.2. Counter-Ion Condensation Theory

Manning's counter-ion condensation theory describes the influence of electrostatic effects on diffusion.[30] When $\xi > 1$, counter-ion condensation must be considered, and condensed counter-ions have no mobility. As a result, the counter-ion diffusion coefficient in the membrane phase, D_M^m, is suppressed by electrostatics to a larger extent than the co-ion diffusion coefficient in the membrane phase, D_X^m:

$$\frac{D_M^m}{D_M^s} = \left(\frac{X/\xi+1}{X+1}\right)\left[1-\frac{1}{3}A(1,X/\xi)\right] \tag{3.13}$$

$$\frac{D_X^m}{D_X^s} = 1-\frac{1}{3}A(1,X/\xi) \tag{3.14}$$

where $A(1,X/\xi) = \sum_{c_1=-\infty}^{\infty}\sum_{c_2=-\infty}^{\infty}\left[\pi(c_1^2+c_2^2)+1+\frac{2\xi}{X}\right]^{-2}$ and $(c_1,c_2) \neq (0,0)$. This sum can be calculated numerically or approximated analytically.[30,31] When $\xi < 1$, counter-ion condensation does not occur, and the counter-ion and co-ion diffusion coefficients in the membrane phase are suppressed by electrostatics to an equivalent extent:

$$\frac{D_M^m}{D_M^s} = \frac{D_X^m}{D_X^s} = 1-\frac{1}{3}A(\xi,X) \tag{3.15}$$

where $A(\xi,X) = \sum_{c_1=-\infty}^{\infty}\sum_{c_2=-\infty}^{\infty}\left[\frac{\pi}{\xi}(c_1^2+c_2^2)+1+\frac{2}{X}\right]^{-2}$ and $(c_1,c_2) \neq (0,0)$.[30]

Combining Equation 3.12, 3.14 and 3.15 provides an approach for calculating the membrane phase diffusion coefficients, relative to that in solution, when counter-ion condensation occurs ($\xi > 1$):[31]

$$\frac{D_M^m}{D_M^s} = \left(\frac{k_w}{2-k_w}\right)^2\left(\frac{X/\xi+1}{X+1}\right)\left[1-\frac{1}{3}A(1,X/\xi)\right] \tag{3.16}$$

$$\frac{D_X^m}{D_X^s} = \left(\frac{k_w}{2-k_w}\right)^2\left[1-\frac{1}{3}A(1,X/\xi)\right] \tag{3.17}$$

When counter-ion condensation does not occur ($\xi < 1$), combining Equation 3.12, 3.16 and 3.17 provides an approach to calculating the membrane phase diffusion coefficients relative to that in solution:

$$\frac{D_M^m}{D_M^s} = \frac{D_X^m}{D_X^s} = \left(\frac{k_w}{2-k_w}\right)^2\left[1-\frac{1}{3}A(\xi,X)\right] \tag{3.18}$$

3.3. References

(1) Geise, G. M.; Paul, D. R.; Freeman, B. D. Fundamental Water and Salt Transport Properties of Polymeric Materials. *Prog. Polym. Sci.* **2014**, *39* (1), 1–42.

(2) Geise, G. M.; Lee, H.; Miller, D. J.; Freeman, B. D.; McGrath, J. E.; Paul, D. R. Water Purification by Membranes: The Role of Polymer Science. *J. Polym. Sci. Part B Polym. Phys.* **2010**, *48* (15), 1685–1718.

(3) Kamcev, J.; Galizia, M.; Benedetti, F. M.; Jang, E.-S.; Paul, D. R.; Freeman, B. D.; Manning, G. S. Partitioning of Mobile Ions between Ion Exchange Polymers and Aqueous Salt Solutions: Importance of Counter-Ion Condensation. *Phys Chem Chem Phys* **2016**, *18* (8), 6021–6031.

(4) Kamcev, J.; Paul, D. R.; Freeman, B. D. Ion Activity Coefficients in Ion Exchange Polymers: Applicability of Manning's Counterion Condensation Theory. *Macromolecules* **2015**, *48* (21), 8011–8024.

(5) Bird, R.; Stewart, W.; Lightfoot, E. Transport Phenomena 2nd Ed., John Wiley&Sons. *Inc Hoboken NJ* **2002**.

(6) Kenneth, S. P. Thermodytriarnics of Electrolytes. I. Theoretical Basis and General Equation. *J Phys Chem A* **1973**, *77*, 268–277.

(7) Pitzer, K. S.; Mayorga, G. Thermodynamics of Electrolytes.: II. Activity and Osmotic Coefficients for Strong Electrolytes with One or Both Ions Univalent. In *Molecular Structure And Statistical Thermodynamics: Selected Papers of Kenneth S Pitzer*; World Scientific, 1993; pp 396–404.

(8) Manning, G. S. Limiting Laws and Counterion Condensation in Polyelectrolyte Solutions I. Colligative Properties. *J. Chem. Phys.* **1969**, *51* (3), 924–933.

(9) Wijmans, J. G.; Baker, R. W. The Solution-Diffusion Model: A Review. *J. Membr. Sci.* **1995**, *107* (1–2), 1–21.

(10) Geise, G. M.; Falcon, L. P.; Freeman, B. D.; Paul, D. R. Sodium Chloride Sorption in Sulfonated Polymers for Membrane Applications. *J. Membr. Sci.* **2012**, *423*, 195–208.

(11) Paul, D. R. Reformulation of the Solution-Diffusion Theory of Reverse Osmosis. *J. Membr. Sci.* **2004**, *241* (2), 371–386.

(12) Helfferich, F. G. *Ion Exchange*; Courier Corporation, 1995.

(13) Zhang, H.; Geise, G. M. Modeling the Water Permeability and Water/Salt Selectivity Tradeoff in Polymer Membranes. *J. Membr. Sci.* **2016**, *520*, 790–800.

(14) Warshel, A.; Russell, S. T. Calculations of Electrostatic Interactions in Biological Systems and in Solutions. *Q. Rev. Biophys.* **1984**, *17* (3), 283–422.

(15) Parsegian, A. Energy of an Ion Crossing a Low Dielectric Membrane: Solutions to Four Relevant Electrostatic Problems. *Nature* **1969**, *221* (5183), 844–846.

(16) Bowen, W. R.; Welfoot, J. S. Modelling the Performance of Membrane Nanofiltration—Critical Assessment and Model Development. *Chem. Eng. Sci.* **2002**, *57* (7), 1121–1137.

(17) Boström, M.; Ninham, B. Energy of an Ion Crossing a Low Dielectric Membrane: The Role of Dispersion Self-Free Energy. *Biophys. Chem.* **2005**, *114* (2–3), 95–101.

(18) Kunz, W.; Belloni, L.; Bernard, O.; Ninham, B. W. Osmotic Coefficients and Surface Tensions of Aqueous Electrolyte Solutions: Role of Dispersion Forces. *J. Phys. Chem. B* **2004**, *108* (7), 2398–2404.

(19) Boström, M.; Williams, D. R.; Ninham, B. W. Surface Tension of Electrolytes: Specific Ion Effects Explained by Dispersion Forces. *Langmuir* **2001**, *17* (15), 4475–4478.

(20) Tavares, F. W.; Bratko, D.; Blanch, H. W.; Prausnitz, J. M. Ion-Specific Effects in the Colloid− Colloid or Protein− Protein Potential of Mean Force: Role of Salt− Macroion van Der Waals Interactions. *J. Phys. Chem. B* **2004**, *108* (26), 9228–9235.

(21) Boström, M.; Williams, D.; Ninham, B. Ion Specificity of Micelles Explained by Ionic Dispersion Forces. *Langmuir* **2002**, *18* (16), 6010–6014.

(22) Boström, M.; Williams, D. R.; Ninham, B. W. Influence of Hofmeister Effects on Surface PH and Binding of Peptides to Membranes. *Langmuir* **2002**, *18* (22), 8609–8615.

(23) Boström, M.; Williams, D.; Stewart, P.; Ninham, B. Hofmeister Effects in Membrane Biology: The Role of Ionic Dispersion Potentials. *Phys. Rev. E* **2003**, *68* (4), 041902.

(24) Boström, M.; Deniz, V.; Ninham, B. Ion Specific Surface Forces between Membrane Surfaces. *J. Phys. Chem. B* **2006**, *110* (19), 9645–9649.

(25) Mahanty, J.; Ninham, B. W. Theory of Dispersion Interactions between Macroscopic Bodies. *J. Chem. Soc. Faraday Trans. 2 Mol. Chem. Phys.* **1975**, *71*, 119–137.

(26) Mahanty, J.; Ninham, B. W. *Dispersion Forces*; Academic Press, 1976; Vol. 1.

(27) Mackie, J.; Meares, P. The Diffusion of Electrolytes in a Cation-Exchange Resin Membrane I. Theoretical. *Proc. R. Soc. Lond. Ser. Math. Phys. Sci.* **1955**, *232* (1191), 498–509.

(28) Mackie, J.; Meares, P. The Diffusion of Electrolytes in a Cation-Exchange Resin Membrane. II. Experimental. *Proc. R. Soc. Lond. Ser. Math. Phys. Sci.* **1955**, *232* (1191), 510–518.

(29) Kamcev, J.; Paul, D. R.; Manning, G. S.; Freeman, B. D. Ion Diffusion Coefficients in Ion Exchange Membranes: Significance of Counterion Condensation. *Macromolecules* **2018**, *51* (15), 5519–5529.

(30) Manning, G. S. Limiting Laws and Counterion Condensation in Polyelectrolyte Solutions II. Self-diffusion of the Small Ions. *J. Chem. Phys.* **1969**, *51* (3), 934–938.

(31) Kamcev, J.; Paul, D. R.; Manning, G. S.; Freeman, B. D. Predicting Salt Permeability Coefficients in Highly Swollen, Highly Charged Ion Exchange Membranes. *ACS Appl. Mater. Interfaces* **2017**, *9* (4), 4044–4056.

Chapter 4: Materials and Methods

4.1. Polymeric Membranes

4.1.1. Commercial Membranes

Two commercially available, sulfonated CEMs, Selemion CMV (Asahi Glass, Co., Tokyo, Japan) and CMI-7000s (Membranes International Inc., NJ, USA) were used in this study (Figure 4.1). The ion exchange capacity (*IEC*) of a charged membrane is a measure of the degree of charged group functionalization of the polymer. The reported *IEC* values of these two commercially available membranes were 2.08 meq/g(dry polymer) for Selemion CMV[1] and 1.6±0.1 meq/g(dry polymer) for CMI-7000s.[2] Other properties of the two membranes were measured using the methods specified in Section 4.4 and presented in Table 4.1.

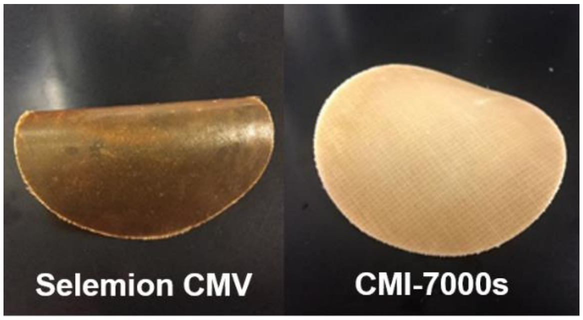

Figure 4.1. Two commercially available CEMs, the Selemion CMV (left) and CMI-7000s (right) used in this study.

Table 4.1. Physical properties of the commercially available polymeric ion exchange membranes. For the water uptake measurements, the membranes were initially hydrated in either 0.1 or 0.5 mol/L sodium chloride solutions at ambient temperature, and the uncertainty is reported as the standard deviation from the mean value of six measurements. The membrane thickness values are reported as an average and standard deviation of four to five measurements made on hydrated as-received membrane sheets.

Membrane	Ion Exchange Capacity (*IEC*) [mequiv/g(dry polymer)]	Water Uptake (w_u) [g(water)/g(dry polymer)]		Hydrated Membrane Thickness(δ) [μm]
		0.1 mol/L NaCl	0.5 mol/L NaCl	
Selemion CMV	2.08	0.28±0.01	0.25±0.02	109±2
CMI-7000s	1.6±0.1	0.32±0.01	0.35±0.02	590±3

4.1.2. XLPEGDA and Sulfonated XLAMPS Membranes

Crosslinked poly(ethylene glycol diacrylate) (XLPEGDA) polymeric membranes serve as uncharged control materials and a crosslinked sulfonated CEM based on sodium neutralized 2-acrylamido-2-methyl-1-propanesulfonic acid (AMPS) that was crosslinked using poly(ethylene glycol diacrylate) (n=10) was used (Figure 4.2). Prior to curing the XLAMPS membranes, 50wt% 2-acrylamido-2-methyl-1-propanesulfonic acid (AMPS) sodium salt solution (catalog number 655821, Sigma-Aldrich, St. Louis, MO) was mixed with poly(ethylene glycol) diacrylate (PEGDA) crosslinker (average M_n = 525g/mol, catalog number 437441, Sigma-Aldrich, St. Louis, MO) to form a homogeneous 1:3 (by mass) AMPS:PEGDA solution. For the XLPEGDA membranes, PEGDA with either 3, 10, or 13 ethylene oxide repeat units between crosslinks (i.e., the value of n in Figure 4.2) was used. The PEGDA (obtained from Sigma-Aldrich) with n = 3, 10, or 13 corresponded to average PEGDA number average molecular weights of M_n = 250g/mol (catalog number 475629), M_n = 525g/mol (catalog number 437441), and M_n = 700g/mol (catalog number 455008), respectively. A free radical initiator, 1-hydroxycyclohexyl phenyl ketone (HCPK, catalog number 405612, Sigma-Aldrich, St. Louis, MO), was added to all of the pre-polymerization solution at a concentration of 0.1% (by mass).

The XLAMPS and XLPEGDA membranes were cured via a free radical UV-initiated photopolymerization process.[3,4] The pre-polymerization solutions were confined between two quartz plates, and plates were used to control the separation of the plates and the resulting membrane thickness. Transparent and colorless membranes were formed by irradiating the pre-polymerization solution with 120μJ/cm^2 of 254nm UV light for 300sec (XLAMPS) and 120sec (XLPEGDA).[4] After curing, the films were soaked in de-ionized (DI) water to hydrate the membranes and extract any unreacted hydrophilic molecules. The final hydrated thickness of the XLAMPS and XLPEGDA membranes was in the range of 200μm – 300μm. The properties of XLAMPS and XLPEGDA membranes were measured using the methods discussed specified in Section 4.4 and presented in Table 4.2 and 4.3.

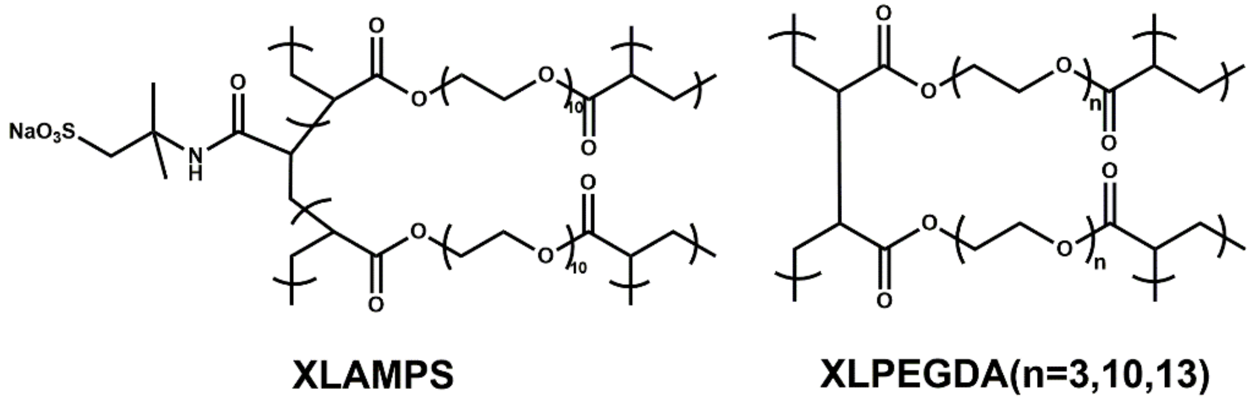
XLAMPS

XLPEGDA(n=3,10,13)

Figure 4.2. Chemical structures of the XLAMPS and XLPEGDA Membranes. XLPEGDA materials were prepared using PEGDA with either *n* = 3, 10, or 13.

Table 4.2. Physical and chemical properties of the XLAMPS and XLPEGDA membranes considered in this study. Water uptake and dry polymer density data were measured under room temperature, and the water uptake sorption k_w was calculated using the method specified in Section 4.4.2. No fixed charge groups are expected to exist in the XLPEGDA membranes, so their *IEC* values are not reported. For water uptake measurements, the membranes were initially hydrated in either 0.1 or 0.5 mol/L sodium chloride solutions, and the uncertainty is reported as the standard deviation of six measurements. The water uptake of XLPEGDA membranes were only measured in 0.1 mol/L sodium chloride solution, so the water uptake in 0.5 mol/L sodium chloride solution was not reported.

Membranes	Ion Exchange Capacity (*IEC*) [mequiv/g(dry polymer)]	Water Uptake (w_u) [g(water)/g(dry polymer)]		Dry Polymer Density (ρ_P) [g/cm^3]	Water Sorption Coefficient (k_w)	
		0.1 mol/L NaCl	0.5 mol/L NaCl			
XLAMPS	1.09	0.81±0.01	0.78±0.02	1.34	0.51±0.01	0.51±0.03
XLPEGDA (n=3)	-	0.054±0.003	-	1.27	0.064±0.004	-
XLPEGDA (n=10)	-	0.34±0.01	-	1.21	0.29±0.01	-
XLPEGDA (n=13)	-	0.52±0.02	-	1.19	0.38±0.02	-

Table 4.3. Room temperature water uptake (w_u) data measured using four aqueous electrolyte solutions. Samples were equilibrated with either 0.1 mol/L or 0.5 mol/L solution prior to the water uptake measurement.

Electrolyte	Selemion CMV		CMI-7000s		XLAMPS	
	0.1 mol/L	0.5 mol/L	0.1 mol/L	0.5 mol/L	0.1 mol/L	0.5 mol/L
NaCl	0.28±0.01	0.25±0.02	0.32±0.01	0.35±0.02	0.81±0.01	0.78±0.02
NaBr	0.22±0.06	0.24±0.02	0.35±0.02	0.34±0.04	0.80±0.02	0.78±0.01
$NaNO_3$	0.24±0.07	0.24±0.03	0.30±0.02	0.31±0.01	0.81±0.02	0.78±0.02
$NaClO_4$	0.27±0.01	0.30±0.02	0.34±0.01	0.33±0.01	0.80±0.02	0.75±0.01

4.1.3. Trimethyl Ammonium Charged PVBAN-TMA and 1,4-Dimethyl Imidazolium Charged PVBAN-DMI Membranes

A crosslinked trimethyl ammonium charged AEM and a crosslinked 1,4-dimethyl ammonium charged AEM were used (Figure 4.3). The two AEMs were synthesized by crosslinking a mixture of styrene and acrylonitrile (1:3 weight ratio), (vinyl benzyl) trimethylammonium chloride or 1,2-dimethyl-3-(4-vinylbenzyl) imidazolium chloride (22 or 25 wt% to ensure the theoretical membrane *IEC* =1.0 mequiv/g). Divinylbenzene and benzoin ethyl ether were added (4wt% and 2wt% based on the weight of all monomers, respectively) as crosslinker and photoinitiator. Dimethyl sulfoxide (DMSO) was added at a ratio of 1.6g per g/(total co-monomer), and the mixture was stirred and ultrasonicated until the solution became transparent and homogeneous. The formulation of these two AEMs were based on some widely reported recipes in the alkaline fuel cell membrane field.[3,5–8]

The transparent and homogeneous solution was then confined between two quartz plates, and spacers were used to control the separation of the plates and the resulting membrane thickness.[3,4] Transparent slightly brown membranes were formed by irradiating the solution with 120 μJ/cm^2 of 254 nm UV light for 1-hour.[5,6,9] After curing, the membranes were carefully peeled from the glass plates and placed into a Teflon mold, then placed into a convection oven with temperature being maintained at 60^{o}C for 1 hour. The membranes were subsequently transferred into a vacuum oven with temperature being maintained at 60^{o}C and under vacuum for 48 hours. The solvent evaporation process could substantially decrease the water uptake of the membranes. Lower membrane uptake, therefore, could make the effects of polymer structure more pronounced in influencing membrane performance, and enhance the membrane mechanical strength to ease the following handling. The entire solvent evaporation process removed at least 98wt% of the solvent from the membrane. The final membranes were soaked in de-ionized (DI) water to be hydrated and any unreacted hydrophilic molecules or unevaporated DMSO should be removed in this process.

The polymer backbones of the two AEMs are therefore composed of styrene, acrylonitrile, divinyl benzene and styrene-based charged monomers. The co-monomer compositions of the two AEMs should be controlled similar during the synthesis processes. Ideally, the only difference between the two AEMs should be the fixed charge group. The two AEMs were named "PVBAN-TMA[X]" and "PVBAN-DMI[X]", where "PVBAN" indicates that the polymeric membranes mainly contain styrene and acrylonitrile co-monomers, "TMA" or "DMI" indicates that the fixed charge group is trimethyl ammonium or 1,4-dimethyl imidazolium, respectively, and "[X]" represents for different counter-ions. The physical and chemical properties of the two AEMs were measured when the samples were equilibrated with DI water and 0.5 mol/L aqueous electrolyte solutions, and presented in Table 4.4 and Table 4.5. The methods used to measure those properties will be discussed in detail in Section 4.4.

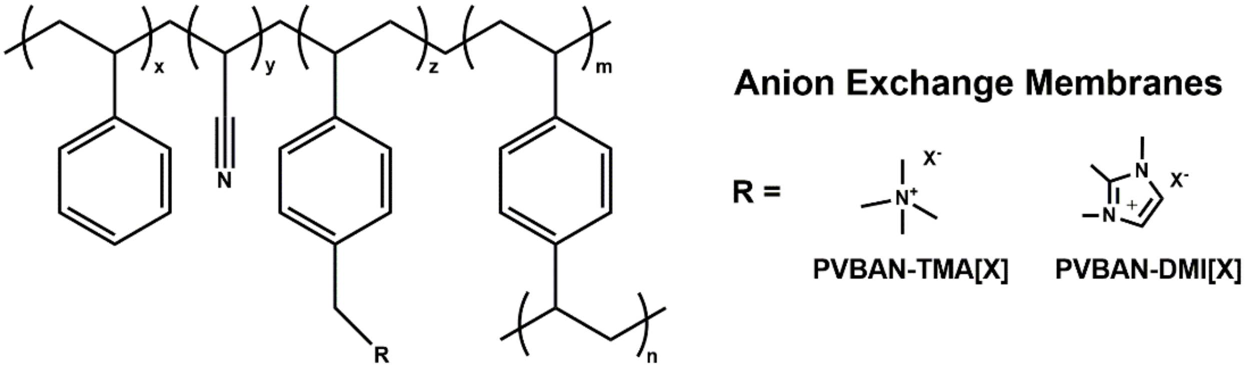

Figure 4.3. Chemical structure and nomenclature of the two AEMs in this study. "PVBAN" indicates that the membranes are mainly composed of styrene and acrylonitrile co-monomers, "TMA" stands for trimethyl ammonium fixed charge group, "DMI" stands for 1,4-dimethyl imidazolium fixed charge group and "[X]" represents for the counter-ions.

Table 4.4. Physical and chemical properties of the two AEMs measured in chloride-form and when samples were equilibrated with DI water. For water uptake measurements, uncertainty is reported as the standard deviation from the mean values of four measurements. The membrane thickness values are reported as an average and standard deviation of four measurements made on different places of hydrated membranes.

Membranes	Thickness (δ) [µm]	Dry Density (ρ_d) [g/cm^3]	Ion Exchange Capacity (*IEC*) [mequiv (fixed charge group)/g(dry polymer)]	Water Uptake (w_u) [g(water)/g(dry polymer)]
PVBAN-TMA[Cl]	600±10	1.22±0.03	1.21±0.15	0.61±0.03
PVBAN-DMI[Cl]	450±3	1.16±0.02	1.15±0.12	0.51±0.04

Table 4.5. Physical and chemical properties of the two AEMs when samples were equilibrated with 0.5 mol/L aqueous solutions of lithium chloride, sodium chloride, ammonium chloride, sodium bromide and sodium nitrate, respectively. In the measurements, the membranes were soaked in 0.5 mol/L solutions for 48 – 72 hours to ensure full equilibrium and ion exchange. The water uptake was reported as an average and standard deviation of four measurements.

Electrolytes	PVBAN-TMA[X]			PVBAN-DMI[X]		
	w_u	Water Sorption Coefficient (k_w)	Fixed Charge Group Concentration, c_m^A [mequiv(fixed charge group group) / cm^3(water sorbed)]	w_u	k_w	c_m^A
LiCl	0.47±0.02	0.36±0.01	2.60±0.34	0.30±0.00	0.26±0.00	3.83±0.40
NaCl	0.46±0.01	0.36±0.01	2.65±0.33	0.30±0.00	0.26±0.00	3.83±0.40
NH_4Cl	0.44±0.01	0.35±0.01	2.74±0.35	0.29±0.00	0.25±0.00	4.02±0.42
NaBr	0.38±0.02	0.32±0.02	3.20±0.42	0.26±0.02	0.23±0.02	4.40±0.61
$NaNO_3$	0.36±0.01	0.31±0.01	3.33±0.43	0.22±0.07	0.20±0.05	5.25±1.82

4.2. Electrolytes

Monovalent strong electrolytes were used in this study. Electrolytes with fixed sodium cation and different anions, such as sodium chloride (NaCl), sodium bromide (NaBr), sodium nitrate ($NaNO_3$) and sodium perchlorate ($NaClO_4$), as well as electrolytes with fixed chloride anion and different cations, such as lithium chloride (LiCl) and ammonium chloride (NH_4Cl) were used. The dielectric, size, polarizability and hydration enthalpy properties[10] of the different cations and anions associated with these electrolytes will be presented and discussed in the following chapters.

4.3. Experimental Methods

4.3.1. Dry Density

The dry polymer density of all membrane samples was measured using an Archimedes' principle method.[4] A Mettler Toledo density kit (Part # 11106706) was used in conjunction with an analytical balance (Model XSE204). The mass of the dry polymer sample first was measured in air, m_1, and subsequently was measured in an auxiliary liquid, i.e., a non-solvent for the polymer, m_2. The dry polymer density, ρ_p, was calculated as:

$$\rho_p = \frac{m_1}{m_1 - m_2}(\rho_2 - \rho_1) + \rho_1 \tag{4.1}$$

where ρ_1 and ρ_2 are the density values, at the measurement temperature, of air and the auxiliary liquid, respectively. The auxiliary liquid was chosen to be *n*-heptane for XLAMPS, XLPEGDA, PVBAN-TMA and PVBAN-DMI membranes. The reason for choosing *n*-heptane for XLAMPS and XLPEGDA was that *n*-heptane has little affinity for the ethylene oxide groups present in PEGDA.[4,11] The reason for choosing *n*-heptane for PVBAN-TMA and PVBAN-DMI was that the molar composition of acrylonitrile is over 85% in both two AEMs, and polyacrylonitrile has negligible solubility in *n*-heptane.[12] The measured temperature (i.e., the air and auxiliary liquid temperatures) was recorded for each measurement, and the density of air and *n*-heptane was evaluated at the measurement temperature.[12]

4.3.2. Water Uptake

In this research, the water uptake of membranes was measured when samples were equilibrated with DI water, 0.1 and 0.5mol/L aqueous electrolyte solutions. Prior to measurements in DI water, a single membrane sheet was cut into small circular coupons with diameter ranging from 0.95 to 2.22cm and soaked in DI water for over 48 hours. The samples were then removed from DI water, and the wet mass, m_{wet}, was measured quickly after the excess DI water was wiped off the sample surface using a laboratory wipe. The sample was subsequently dried under vacuum at ambient temperature until a stabilized dry mass, m_{dry}, was obtained. The drying process typically required 36 to 48 hours. The dry mass was measured immediately after the drying process to prevent sorption of moisture from the atmosphere. The membrane water uptake, w_u, was calculated as:

$$w_u = \frac{m_{wet} - m_{dry}}{m_{dry}} \tag{4.2}$$

The water uptake measurements in 0.1 mol/L or 0.5 mol/L aqueous electrolytes solution follows similar procedures as the measurement in DI water. Prior to measurements in aqueous electrolyte solutions, the membrane samples were soaked in 0.1 or 0.5 mol/L solution for another 48 to 72 hours, and fresh solution was supplied to replace the old solution every 12 hours. This step was conducted to ensure full ion exchange when the counter-ions in the solution was different from the counter-ion of the membrane sample.

The samples were considered to be equilibrated with electrolyte solution following that process. The sample wet mass, m_{wet}, and dry mass, m_{dry}, were measured and the water uptake in electrolytes solution was calculated following Equation 4.2. Water uptake for each membrane was reported as the average of at least four measurements, and the uncertainty was taken as one standard deviation from the mean. Samples were discarded following the water uptake measurement.

The membrane water content, i.e., volume fraction of water in the membrane, ϕ_w, was calculated using the measured membrane dry density and water uptake data using a volume additivity assumption:[13]

$$\phi_w = \frac{w_u/\rho_w}{w_u/\rho_w + \frac{1-w_u}{\rho_w}} \tag{4.3}$$

where ρ_w is the density of water, which was taken as 1 g/cm^3.[12] The volume fraction of water in the polymer is essentially equivalent to the water sorption coefficient, k_w, which represents the ratio of concentration of water in the polymer to that in the external solution.[14–16]

4.3.3. Ion Exchange Capacity and Fixed Charge Group Concentration

The ion exchange capacity (*IEC*) of the XLAMPS was calculated theoretically. The *IEC* of PVBAN-TMA[X] and PVBAN-DMI[X] membranes was determined using an ion exchange method. The membranes were prepared in chloride form and rinsed with DI water. Prior to *IEC* measurements, the crosslinked membranes were cut into circular coupons with diameters of 0.95 or 1.27cm. The coupons were then soaked in 1mol/L sodium nitrate solution of volume, V_E (50mL for sample with diameter of 0.95cm and 80mL for sample with diameter of 1.27cm). The nitrate will then replace the chloride counter-ion of the sample. The samples were soaked for at least 48 hours to ensure full ion exchange. The chloride concentration in the external solution, c_E, was determined using an Ion Chromatography (ICS-2100, Thermo Scientific). The samples were then soaked in DI water to desorb the sodium nitrate, and dried under vacuum afterwards. The sample dry mass was then measured as mdry, and the IEC was calculated as:

$$IEC = \frac{V_E c_E}{m_{dry}} \tag{4.4}$$

The membrane fixed charge group concentration, c_m^A, is defined as the concentration of fixed charge group within the water sorbed by the polymeric membrane, and has the unit of mol of fixed charge groups per liter of sorbed water. It is calculated using the membrane ion exchange capacity, *IEC*, membrane water uptake, w_u, and the density of water, ρ_w:

$$c_m^A = \frac{IEC}{w_u} \rho_w \tag{4.5}$$

4.3.4. Salt Sorption and Diffusivity

The salt sorption coefficient and diffusivity were measured by kinetic desorption.[4,17] Kinetic desorption measurements started from placing salt-saturated membrane samples into a container filled with DI water. The salt will then desorb from the membrane phase into the DI water, and the concentration of external solution will change accordingly. By tracking the concentration change at different time points, a concentration-versus-time curve can be obtained and salt sorption coefficients and diffusivities can be obtained by modeling the desorption curve. It should be noted that when conducting kinetic desorption measurements, the carbon dioxide (CO_2) from atmosphere can greatly impact the performance of IEMs, especially AEMs. When CO_2 dissolves in water, it forms carbonic acid, which dissociates into proton, bicarbonate and carbonate ions.[18,19] The carbonate and bicarbonate ions can displace some counter-ions in AEMs, resulting in inaccurate measurements in solution concentration. A modest amount of ion exchange might occur between the proton and the counter-ions of CEMs, but the effect is negligible compared with the situation of AEMs.[18] To minimize the effects of CO_2 on the salt sorption coefficients and discursivity on AEMs. The entire kinetic desorption process was done under the protection of nitrogen. The desorption steps for CEMs and AEMs will be discussed in separate paragraphs.

To measure the salt sorption coefficients and diffusivity of CEMs, the salt-saturated circular coupon samples were removed from salt solution, and excess solution on the sample surface was carefully removed using a lab tissue. Then, the sample was carefully transferred into a volume (ranging from 25mL to 150mL) of well-stirred atmospherically equilibrated DI water. The desorption solution volume was chosen such that the final concentration (following salt desorption from the polymer) would be in the range of 1 – 3mg(salt)/L.[17] The conductivity of the desorption solution was recorded every 10 – 60s using a conductivity meter (inoLab* Cond 7310, WTW Corp Inc., CA, USA). The measurement time interval was chosen based on the desorption rate. The measurement was stopped when desorption solution concentration stabilized, i.e., the concentration of desorption solution remained constant for at least a time period equivalent to the sample's characteristic time for diffusion (typically between 200 and 500s). This time was determined iteratively as $\delta^2/(4D_s^m)$, where δ is the hydrated membrane thickness, and D_s^m is the salt diffusion coefficient in the membrane. The kinetic desorption measurement was conducted five times for each sample, electrolyte, and concentration.

The desorption solution conductivity was converted to salt concentration using a calibration curve and then to the mass of salt desorbed from the polymer using the volume of the desorption solution. A flat-sheet diffusion model was used to determine the salt diffusion coefficient, D_s^m, in the membrane using the desorption data:

$$D_s^m \cong \left\{\frac{\pi\delta^2}{16}\left[\frac{\partial(M_t/M_\infty)}{\partial t^{1/2}}\right]^2\right\} t^{\frac{1}{2}} \tag{4.6}$$

where M_t is the mass of salt desorbed from the polymer at time *t* and M_∞ is the total mass of salt desorbed from the polymer during the entire process.[20] Equation 4.6 is an approximation that is only valid when $M_t/M_\infty < 0.6$. Thus, the early-time desorption data were plotted as M_t/M_∞ versus $t^{\frac{1}{2}}$, and the term in square brackets is the slope of the plot.[20]

The salt sorption coefficient, k_s^m is defined as the salt concentration in the water sorbed by the membrane, c_s^m, relative to that in the external solution, c_s^s:

$$k_s^m = \frac{c_s^m}{c_s^s} = \frac{c_\infty^s V_d}{c_s^s V_p \phi_w} \tag{4.7}$$

The measurements on AEMs were done under the protection of nitrogen. A container filled with DI water was sealed and purged with nitrogen until the conductivity dropped down to and stabilized at 0.10 µS/cm. Salt-equilibrated membrane coupons were removed from the salt solution and wiped. Then the container was open and the sample was immediately transferred into the container and the container was quickly sealed again. The desorption then started and the conductivity of the solution was recorded every 60 seconds using the same conductivity meter. The entire apparatus was purged with nitrogen, and the water-saturated nitrogen removed water from the container and caused conductivity reduction as well. To account for the conductivity reduction caused by purging nitrogen, background curves were obtained using 5ppm solutions of all electrolytes. For example, the sodium chloride background curve was obtained by purging a 5ppm sodium chloride solution with nitrogen without putting the membrane samples in. The nitrogen pressure (i.e., flow rate) was controlled to be 2.0 psig using a pressure gauge for all measurement. The measurement was stopped when desorption solution concentration stabilized, i.e., the conductivity decrease follows the background curve for at least a time period equivalent to the sample's characteristics time for diffusion. The actual desorption conductivity curve was obtained by subtracting the background conductivity change from the measured desorption conductivity. The diffusion and sorption coefficients were obtained using Equation 4.6 and 4.7.

4.3.5. Membrane Permselectivity

Membrane permselectivity was measured as apparent permselectivity defined by Strathmann,[21,22] using a static method that is not affected by boundary layers and the solution-membrane interfaces. The method also neglects osmotic water transport through the membrane. The decision to study apparent permselectivity was motivated by the common use of the static measurement approach throughout the literature.[23–25]

4.3.5.1. Measurement Apparatus and Principles

Apparent permselectivity is determined from a membrane potential, E_m, that is measured while the membrane separates solutions of high, $a_{\pm}^{sL}$, and low, $a_{\pm}^{s0}$, mean electrolyte activity:

$$\alpha = \frac{\left[E_m \Big/ \left(\frac{RT}{F} ln \frac{a_{\pm}^{sL}}{a_{\pm}^{s0}}\right)\right] + 1 - 2t_M^s}{2t_X^s} \tag{4.8}$$

Where R is the gas constant, T is the absolute temperature, and F is the Faraday's constant.[21,26] The solution concentration in each chamber of the measurement cell (Figure 4.4) is held constant by supplying fresh solution to the chamber, so the mean electrolyte activity of the solution in each chamber is fixed. The electric potential difference across the membrane, E_x, is measured using double junction reference electrodes. To account for asymmetry in the reference electrodes, an offset potential, E_{offset}, is measured between the two electrodes, so the membrane potential, E_m, is obtained as:

$$E_m = E_x - E_{offset} \tag{4.9}$$

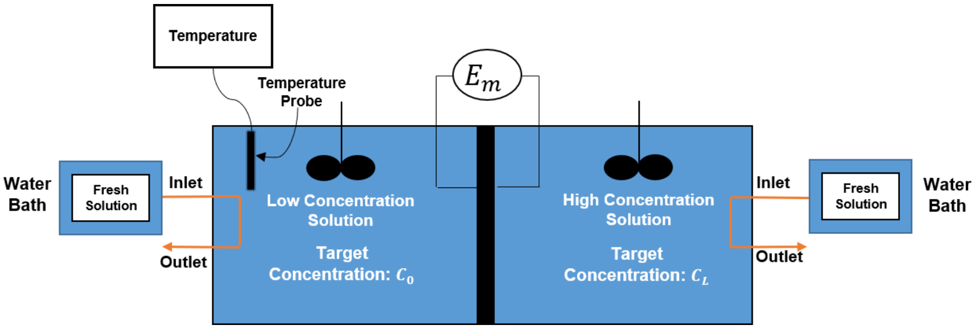

Figure 4.4. Apparent permselectivity of an ion exchange membrane can be measured by placing the membrane between solutions of different salt concentration.[21] When the concentrations of these solutions are held constant (by stirring and single pass fresh solution feeds), the electric potential difference across the membrane can be measured and ultimately related to the apparent permselectivity of the membrane. The temperature of the solutions in the cell is monitored using a temperature probe places in the low concentration solution

In the measurements, the salt equilibrated membrane sample was placed between the two cell chambers, and the chambers subsequently were filled with aqueous salt solutions of different concentrations. Each chamber contained 100mL of solution, and cross-sectional area of exposed membrane was 5.09cm^2. Overhead mechanical stirring at 460rpm ensured that the solution in each chamber was well mixed without creating cavitation-induced bubbles in the chambers. Additionally, the concentrations of the solutions in each chamber were maintained by a continuous, single-pass flow of fresh solution. Double-junction Ag/AgCl reference electrodes (RREF 0024, Pine Instrument Co., Grove City, PA), filled with 10% KNO_3 solution, were placed in the solutions on either side of the membrane. Double junction reference electrodes provided a more stable potential reading as compared to single junction reference electrodes. The electric potential difference across the reference electrodes, E_x, was recorded using a multimeter (model 2999, Keithley, Cleveland, OH) as a function of time using a LabView program. Typically, the electric potential stabilized after 20 – 30 minutes. The potential, E_x, was recorded every 10s, and the stabilized condition was defined as the point when the rate of change in E_x was less than 0.3 mV over 20 minutes. The value of E_x was taken as a time average of the electric potential difference measurements made over 30 minutes following stabilization of the potential.

The offset potential of the reference electrodes, E_{offset}, was measured after completion of the E_x measurement. This offset potential captured the asymmetry of the specific reference electrodes that were used in the measurement. Both reference electrodes were placed in the high concentration solution, and the electric potential difference between the reference electrodes was measured using a multimeter. The value of E_{offset} was determined by averaging the offset potential over a period of 30 minutes to 1 hour once the offset potential had stabilized, and the magnitude of the offset potential was typically found to be 2.0 ± 0.3 mV. Equation 4.9 was used to determine the membrane potential.

Solution concentration was chosen on the basis of a typical concentration range reported in the literature (c_0 = 0.1mol/L and c_L = 0.5mol/L). [24,25] Using these concentrations also ensured that the electric potential, E_x, would be significantly large to measure accurately. The average electrolyte activity values were determined as:

$$a_{\pm}^{s0} = \gamma_{\pm}^{s0} c_0 \tag{4.10}$$

$$a_{\pm}^{sL} = \gamma_{\pm}^{sL} c_L \tag{4.11}$$

where $\gamma_{\pm}^{s0}$ and $\gamma_{\pm}^{sL}$ are the average electrolyte activity coefficients on the low and high concentration sides of the membrane, respectively. The activity coefficients and their temperature dependence were determined from reported values.[27]

Apparent permselectivity measurements were made on a given membrane sample. The membrane potential for the sample was measured three times, and the cell was disassembled and reassembled between each measurement. Each experimentally measured apparent permselectivity data point represents the average of three replicates, and the uncertainty in this average is reported as one standard deviation from the mean value. This approach facilitated study of the influence of temperature and flow rate on apparent permselectivity without complications that could arise from sample-to-sample variability, which is reported elsewhere[24] for these membranes.

4.3.5.2.Influence of Experimental Factors

The terms in Equation 4.8 are fixed on the basis of the experimental conditions and suggest potential sources of uncertainty in the apparent permselectivity potential measurement. Three sources of uncertainty were identified: temperature variations, concentration deviations and electric potential fluctuations. The influence of the three factors can be quantified either through experiments or error propagation analysis.

To probe the influence of temperature on apparent permselectivity, fresh solution baths (Figure 4.4) were cooled or heated using a water bath. To prevent evaporation, the solution baths were connected to the measurement apparatus such that the solution was not exposed to the atmosphere until it excited the tubing after passing through the measurement cell. A probe was placed in the low concentration solution chamber to measure the temperature, and the water bath temperature was set such that the desired chamber temperature was achieved. Chamber temperatures were set in the range of 14 – 31°C. These temperatures were selected to be both above and below typical room temperature to determine whether modest temperature fluctuations appreciably influence the apparent membrane permselectivity measurement. The temperature dependent parameters used in Equation 4.8 to calculate apparent permselectivity are provided in Appendix B.

Apparent permselectivity was also measured using a series of single pass solution flow rates, ranging from 1 to 15mL/min, to determine the minimum flow rate that would maintain the solution concentration in both chambers of the experimental apparatus (i.e., maintain the pseudo-steady-state condition during the measurement). Flow rates were controlled using a digital peris pump (Masterflex L/S Digital Drive, ColeParmer, U.S.). Fresh solution was fed to the chambers, and the displaced solution was not recycled to the chambers.

Uncertainty resulting from the electric potential measurements and the solution preparation process was taken into consideration using standard error propagation analysis.[28] The magnitude of electric potential measurement fluctuations, ΔE, an independent variable for the purpose of error propagation analysis, was taken to be a series of values of this error propagation analysis, was taken to be a series of values ranging from 0 to 0.4mV, which was found to be an experimentally relevant range. The uncertainty of the membrane apparent permselectivity, $\Delta\alpha$, was calculated using ΔE and standard error propagation techniques. The deviations from the target solution concentrations for low concentration, Δc_0, and high concentration, Δc_0, solutions, independent variables for the purpose of this error propagation analysis, were taken to be a series of values ranging from 0 to 0.015mol/L and 0 to 0.075mol/L, respectively, and values of $\Delta\alpha$ were calculated using Δc_0 or Δc_L and standard error propagation techniques. The effect of error in the salt mass measurement, Δm, associated with the preparation of 1L of low and high concentration solution on the membrane permselectivity was also investigated. Values of Δm ranging from 0 to 100mg (NaCl) were considered, and standard error propagation techniques were used to determine the influence of Δm on the uncertainty of the apparent permselectivity. Additional details and sample calculations for the error propagation analysis are discussed in Chapter 5 and provided in the Appendix B.

4.3.6. Ionic Conductivity

The membrane ionic conductivity was measured using electrochemical impedance spectroscopy (EIS, SP 150, Biologic).[29,30] The measurement was performed while the membrane separated two chambers with a cross-sectional membrane area of 4.52cm^2 that was filled with 50mL of 0.5mol/L aqueous solutions of lithium chloride, sodium chloride, ammonium chloride, sodium nitrate and sodium bromide. Ag/AgCl reference electrodes (MR 5275, Bioanalytical Systems Inc., Lafayette, IN) were inserted on both sides of the membrane, and the impedance response was measured from 1Hz to 50kHz with a current amplitude of 1mA and 100 points were recorded in total. The Ohmic resistance of the cell (i.e., the solution and the membrane), R_{m+s}, was taken as the value of the real impedance when the imaginary impedance was zero (i.e., when the data on a Nyquist plot crossed the real axis. The cell was then disassembled, and the thickness of the membrane, δ, was measured. The cell was then reassembled without the membrane and the measurement was repeated to obtain the resistance of aqueous solution, R_s. The conductivity of the membrane, σ_m^s, was calculated as:

$$\sigma_m^s = \frac{\delta}{A(R_{m+s} - R_s)} \tag{4.12}$$

where A was the cross-sectional area of the cell and δ was the membrane thickness.

4.4. References

(1) Miyoshi, H.; Chubachi, M.; Yamagami, M.; Kataoka, T. Characteristic Coefficients for Equilibrium between Solution and Neosepta or Selemion Cation Exchange Membranes. *J. Chem. Eng. Data* **1992**, *37* (1), 120–124.

(2) Manufacture Specifications.

(3) Ju, H.; McCloskey, B. D.; Sagle, A. C.; Kusuma, V. A.; Freeman, B. D. Preparation and Characterization of Crosslinked Poly (Ethylene Glycol) Diacrylate Hydrogels as Fouling-Resistant Membrane Coating Materials. *J. Membr. Sci.* **2009**, *330* (1–2), 180–188.

(4) Ju, H.; Sagle, A. C.; Freeman, B. D.; Mardel, J. I.; Hill, A. J. Characterization of Sodium Chloride and Water Transport in Crosslinked Poly (Ethylene Oxide) Hydrogels. *J. Membr. Sci.* **2010**, *358* (1–2), 131–141.

(5) Qiu, B.; Lin, B.; Qiu, L.; Yan, F. Alkaline Imidazolium-and Quaternary Ammonium-Functionalized Anion Exchange Membranes for Alkaline Fuel Cell Applications. *J. Mater. Chem.* **2012**, *22* (3), 1040–1045.

(6) Ran, J.; Wu, L.; Varcoe, J. R.; Ong, A. L.; Poynton, S. D.; Xu, T. Development of Imidazolium-Type Alkaline Anion Exchange Membranes for Fuel Cell Application. *J. Membr. Sci.* **2012**, *415*, 242–249.

(7) Ran, J.; Wu, L.; He, Y.; Yang, Z.; Wang, Y.; Jiang, C.; Ge, L.; Bakangura, E.; Xu, T. Ion Exchange Membranes: New Developments and Applications. *J. Membr. Sci.* **2017**, *522*, 267–291.

(8) Varcoe, J. R.; Atanassov, P.; Dekel, D. R.; Herring, A. M.; Hickner, M. A.; Kohl, P. A.; Kucernak, A. R.; Mustain, W. E.; Nijmeijer, K.; Scott, K. Anion-Exchange Membranes in Electrochemical Energy Systems. *Energy Environ. Sci.* **2014**, *7* (10), 3135–3191.

(9) Yang, C.; Wang, S.; Jiang, L.; Hu, J.; Ma, W.; Sun, G. 1, 2-Dimethylimidazolium-Functionalized Cross-Linked Alkaline Anion Exchange Membranes for Alkaline Direct Methanol Fuel Cells. *Int. J. Hydrog. Energy* **2015**, *40* (5), 2363–2370.

(10) Marcus, Y. *Ion Properties*; CRC Press, 1997.

(11) Cruise, G. M.; Scharp, D. S.; Hubbell, J. A. Characterization of Permeability and Network Structure of Interfacially Photopolymerized Poly (Ethylene Glycol) Diacrylate Hydrogels. *Biomaterials* **1998**, *19* (14), 1287–1294.

(12) Lide, D. R. *Handbook of Chemistry and Physics*; CRC Press, 2003.

(13) Xie, W.; Cook, J.; Park, H. B.; Freeman, B. D.; Lee, C. H.; McGrath, J. E. Fundamental Salt and Water Transport Properties in Directly Copolymerized Disulfonated Poly (Arylene Ether Sulfone) Random Copolymers. *Polymer* **2011**, *52* (9), 2032–2043.

(14) Geise, G. M.; Paul, D. R.; Freeman, B. D. Fundamental Water and Salt Transport Properties of Polymeric Materials. *Prog. Polym. Sci.* **2014**, *39* (1), 1–42.

(15) Geise, G.; Freeman, B. D.; Paul, D. R. Characterization of a Sulfonated Pentablock Copolymer for Desalination Applications. *Polymer* **2010**, *51* (24), 5815–5822.

(16) Luo, H.; Aboki, J.; Ji, Y.; Guo, R.; Geise, G. M. Water and Salt Transport Properties of Triptycene-Containing Sulfonated Polysulfone Materials for Desalination Membrane Applications. *ACS Appl. Mater. Interfaces* **2018**, *10* (4), 4102–4112.

(17) Yasuda, H.; Lamaze, C.; Ikenberry, L. Permeability of Solutes through Hydrated Polymer Membranes. Part I. Diffusion of Sodium Chloride. *Makromol. Chem. Macromol. Chem. Phys.* **1968**, *118* (1), 19–35.

(18) Kamcev, J.; Jang, E.-S.; Yan, N.; Paul, D. R.; Freeman, B. D. Effect of Ambient Carbon Dioxide on Salt Permeability and Sorption Measurements in Ion-Exchange Membranes. *J. Membr. Sci.* **2015**, *479*, 55–66.

(19) Stumm, W.; Morgan, J. J. *Aquatic Chemistry: Chemical Equilibria and Rates in Natural Waters*; John Wiley & Sons, 2012; Vol. 126.

(20) Crank, J. *The Mathematics of Diffusion*; Oxford university press, 1979.

(21) Strathmann, H.; Giorno, L.; Drioli, E. *Introduction to Membrane Science and Technology*; Wiley-VCH Weinheim, 2011; Vol. 544.

(22) Strathmann, H.; Grabowski, A.; Eigenberger, G. Ion-Exchange Membranes in the Chemical Process Industry. *Ind. Eng. Chem. Res.* **2013**, *52* (31), 10364–10379.

(23) Bauer, B.; Strathmann, H.; Effenberger, F. Anion-Exchange Membranes with Improved Alkaline Stability. *Desalination* **1990**, *79* (2), 125–144.

(24) Geise, G. M.; Cassady, H. J.; Paul, D. R.; Logan, B. E.; Hickner, M. A. Specific Ion Effects on Membrane Potential and the Permselectivity of Ion Exchange Membranes. *Phys Chem Chem Phys* **2014**, *16* (39), 21673–21681.

(25) Cassady, H. J.; Cimino, E. C.; Kumar, M.; Hickner, M. A. Specific Ion Effects on the Permselectivity of Sulfonated Poly(Ether Sulfone) Cation Exchange Membranes. *J. Membr. Sci.* **2016**, *508*, 146–152.

(26) Silvester, L. F.; Pitzer, K. S. Thermodynamics of Electrolytes. X. Enthalpy and the Effect of Temperature on the Activity Coefficients. *J. Solut. Chem.* **1978**, *7* (5), 327–337.

(27) Pitzer, K. S.; Peiper, J. C.; Busey, R. H. Thermodynamic Properties of Aqueous Sodium Chloride Solutions. *J Phys Chem Ref Data U. S.* **1984**, *13:1*.

(28) Ku, H. H. Notes on the Use of Propagation of Error Formulas. *J. Res. Natl. Bur. Stand.* **1966**, *70* (4).

(29) Kamcev, J.; Sujanani, R.; Jang, E.-S.; Yan, N.; Moe, N.; Paul, D. R.; Freeman, B. D. Salt Concentration Dependence of Ionic Conductivity in Ion Exchange Membranes. *J. Membr. Sci.* **2018**, *547*, 123–133.

(30) Park, J.-S.; Choi, J.-H.; Woo, J.-J.; Moon, S.-H. An Electrical Impedance Spectroscopic (EIS) Study on Transport Characteristics of Ion-Exchange Membrane Systems. *J. Colloid Interface Sci.* **2006**, *300* (2), 655–662.

Chapter 5: Effects of Experimental Factors on Permselectivity Measurement Accuracy†

This study investigated the magnitude of three origins of experimental uncertainty in membrane apparent permselectivity measurements using a static method, i.e., temperature variations, concentration deviations and membrane potential measurement fluctuations. The main objective of this study was to understand whether the uncertainty from experimental factors substantially disturbed permselectivity values measured by such method, therefore set the foundation for evaluating permselectivity difference originated from other factors such as the specific nature of ion or polymer structure.

5.1. Introduction

IEMs are widely used in separation and energy generation technologies, such as ED and RED.[2–12] In general, these processes rely on ion exchange membranes to regulate electric field-driven ion migration.[13] CEMs, which have negatively charged groups bound to the matrix, enable selective transport of cations in an electric field, and AEMs, which have positively charged groups bound to the matrix, enable selective transport of anions in an electric field.[6,13] The permselectivity of these CEMs and AEMs is a measure of how exclusively CEMs transport cations or how exclusively AEMs transport anions.[7] ED and RED processes use stacks of alternating CEMs and AEMs to establish a selective ionic current that either deionizes water when electricity is applied to the system or generates electricity when solutions of different electrolyte activity are used to generate an electric potential difference, which drives ionic current, across the stack (RED).[7,13,14]

The permselectivity of an ion exchange membrane affects the energy efficiency of electric field-driven membrane applications. In RED, for example, the open circuit voltage of the membrane stack varies linearly with permselectivity, and maximum power density scales with the permselectivity squared. Therefore, membranes with low permselectivity result in low RED power output.[10,11,14,15] In ED, low

---

† This section has been adapted with permission from: Ji, Y.; Geise, G. M. The Role of Experimental Factors in Membrane Permselectivity Measurements. *Ind. Eng. Chem. Res.* **2017**, *56* (26), 7559–7566.

permselectivity results in less efficient desalination because more power must be supplied to this system, as compared to a high permselectivity membrane, to accomplish an equivalent separation.[4,16]

As discussed in previous chapters, membrane permselectivity α is defined using the transport numbers of counterions and coions in solution phase and membrane phase, respectively. Transport numbers represent the fraction of current carries by each ion in each phase.[7] In a perfectly permselective membrane, only counterions carry current through the membrane. For a nonpermselective membrane, ion transport in the membrane is analogous to that in solution, and the permselectivity is equal to zero.

Membrane apparent permselectivity was typically measured using a static method as described in previous chapter.[17–19] Apparent permselectivity values that exceed unity using such method have been reported.[19–21] In these cases, the values are typically close to unity (e.g., typical values are reported up to an apparent permselectivity of 1.04). These nonphysical results, in some cases, have been attributed to fluctuations in room temperature.[19–21] Presumably, these room temperature variations are relatively small (i.e., likely no more than a few degrees Celsius). Such reports, though, raise questions about the selectivity of the apparent permselectivity to temperature. Experimental measurements of apparent permselectivity as a function of temperature would help to address and inform this issue.

According to the static method, apparent permselectivity often is determined from a membrane potential, E_m, that is measured while the membrane separates solutions of high, high, $a_{\pm}^{SL}$, and low, $a_{\pm}^{S0}$, mean electrolyte activity:

$$\alpha = \frac{\left[E_m \Big/ \left(\frac{RT}{F} ln \frac{a_{\pm}^{SL}}{a_{\pm}^{S0}}\right)\right] + 1 - 2t_M^s}{2t_X^s} \tag{5.1}$$

The solution concentration in each chamber of the measurement cell (Figure 4.4) is held constant by supplying fresh solution to the chamber, so the mean electrolyte activity of the solution in each chamber is fixed. The electric potential difference across the membrane, E_x, is measured using double junction reference electrodes. To account for asymmetry in the reference electrodes, an offset potential, E_{offset}, is measured between the two electrodes, so the membrane potential, E_m, is obtained as:

$$E_m = E_x - E_{offset} \tag{5.2}$$

The membrane potential, E_m, can then be used to calculate the apparent permselectivity of the membrane using Equation 5.1.

The other terms in Equation 5.1 are fixed on the basis of the experimental conditions and suggest potential sources of uncertainty in the apparent membrane potential measurement. Temperature enters the analysis both directly and indirectly (the transport numbers and activity values are expected to depend on temperature[22–26]). Additionally, error is introduced into the apparent permselectivity measurement if the actual salt solution concentrations in the chambers are different from those concentrations used to determine the activity values for use in Equation 5.1. Finally, uncertainty in the measured value of E_x (and, thus, E_m) could contribute uncertainty to the overall measurement.

Here, we reported an investigation of three factors that may influence the accuracy of apparent permselectivity measurements. First, the Nernst potential calculations used to convert membrane potential measurements to permselectivity require a fixed temperature. Researchers often report room temperature conditions, which may fluctuate from day to day, when measuring apparent permselectivity. In some cases, nonphysical permselectivity data are attributed to such temperature fluctuations, but the magnitude of the influence of temperature on apparent permselectivity is not well established. Second, the mean electrolyte activity (ultimately, concentration) of the two solutions used in the measurement must be kept constant. We investigated the sensitivity of the apparent permselectivity to relevant deviations from these fixed concentrations and the effects of failing to provide a sufficiently high flow rate of fresh solution to the cell. Third, the influence of electric potential measurement fluctuations on apparent permselectivity was considered. Figure 5.1 illustrates these fluctuations (characterized by ΔE) using representative data that show the electric potential difference across a membrane stabilizing as the system reaches a pseudo steady state. The standard deviation, ΔE, from the average membrane potential, E_x, could be a source of membrane permselectivity uncertainty. We report and discuss the influence of temperature fluctuations, deviations in salt concentration, and membrane potential measurement fluctuations on membrane apparent permselectivity measurements.

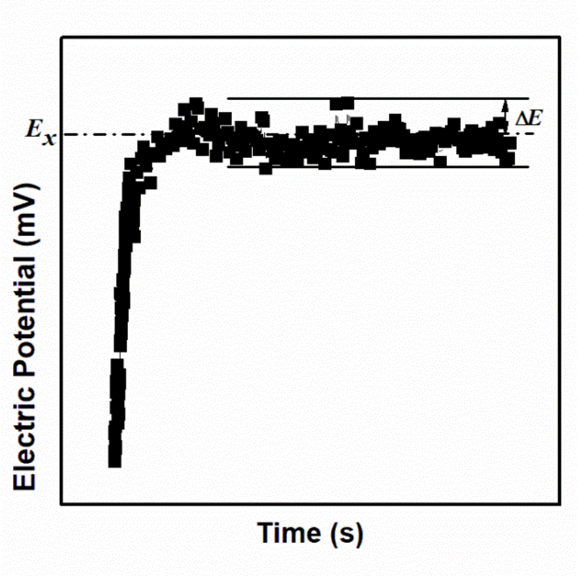

Figure 5.1. Representative electric potential difference, E_x, data measured, as a function of time and using reference electrodes, across a membrane that separates solutions of different salt concentration. The measured membrane potential approaches the pseudo-steady-state values, E_x, and fluctuations in the measured values of E_x can be quantified as ΔE.

5.2. Results and Discussion

5.2.1. Temperature Dependence of Apparent Permselectivity

Temperature variations around room temperature could affect apparent permselectivity, and little is known about the temperature sensitivity of this property. The membrane apparent permselectivity decreases slightly as temperature increases (Figure 5.2). These effects are relatively small as increasing temperature from 14 to 31^{o}C results in a decrease in apparent permselectivity that is less than 2% for both commercial membranes. Therefore, under typical experimental conditions (i.e., room temperature with fluctuations that do not exceed ± 5^{o}C), some temperature-induced apparent permselectivity fluctuations may occur, but these fluctuations should be relatively small (no larger than 2%). The standard deviation from the mean of three replicate values (i.e., the error bars in Figure 5.2) is generally in the range of 1% to 2% for these measurements, so the dependence of apparent permselectivity on temperature, over this temperature range, is on the order of the uncertainty that results from simply dismantling the cell and reassembling the cell to conduct replicate measurements.

The observed changes in apparent permselectivity as a function of temperature may result from uneven increase in the diffusion coefficients of counterions and coions in the membrane phase. As temperature increases, the counterion and coion diffusion coefficients in solution generally increase to different extents,[24,27] so the transport numbers in the solution phase depend on temperature (Table B.1).[28] For sodium chloride, a temperature rise from 14°C to 31°C will cause t_M^s to increase from 0.392 to 0.399 and t_X^s to decrease from 0.608 to 0.601 (Table B.1),[28] and the apparent permselectivity (calculated using Equation 5.1) would decrease as a result of the decrease in t_X^s, provided that the transport number in the membrane phase did not change. The membrane phase transport number may be affected by temperature to a different extent than solution transport numbers (due to differences in the activation energy for diffusion in the two phases), but this solution-phase example and the results reported in Figure 5.2 suggest that these temperature effects may be small, particularly over small temperature ranges.

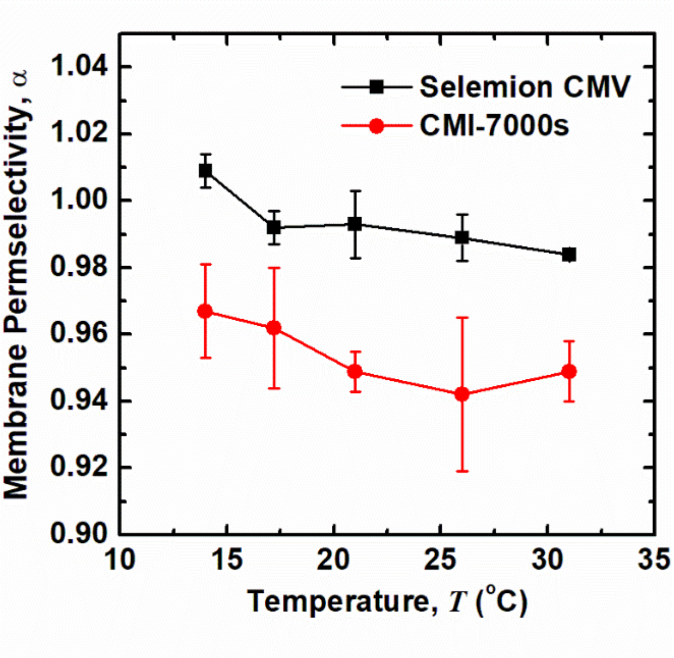

Figure 5.2. Apparent permselectivity decreases slightly as temperature increases over a modest range of temperatures surrounding room temperature. The apparent permselectivity was characterized using 0.1mol/L and 0.5mol/L aqueous sodium chloride solutions. Fresh solution single-pass flow rates were 5mL/min. Each data point corresponds to the average of three replicate measurements made on a membrane sample (the cell was disassembled and reassembled between measurements), and the error bars correspond to one standard deviation from this average.

5.2.2. Deviations in Electrolyte Concentrations

While measuring apparent permselectivity, the concentrations of the solutions on both sides of the membrane must be held constant. The difference in the thermodynamic activity must be held constant. The difference in the thermodynamic activity of the electrolyte solutions on either side of the membrane generates the membrane potential as described by the Nernst equation,[29] so deviations in concentration (ultimately thermodynamic activity) will influence permselectivity. The concentration difference across the membrane can drive salt permeation from the high salt concentration chamber to the low salt concentration chamber, and this process acts to reduce the concentration difference between the solutions on the low and high concentration sides of the membrane.[6,30] To combat this salt transport process, fresh solution is fed to the chambers throughout the measurement, so the flow rate for this single pass feed should be set at a sufficiently high value to maintain the solution concentrations on either side of the membrane. Furthermore, because permselectivity depends on the thermodynamic activity of the solutions, errors in the solution preparation process, particularly the low concentration solution, also can affect the apparent permselectivity measurement.

5.2.2.1. Solution Flow Rates

The rate of fresh solution addition to each chamber will influence the solution residence time in the chamber, and this residence time influences the formation of the pseudo-steady-state measurement condition. During the measurement, the solution concentration on both sides of the membrane should be effectively constant,[7] and achieving this pseudo-steady-state condition requires a sufficiently high flow rate of fresh solution to be provided to each chamber. To maintain the concentration on both sides of the membrane, the solution residence time, τ, must be much shorter than the diffusion time scale, $t_{diff,}$ for salt permeation through the membrane. Thus, $\tau/t_{diff} = (V_c/f)/(\delta^2/D_s) \ll 1$, where V_c is the volume of the chamber, f is the solution flow rate, δ is the membrane thickness, and D_s is the salt diffusion coefficient in the membrane.

Apparent permselectivity values were measured using a series of flow rates (1mL/min to 15mL/min). Above 5mL/min, the apparent permselectivity stabilize for both membranes (Figure 5.3), suggesting that those flow rates are sufficient to achieve the pseudo-steady-state condition. The sensitivity of apparent permselectivity to flow rate is more pronounced for the Selemion CMV membrane, and the CMI membrane achieves the pseudo-steady-state condition at the flow rate of 3mL/min, which is lower than that required for the CMV membrane. This situation could be explained by the time scale relationship described above. The CMV membranes are thinner than the CMI membranes (Table 4.1), so the diffusion time scale of the CMV membrane is much shorter than that of the CMI membrane. Thus, a greater flow rate must be used with the CMV membrane to reduce the solution residence time as compared to what is required for the CMI membrane. This analysis also explains why the CMI membrane is less sensitive to flow rate than CMV membrane. Thicker membranes, such as the CMI membrane, have larger diffusion time scale, so the pseudo-steady-state condition can be achieved at lower flow rates.

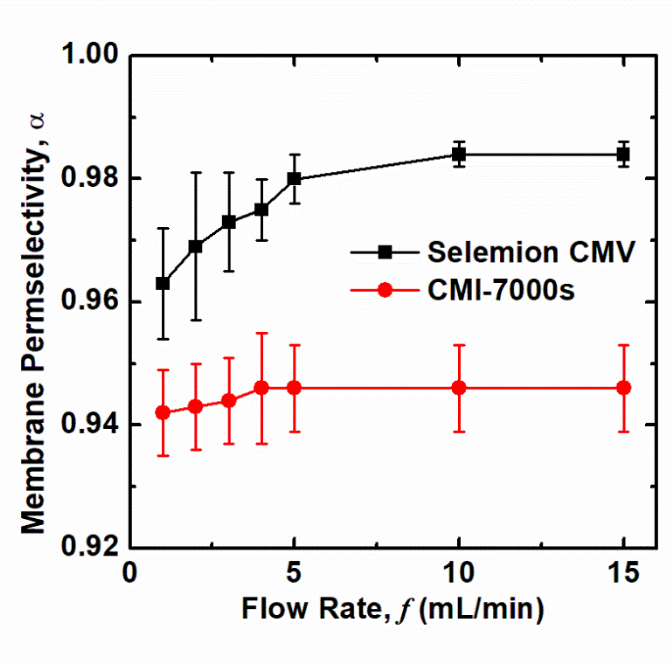

Figure 5.3. Apparent permselectivity as a function of solution flow rate at 21°C. The apparent permselectivity was characterized using 0.1mol/L and 0.5mol/L aqueous sodium chloride solutions. Each data point corresponds to the average of three replicate measurements made on a membrane sample (the cell was disassembled and reassembled between measurements), and the error bars correspond to one standard deviation from this average.

5.2.2.2. Solution Preparation

The relationship between concentration deviations and apparent permselectivity uncertainty for low concentration solution and high concentration solution is shown in Figure 5.4A and B. Figure 5.4A shows the situation for deviations around a c_L = 0.5mol/L sodium chloride solution, and Figure 5.4B shows the situation for deviations around a c_0 = 0.1mol/L sodium chloride solution. The actual solution concentration is normalized by the target concentration (i.e., 0.1mol/L or 0.5mol/L sodium chloride), and the actual apparent permselectivity is also normalized by the value measured using the target solution concentrations (additional details and sample calculations are provided in the Appendix B.2)

The influence of concentration changes on apparent permselectivity depends on whether the change increases or decreases the difference of the thermodynamic activity values of the solutions on either side of the membrane. When the value of c_L increases (i.e., $\Delta c_L > 0$) with a fixed value of c_0, the difference of thermodynamic activity values of the solutions on either side of the membrane increases. The situation results in an increase in the apparent permselectivity (Figure 5.4A) as compared to the base case (i.e., c_L = 0.5mol/L). For example, if the concentration of the high concentration solution was 5% greater than the base case (i.e., Δc_L = 0.025mol/L), the measured apparent permselectivity would increase by approximately 2.8% as compared to the base case. When the value of c_0 increases (i.e., $\Delta c_0 > 0$) with a fixed value of c_L, the difference of the thermodynamic activity values of the solutions on either side of the membrane decreases. This situation results in a decrease in the apparent permselectivity (Figure 5.4B) as compared to the base case (i.e., c_0 = 0.1mol/L). For example, if the concentration of the low concentration solution was 5% greater than the base case (i.e., Δc_0 = 0.005mol/L), the measured apparent permselectivity would decrease by approximately 2.8% as compared to the base case. Therefore, concentration changes that increase the activity difference across the membrane cause an increase in apparent permselectivity and vice versa.

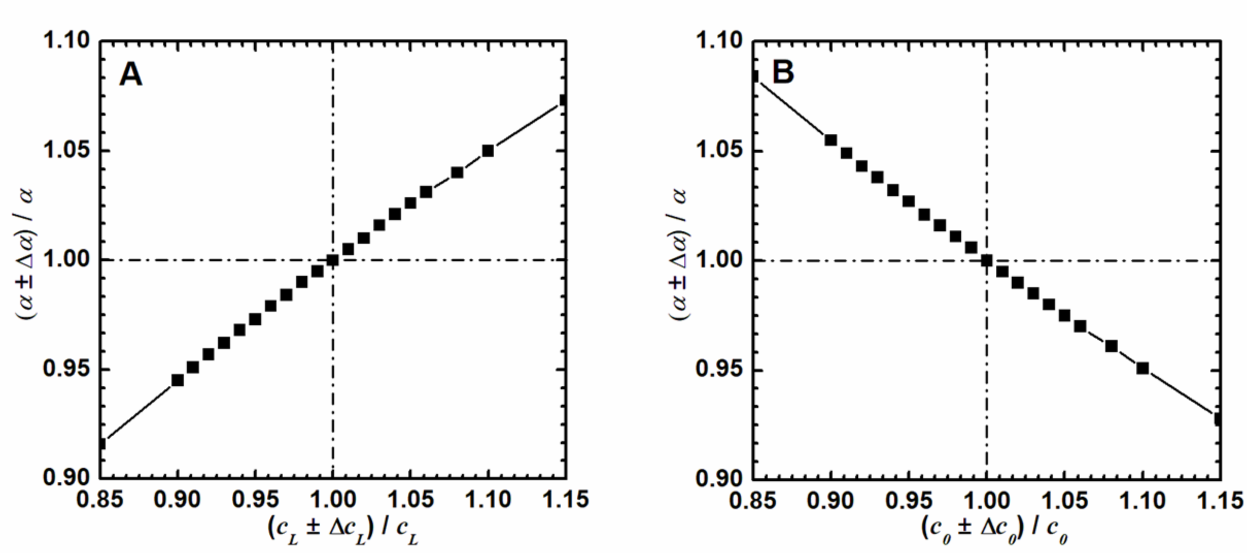

Figure 5.4. Error analysis reveals the relative deviation of the apparent permselectivity as a function of the relative deviation of solution centration for (A) the high concentration solution and (B) the low concentration solution.

Uncertainty in the measurement of salt mass, while preparing the salt solutions, is one possible source of error in the salt solution concentrations. While the relationship between the relative magnitude of concentration and apparent permselectivity is similar for high and low concentration solutions (as discussed in the preceding paragraph and Figure 5.5), the influence of absolute magnitude of uncertainty in the solution preparation process (e.g., uncertainty in the mass of salt measured during the solution preparation process) has a more significant effect on apparent permselectivity if the uncertainty is in the low concentration solution as compared to the high concentration solution (Figure 5.5). For example, preparation of 1L of 0.1mol/L and 0.5mol/L aqueous sodium chloride solution requires measuring 5.844g and 29.22g of sodium chloride, respectively. A 10mg salt mass deviation in the 0.1mol/L solution will introduce a 0.1% deviation in apparent permselectivity. The same mass deviation in the 0.5mol/L solution will only introduce a 0.015% deviation in the apparent permselectivity. Therefore, uncertainty in the salt mass measured during the solution preparation process will influence the low concentration solution to a greater extent than the high concentration solution.

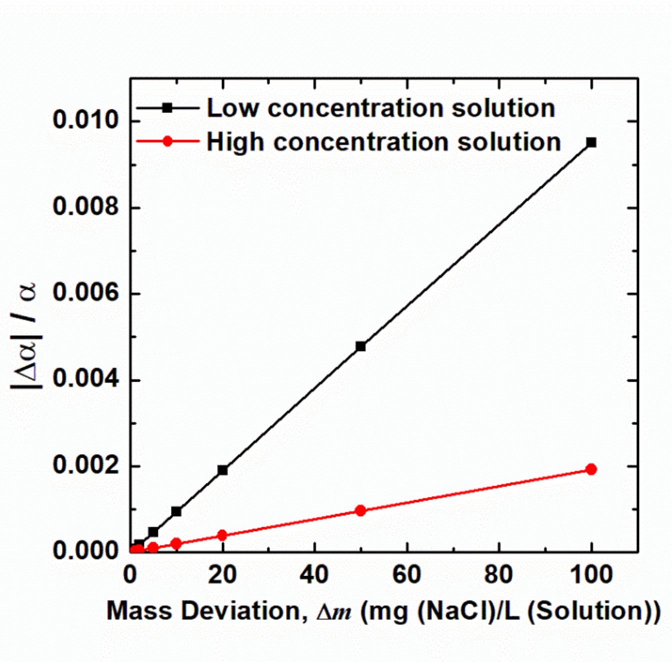

Figure 5.5. Uncertainty in the salt mass measured during the solution preparation process, Δ*m*, has a more significant influence on apparent permselectivity if the uncertainty is in the low concentration solution as compared to the high concentration solution.

In addition to the potential salt mass measurement errors, which could contribute to Δ*m*, sorption of atmospheric moisture into the salt crystals and/or losses during solute transfer (after mass measurement) could also contribute to Δm and thus affect the apparent permselectivity. These contributions, however, may be small in practice. Deviations from target sodium chloride solution concentrations of 10ppm in the high and low concentration solutions introduce approximately 0.015% and 0.1% error, respectively, in apparent permselectivity, and this uncertainty is within the replicate uncertainty that results from disassembling and reassembling the measurement cell between replicate apparent permselectivity measurements.

5.2.3. Uncertainty from Membrane Potential Measurement

During the apparent permselectivity measurement, the measured value of E_x increased and reached a stabilized value (cf., Figure 5.1). The final measured value of E_x was taken as the average electric potential, and the standard deviation ΔE was taken as the measurement uncertainty. The membrane potential, E_m, was determined using the measured electrode offset potential (Equation 5.2). The uncertainty in the measurement of E_{offset} was typically more than 2 orders of magnitude smaller than the value of ΔE, so the value of ΔE was taken as the uncertainty in E_m. A ΔE value that is 1% of E_m will introduce approximately a 1% deviation in the final membrane apparent permselectivity (Figure 5.6). For the conditions (0.1mol/L and 0.5mol/L sodium chloride solutions) used in this study, average membrane potential values, E_m, were around 37mV, and in this case, typical values of ΔE ranged from 0.1mV to 0.2mV. Therefore, fluctuations in the measurement of E_m contribute roughly 0.2% to 0.5% uncertainty in the final apparent permselectivity. In contrast, the concentration variability of low concentration solution and high concentration solution typically introduce about 0.015% to 0.1% uncertainty in the final apparent permselectivity, and the uncertainty from temperature fluctuations is expected to be no large than 2%.

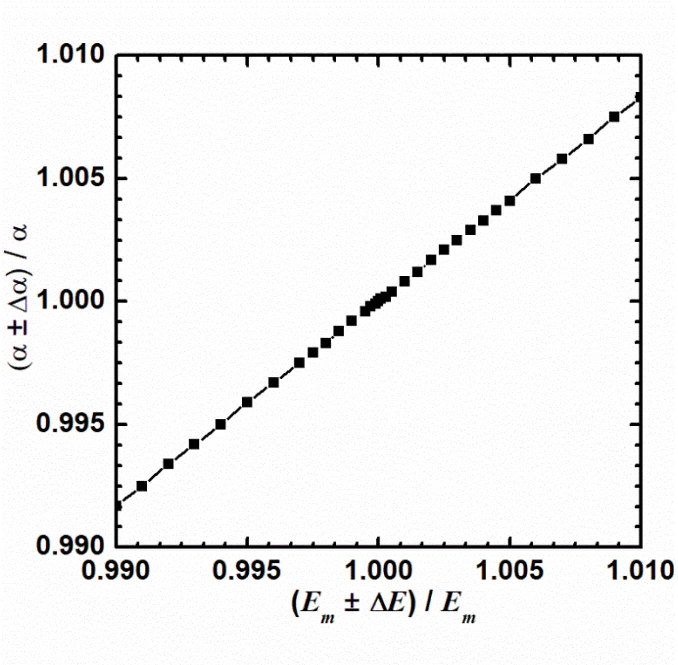

Figure 5.6. Fluctuations in the membrane potential measurement (ΔE) introduce uncertainty in the apparent permselectivity

5.3. Conclusions

This work discussed three origins of uncertainty in the apparent permselectivity measurement: temperature variations, concentration deviations, and membrane potential measurement fluctuations. Of the three issues considered, the influence of small temperature variations around room temperature on apparent permselectivity was greatest. Apparent permselectivity decreased by approximately 2% as the temperature decreased from 14°C to 31°C. This uncertainty, however, was of magnitude comparable to the replicate uncertainty, which was determined by disassembling and reassembling the measurement cell between multiple apparent permselectivity measurements made on a given sample. Second, membrane potential measurement fluctuations were found to contribute likely 0.2% to 0.5% uncertainty to the apparent permselectivity measurement. Finally, the influence of solution preparation errors was found to be the smallest contributor of apparent permselectivity uncertainty (approximately 0.015% to 0.1%). The low concentration solution is more sensitive to salt mass deviations than the high concentration solution, so the low concentration solution is more likely to be the source of solution concentration-related apparent permselectivity uncertainty as compared to the high concentration solution.

5.4. References

(1) Miyoshi, H.; Chubachi, M.; Yamagami, M.; Kataoka, T. Characteristic Coefficients for Equilibrium between Solution and Neosepta or Selemion Cation Exchange Membranes. *J. Chem. Eng. Data* **1992**, *37* (1), 120–124.

(2) McGinnis, R. L.; McCutcheon, J. R.; Elimelech, M. A Novel Ammonia–Carbon Dioxide Osmotic Heat Engine for Power Generation. *J. Membr. Sci.* **2007**, *305* (1), 13–19.

(3) Kamcev, J.; Freeman, B. D. Charged Polymer Membranes for Environmental/Energy Applications. *Annu. Rev. Chem. Biomol. Eng.* **2016**, *7*, 111–133.

(4) Strathmann, H. Electrodialysis, a Mature Technology with a Multitude of New Applications. *Desalination* **2010**, *264* (3), 268–288.

(5) Cusick, R. D.; Kim, Y.; Logan, B. E. Energy Capture from Thermolytic Solutions in Microbial Reverse-Electrodialysis Cells. *Science* **2012**, *335* (6075), 1474–1477.

(6) Geise, G. M.; Paul, D. R.; Freeman, B. D. Fundamental Water and Salt Transport Properties of Polymeric Materials. *Prog. Polym. Sci.* **2014**, *39* (1), 1–42.

(7) Strathmann, H.; Giorno, L.; Drioli, E. *Introduction to Membrane Science and Technology*; Wiley-VCH Weinheim, 2011; Vol. 544.

(8) Logan, B. E.; Elimelech, M. Membrane-Based Processes for Sustainable Power Generation Using Water. *Nature* **2012**, *488*, 313–319.

(9) Ramon, G. Z.; Feinberg, B. J.; Hoek, E. M. V. Membrane-Based Production of Salinity-Gradient Power. *Energy Env. Sci* **2011**, *4* (11), 4423–4434.

(10) Długołęcki, P.; Gambier, A.; Nijmeijer, K.; Wessling, M. Practical Potential of Reverse Electrodialysis As Process for Sustainable Energy Generation. *Environ. Sci. Technol.* **2009**, *43* (17), 6888–6894.

(11) Post, J. W.; Veerman, J.; Hamelers, H. V. M.; Euverink, G. J. W.; Metz, S. J.; Nymeijer, K.; Buisman, C. J. N. Salinity-Gradient Power: Evaluation of Pressure-Retarded Osmosis and Reverse Electrodialysis. *J. Membr. Sci.* **2007**, *288* (1), 218–230.

(12) Geise, G. M.; Lee, H.; Miller, D. J.; Freeman, B. D.; McGrath, J. E.; Paul, D. R. Water Purification by Membranes: The Role of Polymer Science. *J. Polym. Sci. Part B Polym. Phys.* **2010**, *48* (15), 1685–1718.

(13) Strathmann, H.; Grabowski, A.; Eigenberger, G. Ion-Exchange Membranes in the Chemical Process Industry. *Ind. Eng. Chem. Res.* **2013**, *52* (31), 10364–10379.

(14) Veerman, J.; Saakes, M.; Metz, S. J.; Harmsen, G. J. Reverse Electrodialysis: A Validated Process Model for Design and Optimization. *Chem. Eng. J.* **2011**, *166* (1), 256–268.

(15) Długołęcki, P.; Nymeijer, K.; Metz, S.; Wessling, M. Current Status of Ion Exchange Membranes for Power Generation from Salinity Gradients. *J. Membr. Sci.* **2008**, *319* (1–2), 214–222.

(16) Ghyselbrecht, K.; Huygebaert, M.; Bruggen, B. V. der; Ballet, R.; Meesschaert, B.; Pinoy, L. Desalination of an Industrial Saline Water with Conventional and Bipolar Membrane Electrodialysis. *Desalination* **2013**, *318*, 9–18.

(17) Bauer, B.; Strathmann, H.; Effenberger, F. Anion-Exchange Membranes with Improved Alkaline Stability. *Desalination* **1990**, *79* (2), 125–144.

(18) Geise, G. M.; Cassady, H. J.; Paul, D. R.; Logan, B. E.; Hickner, M. A. Specific Ion Effects on Membrane Potential and the Permselectivity of Ion Exchange Membranes. *Phys Chem Chem Phys* **2014**, *16* (39), 21673–21681.

(19) Cassady, H. J.; Cimino, E. C.; Kumar, M.; Hickner, M. A. Specific Ion Effects on the Permselectivity of Sulfonated Poly(Ether Sulfone) Cation Exchange Membranes. *J. Membr. Sci.* **2016**, *508*, 146–152.

(20) Fontananova, E.; Messana, D.; Tufa, R. A.; Nicotera, I.; Kosma, V.; Curcio, E.; Baak, W. van; Drioli, E.; Profio, G. D. Effect of Solution Concentration and Composition on the Electrochemical Properties of Ion Exchange Membranes for Energy Conversion. *J. Power Sources* **2017**, *340*, 282–293.

(21) Le, X. T. Permselectivity and Microstructure of Anion Exchange Membranes. *J. Colloid Interface Sci.* **2008**, *325* (1), 215–222.

(22) Silvester, L. F.; Pitzer, K. S. Thermodynamics of Electrolytes. X. Enthalpy and the Effect of Temperature on the Activity Coefficients. *J. Solut. Chem.* **1978**, *7* (5), 327–337.

(23) Braun, B. M.; Weingärtner, H. Transference Numbers of Aqueous NaCl and Na2SO4 at 25°C from EMF Measurements with Sodium-Selective Glass Electrodes. *J. Solut. Chem.* **1985**, *14* (9), 675–686.

(24) Lide, D. R. *Handbook of Chemistry and Physics*; CRC Press, 2003.

(25) Panopoulos, D. K.; Kaneko, H.; Spiro, M. Transference Numbers of Sodium Chloride in Concentrated Aqueous Solutions and Chloride Conductances in Several Concentrated Electrolyte Solutions. *J. Solut. Chem.* **1986**, *15* (3), 243–252.

(26) Pitzer, K. S.; Peiper, J. C.; Busey, R. H. Thermodynamic Properties of Aqueous Sodium Chloride Solutions. *J Phys Chem Ref Data U. S.* **1984**, *13:1*.

(27) Yuan-Hui, L.; Gregory, S. Diffusion of Ions in Sea Water and in Deep-Sea Sediments. *Geochim. Cosmochim. Acta* **1974**, *38* (5), 703–714.

(28) Robinson, R. A.; Stokes, R. H. *Electrolyte Solutions*; Courier Corporation, 2002.

(29) Newman, J.; Thomas-Alyea, K. E. *Electrochemical Systems*; John Wiley & Sons, 2012.

(30) Geise, G.; Freeman, B. D.; Paul, D. R. Characterization of a Sulfonated Pentablock Copolymer for Desalination Applications. *Polymer* **2010**, *51* (24), 5815–5822.

Chapter 6: Specific Co-Ion Sorption and Diffusion Properties Influence Permselectivity‡

The previous project has demonstrated that the experimental factors will not introduce larger-than-2% uncertainty to membrane permselectivity. The objective of this project was to understand if the permselectivity of a series of commercially available and lab-synthesized CEMs will depend on ion specific factors. Furthermore, the co-ion transport within CEMs was studied in terms of ion sorption and diffusion effects. Ion specific permselectivity behavior of CEMs was observed, and ion specific sorption and diffusion effects were observed and demonstrated to contribute to ion specific permselectivity phenomena. Modeling results were compared with experimental results to illustrate on how the ion specific parameter, i.e., co-ion bare and hydrated radius, polarizability and geometry, contribute the ion specific sorption and diffusion behavior. Additionally, an ion-polymer complexation was detected and demonstrated to facilitate the perchlorate transport.

6.1. Introduction

Ion exchange membranes (IEMs) often are prepared using polymers containing positively charged groups (AEMs) or negatively charged groups (CEMs). The parameter used to quantify the ability of an IEMs to selectively transport certain ions is permselectivity. The permselectivity of an ion exchange membrane describes the extent to which a membrane selectively transports counter-ions and excludes co-ions,[1,2] and it is linked to the efficiency of many electromembrane-based separation (e.g., electrodialysis (ED)[3–5]), energy generation (e.g., reverse electrodialysis (RED)[6–8]), and energy storage (e.g., redox flow batteries (RFB)[9,10]) technologies. Highly permselective IEMs enable efficient ED separation processes, efficient energy recovery in RED, and high coulombic efficiency of and low capacity fade in redox flow batteries.[2,3,5,7,9] Therefore, it is critical to maximize the permselectivity properties of ion exchange membranes of these applications.

---

‡This chapter has been adapted with permission from: Ji, Y.; Luo, H.; Geise, G.M. Specific Co-Ion Sorption and Diffusion Properties Influence Membrane Permselectivity. *J. Membr. Sci*. **2018**, *563*(1), 492 – 504

Traditionally, ion exchange membrane permselectivity has been characterized and studied using sodium chloride. Emerging separation challenges and electro-membrane applications, however, require membrane optimized for solutions containing electrolytes that are different from sodium chloride.[8,11–20] Perhaps one of the more pronounced examples of this situation is the application of membranes as separators in RFB applications. The development of flow batteries has involved the identification of a wide range of battery chemistry options, and vanadium-based ions, bromide, zinc ions, cerium or organic redox shuttles are a few examples of the types of molecules that could be exposed to the membrane separator in RFB systems.[9–11,13] Additionally, many membrane-based energy recovery technologies could expose ion exchange membranes to complex ionic solutions such ammonium bicarbonate,[18] lithium chlorate,[6] or copper and ammonia-based solutions.[17] Furthermore, deionization via ED could be challenged with increasingly contaminated waters containing, for example, chromium,[21] cadmium,[22] fluoride,[23] nitrate,[5] perchlorate,[24] and sulfate.[5] Since IEMs are required in these technologies, membrane permselectivity properties must be understood for electrolytes other than sodium chloride.

Membrane that selectively transport ions via differences in ion valence (e.g., di-valent versus mono-valent ions) are available,[25–35] but fewer studies have addressed the problem of engineering selective ion transport between ions of similar valence (e.g., selectivity between different mono-valent ions).[19,36–38] Li et al. measured the permselectivity properties of three poly(phenylene oxide)-based anion exchange membranes using sodium electrolytes with fluoride, chloride, bromide, iodide, hydroxyl, nitrate and nitrite counter-ions; membrane permselectivity was correlated with the Gibbs free energy of anion hydration and the Stokes radii of the anions.[37] Geise et al. measured the permselectivity properties of four commercial ion exchange membranes using sodium chloride and bicarbonate as well as ammonium chloride and bicarbonate.[19] Cassady et al. subsequently measured the permselectivity properties of a sulfonated poly(ether sulfone) membrane using lithium, sodium, and potassium salts with chloride and sulfate.[36] In the latter two studies, ion specific effects were discussed within the framework of counter-ion binding affinity and co-ion polarizability. Imteyaz et al. measured the permselectivity of a zirconium aluminophosphate-poly(vinyl chloride) composite cation exchange membrane using lithium, sodium potassium salts with chloride and nitrate, and ascribed differences in permselectivity to counter-ion binding affinity, and the hydration radii of the co-ions.[38]

In general, membrane permselectivity has been observed to decrease as the binding affinity between the counter-ion and fixed charge group increases.[19,36] The relationship between co-ion properties and membrane permselectivity is less clear compared to the situation for the counter-ions. Studies suggest that co-ion specific membrane permselectivity properties may be related to the Gibbs free energy of hydration,[37] co-ion Stokes radius,[37] co-ion polarizability,[19,36] and co-ion hydrated radius,[38] but few general conclusions exist. These preliminary studies highlight the need for a deeper understanding of the fundamental interactions that drive co-ion specific permselectivity properties in ion exchange membranes.

Membrane permselectivity, α, is defined using cation and anion transport numbers (Equation 2.1). Increase in the membrane-phase co-ion transport number drive a decrease in permselectivity (Equation 2.1 and 2.2). A perfectly permselective membrane ($\alpha = 1$) passes current via only counter-ions and completely prevents co-ion transport (i.e., $t_X^m = 0$). In the other limiting case, a non-permselective membrane (i.e., $t_X^m = t_X^s$ and $\alpha = 0$). The permselectivity, therefore, varies between zero and unity as the co-ion transport number varies between zero and the value in bulk solution.

The definition of the membrane phase transport numbers, t_i^m, include both the ion concentration and diffusivity in the membrane phase. As a result, permselectivity is expected to increase as either the co-ion concentration or mobility in the membrane phase is suppressed (see Appendix C.1 for additional discussion). Therefore, attempts to understand or model co-ion specific permselectivity properties should recognize the contribution of co-ion specific sorption (or partitioning) and diffusion effects.

In this study, the apparent permselectivity properties of three CEMs were measured using four monovalent electrolytes, sodium chloride (NaCl), sodium bromide (NaBr), sodium nitrate ($NaNO_3$) and sodium perchlorate ($NaClO_4$). These electrolytes all dissociate completely in water and avoid aqueous speciation challenges recognized in other studies.[39] The co-ion sorption and diffusion coefficients of a crosslinked sulfonated polymer membrane (a CEM) were measured using the four electrolytes to quantify specific co-ion sorption and diffusion properties. To determine the underlying phenomena that drive co-ion specific sorption (and, thus, permselectivity) properties, co-ion sorption was modeled using Donnan exclusion theory[4] coupled with three models to describe the mean ionic activity coefficients in the polymer: Manning's counter-ion condensation theory,[40,41] electrostatic (i.e., the Born model),[17,42] and a model combining electrostatic and dispersion force.[43] Ion diffusion coefficients were modeled using a combination of the Mackie and Meares hindered diffusion model[44,45] and Manning's counter-ion condensation theory.[41] Co-ion properties, including polarizability and size, affect co-ion specific sorption and diffusion properties and, thus, permselectivity. Additionally, complexation between sodium perchlorate and the polymer affected permselectivity via both co-ion sorption and diffusion properties.

6.2. Results and Discussion

6.2.1. Apparent Permselectivity

The apparent permselectivity of the CEMs was measured using each of the four electrolytes considered (Figure 6.1). In general, the Selemion CMV membrane had the highest apparent permselectivity, and XLAMPS had the lowest apparent permselectivity. Membrane with high *IEC* and low water content tend to have higher apparent permselectivity compared to materials with low *IEC* and high-water content, so the high-water content of XLAMPS compared to the commercial membranes. Representative membrane permselectivity data analysis was presented in Appendix C.2.

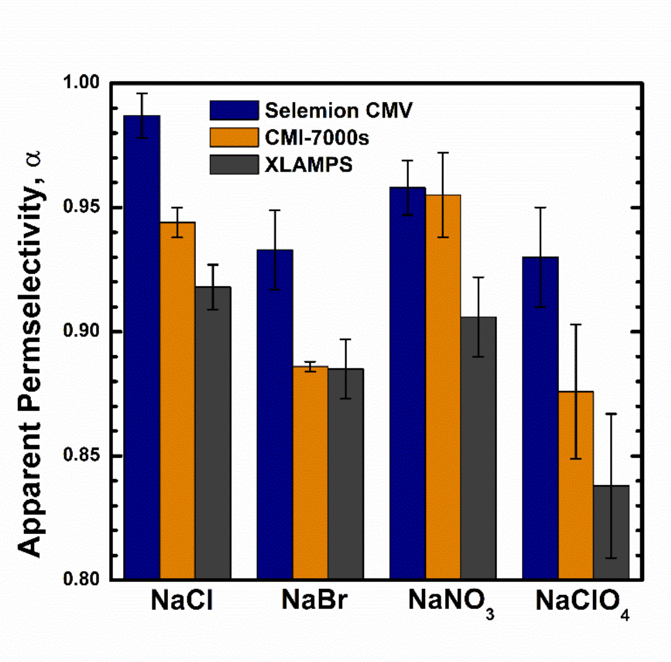

Figure 6.1. Apparent permselectivity values of the commercial and XLAMPS membranes calculated from membrane potential measurements made while the membranes separated solutions of 0.1mol/L and 0.5mol/L aqueous electrolytes. Each data point represents the average of three independent measurements made at room temperature (23±2°C), and the uncertainty was taken as one standard deviation from the mean.

Apparent permselectivity properties, for all three membranes, depended on which co-ion (anion) was used during the measurement (Figure 6.1), i.e., the properties were co-ion specific. Unlike other observations of co-ion specific apparent permselectivity properties made using ions that have different valence or participate in aqueous speciation reactions, the ions considered here have the same valence and do not undergo speciation in aqueous solution. Junction potentials at the reference electrode/solution interface may contribute to the measured apparent permselectivity properties reported in Figure 6.1. These junction potentials can be estimated based on Henderson equation, and apparent permselectivity values adjusted using the estimated junction potential are provided in the Appendix C.3. The junction potential contribution changes the absolute value of the apparent permselectivity, but the qualitative trend is preserved. Therefore, the co-ion specific apparent permselectivity results reported in Figure 6.1 suggest that fundamental properties of the co-ions influence apparent permselectivity properties.

Apparent permselectivity values that are less than unity result from a non-zero value of the co-ion transport number in the membrane (Equation 6.1). As such, differences in apparent permselectivity measured using different co-ions (Figure 6.1) suggest that the monovalent co-ions considered in this study interact with the polymer and influence the co-ion transport number in fundamentally unique ways. Non-zero values of the membrane phase co-ion transport number occur because co-ions sorb into the membrane and then transport (via a diffusion/migration process) through the membrane. As such, co-ion transport in the membrane is sensitive to co-ion sorption and diffusion contributions.[46] Additionally, because the differences in apparent permselectivity measured using the different electrolytes generally are similar between the three membranes considered, intrinsic co-ion properties may be responsible for the observed co-ion specific apparent permselectivity properties.

6.2.2. Co-Ion Sorption

The XLAMPS co-ion sorption coefficients were measured experimentally using the four electrolytes (Figure 6.2). Additionally, the mean ionic activity coefficients for the electrolyte sorbed in the polymer were calculated from the measured sorption data and reported in Appendix C.4. The commercial membrane co-ion sorption coefficients were not measured because the supporting mesh incorporated in those membranes for mechanical strength complicates the interpretation of ion sorption coefficients in those materials.

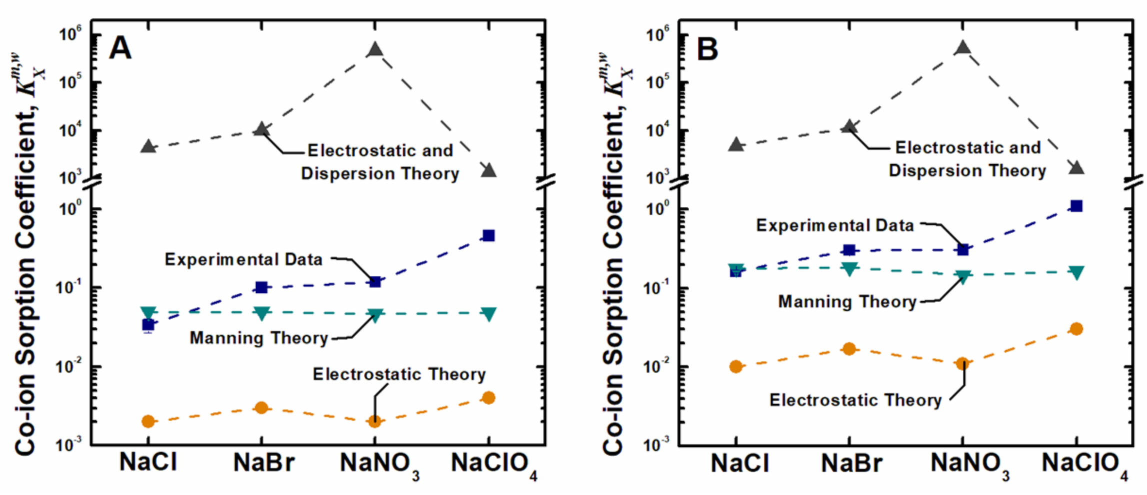

Figure 6.2. XLAMPS co-ion sorption coefficients measured after equilibrating samples with (A) 0.1mol/L or (B) 0.5mol/L aqueous electrolyte solutions (■). Experimental data were compared to sorption coefficients calculated by combining Donnan exclusion theory with either Manning's counter-ion condensation theory (▼), electrostatic theory (●), or an electrostatic and dispersion force-based theory (▲). Each experimental data point represents the average of at least four measurements made at room temperature, and the uncertainty was taken as one standard deviation from the mean. The dashed lines are included to guide the eyes.

The measured XLAMPS co-ion sorption coefficients increase with increasing external salt concentration. This observation is consistent with Donnan theory and other reports.[4,47] Specific co-ion sorption was observed (Figure 6.2) as the sorption coefficients differed depending on the co-ion used during the measurement. Co-ion sorption generally correlated with the apparent permselectivity measurements; co-ions that exhibited larger sorption coefficients generally resulted in lower apparent permselectivity and vice versa.

Comparing the measured and calculated co-ion sorption coefficients (Figure 6.2) provides insight into the co-ion specific properties and/or interactions that may contribute to the co-ion specific sorption behavior. In the following discussion, the results obtained using sodium perchlorate will be excluded due to the presence of additional interactions between sodium perchlorate and the polymer. These interactions are not captured using the sorption models discussed in this section and will be discussed in the next section.

The Manning parameter, ξ, for the XLAMPS material was taken to be 0.18 (estimation of ξ is detailed in the Appendix C.5). Since this value is less than unity, counter-ion condensation does not occur in XLAMPS,[40] and Equation 3.6 was used to calculate the activity coefficients in the membrane phase.

Using Manning's counter-ion condensation theory generally provided a reasonable prediction of the chloride sorption coefficient (Figure 6.2). The theory, however, underestimated the sorption coefficients measured using the other electrolytes. This result is not surprising because ion valence is the only explicit ion-specific parameter in the model. Manning proposed an empirical parameter to capture ion-specific effects,[48] but the model does not describe co-ion specific sorption based on fundamental co-ion properties.

The application of electrostatic and dispersion theories to calculate co-ion sorption coefficients require knowledge of ion, membrane and solution parameters. The parameters used for such calculations were presented and discussed in Appendix C.6 and C.7.

Electrostatic theory contains a bare co-ion radius term (c.f. Equation 3.8), so this approach is able to capture co-ion specific sorption effects to some degree because different monovalent co-ions have different charge density values due to size differences. The theory dictates that the magnitude of the solvation energy barrier increases as ion size decreases (or charge density increases), so smaller ions generally would be expected to have smaller sorption coefficients compared to larger ions. The sorption coefficients predicted using electrostatic theory follow the trend: $k_{\mathrm{NaBr}}^{m} > k_{\mathrm{NaNO_3}}^{m} \cong k_{\mathrm{NaCl}}^{m}$. Unlike the Manning theory, electrostatic theory captures ion specific effects to some extent, but it does not completely capture the experimental sorption coefficient trend, e.g., electrostatic theory predicts a drop in the sodium nitrate sorption coefficient compared to that for sodium bromide that is not observed in the experimentally measured value. The partial agreement between the electrostatic theory-calculated and experimentally measured co-ion sorption coefficients indicates that charge density effects likely contribute to co-ion specific sorption properties, but charge density is not the only contributor to co-ion specific sorption properties.

Dispersion forces can be combined with the electrostatic forces to take into account excess polarizability, which is an additional ion specific parameter. Attractive dispersion forces between the hydrated polymer and co-ions reduce the sorption energy barrier and increase ion sorption coefficients compared to calculations made using electrostatics alone. Increases in excess polarizability are expected to lead to a reduction in the sorption energy barrier and an increase in ion sorption.

Dispersion forces arise from differences in the polarizability properties of the ion and the surrounding medium. Smaller ions of a given valence have larger charge density, and this larger charge density enables smaller ions to more effectively polarize the surrounding medium. As a result, smaller ions of a given valence create a larger polarizability difference between the ion and the surrounding medium.

The ion excess polarizability is a measure of this difference between the polarizability of the ion and the surrounding medium (of equivalent volume). Therefore, larger excess polarizability is correlated with more substantial dispersion interactions, and this correlation ultimately leads to increased ion sorption for more polarizable ions compared to less polarizable ions. Including dispersion energy in the sorption model addresses qualitative disagreement between the sodium chloride, bromide, and nitrate measured sorption coefficients and those values calculated using electrostatic theory (Figure 6.2). For example, dispersion energy contributions address the previously discussed issue where electrostatic theory predicts a sodium nitrate sorption coefficient that is less than the sodium bromide sorption coefficient. The sorption coefficients calculated using the electrostatic and dispersion combined theory followed the trend: $k^m_{\mathrm{NaNO_3}} > k^m_{\mathrm{NaBr}} > k^m_{\mathrm{NaCl}}$. Although the theory predicted a larger difference between sodium nitrate sorption coefficient and sodium bromide sorption coefficient, compared to experimental data, the electrostatic and dispersion combined theory still captured the qualitative increasing tendency, from k^m_{NaBr} to $k^m_{\mathrm{NaNO_3}}$.

Neither the use of electrostatic theory nor the inclusion of dispersion energy results in quantitative agreement between the measured and calculated sorption coefficients. Electrostatic theory overestimates the sorption energy barrier and underestimates co-ion sorption coefficients by approximately two orders of magnitude. Including dispersion energy in the calculation reduced the sorption energy barrier to the point where co-ion sorption coefficients were overestimated by several orders of magnitude. This lack of quantitative agreement may originate from at least two issues. First, the dielectric continuum assumption oversimplifies the membrane as it does not capture molecular details of the material, and this simplification could obscure the interaction energy calculations. Second, even if the dielectric continuum assumption is reasonable, the magnitude of both the electrostatic and dispersion energies is very sensitive to the hydrated membrane dielectric constant, $\varepsilon_m(0)$, and optical dielectric constant, $\varepsilon_m^*(0)$. As discussed previously, the value of $\varepsilon_m(0)$ was taken to be 40 using an empirical relationship,[49] so the specific polymer considered in this study may have different relative permittivity properties compared to the empirical relationship. The value of $\varepsilon_m^*(0)$ was measured experimentally to be 3.0±0.1, but the magnitude of the experimental uncertainty in this value could affect the caluclated sorption coefficients by at least an order of magnitude. Both of these issues may introduce sufficient uncertainty into the energy calculations to prevent quantitative agreement between the experimentally measured and calculated sorption coefficient values.

To explore the issue of uncertainty in more depth, the electrostatic theory was fit to the sorption coefficient data for XLAMPS initially equilibrated in 0.1 mol/L aqueous NaCl with the value of $\varepsilon_m(0)$ left as an adjustable parameter. This approach resulted in a fitted value of $\varepsilon_m(0) = 64$ (compared to the value of 40 that was determined using the empirical approach discussed previously). Electrostatic theory was then used to calculate the NaBr and $NaNO_3$ sorption coefficients using the $\varepsilon_m(0) = 64$ value (open circles in Figure 6.3). The larger value of $\varepsilon_m(0)$ reduces the significance of charge density effects, and as such, the calculated NaBr and $NaNO_3$ sorption coefficients are very similar to that for NaCl.

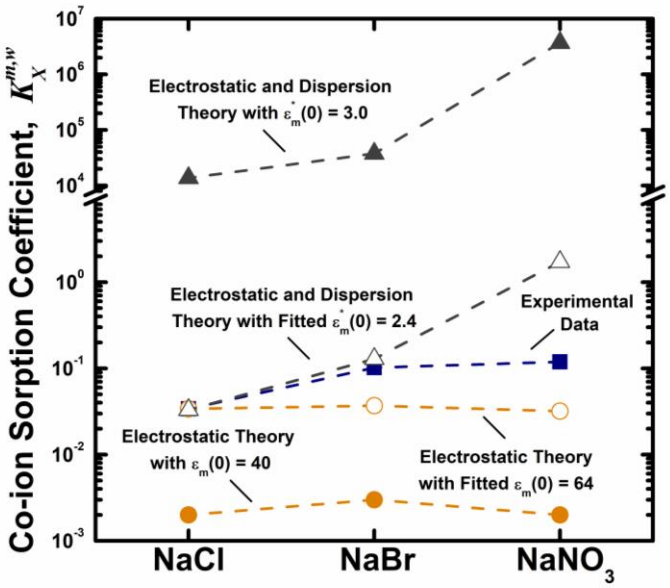

Figure 6.3. XLAMPS co-ion sorption coefficient data measured experimentally after equilibrating samples with 0.1 mol/L aqueous electrolyte solution (■), calculated using electrostatic theory with $\varepsilon_m(0) = 40$ (●) or the fitted $\varepsilon_m(0) = 64$ (○), and calculated using the electrostatic and dispersion energy theory with $\varepsilon_m^*(0) = 3.0$ (▲) or the fitted $\varepsilon_m^*(0) = 2.4$ (△). Experimental data points represent the average of four to five measurements, and the uncertainty was taken as one standard deviation from the mean. The dashed lines are provided to guide the eyes.

Alternatively, the electrostatic theory with dispersion energy contributions was fit to the sorption coefficient data for XLAMPS initially equilibrated in 0.1 mol/L aqueous NaCl with $\varepsilon_m(0) = 40$ and the value of $\varepsilon_m^*(0)$ left as an adjustable parameter. This approach resulted in a fitted value of $\varepsilon_m^*(0) = 2.4$, which is less than the measured value of 3.0±0.1. The theory was then used to calculate the NaBr and $NaNO_3$ sorption coefficients using the $\varepsilon_m^*(0) = 2.4$ value (open triangles in Figure 6.3). Agreement between the experimental and calculated sorption coefficient data is greatly improved with the fitted $\varepsilon_m^*(0)$ value compared to the measured value, and this calculation further highlights the sensitivity of the electrostatic and dispersion energy model to the value of the optical dielectric constant. It further suggests that dispersion energy effects may be important for describing co-ion specific sorption in charged polymers.

6.2.3. Ion-Polymer Complexation

In addition to the continuum modeling approaches described above, specific ion-polymer complexation interactions may also contribute to co-ion specific apparent permselectivity properties.

Evidence for these interactions can be found by analyzing the sodium perchlorate sorption data. For XLAMPS initially equilibrated with 0.5mol/L aqueous sodium perchlorate, $k_{\mathrm{NaClO_4}}^{m} = 1.09 \pm 0.01$ (Figure 6.2). Values of k_X^m greater than unity indicate that, at equilibrium, the electrolyte solution sorbed by the membrane is more concentrated than the external solution. Alternatively, when k_X^m is less than unity, ions are excluded from the polymer matrix. For membrane polymers, k_X^m is typically less than unity, so the situation, described above where $k_{\mathrm{NaClO_4}}^{m} > 1$ is a rare occurrence as polymers generally exclude ion sorption to at least some extent.[50] This situation could be consistent with ion-polymer complex formation as such interactions could increase ion sorption to the point where the internal perchlorate concentration exceeded the perchlorate concentration in the external solution.

The ethylene oxide groups that are present in XLAMPS may form ion-polymer complexes with the perchlorate ions (Figure 6.4).[51,52] Four ethylene oxide repeat units are suggested to be needed to form the complex.[52–54] This type of complexation may occur in XLAMPS because ethylene oxide units are present in the PEGDA crosslinker. To further test the hypothesis that ion-polymer complex formation occurred in XLAMPS, the co-ion sorption coefficients of crosslinked poly(ethylene glycol) diarylate hydrogels (XLPEGDA) with different numbers of ethylene oxide repeat units between crosslinks (n = 3, 10, or 13, cf. Figure 4.2) were measured (Figure 6.5).

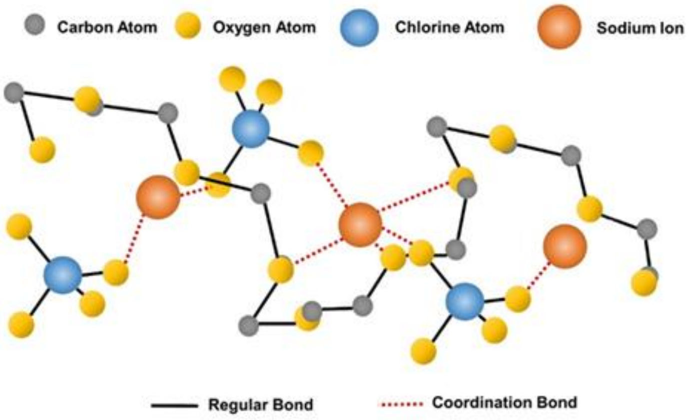

Figure 6.4. Schematic illustration of the structure of the $NaClO_4$-EO complex. Adapted from Ref.[53] with permission from The Royal Society of Chemistry.

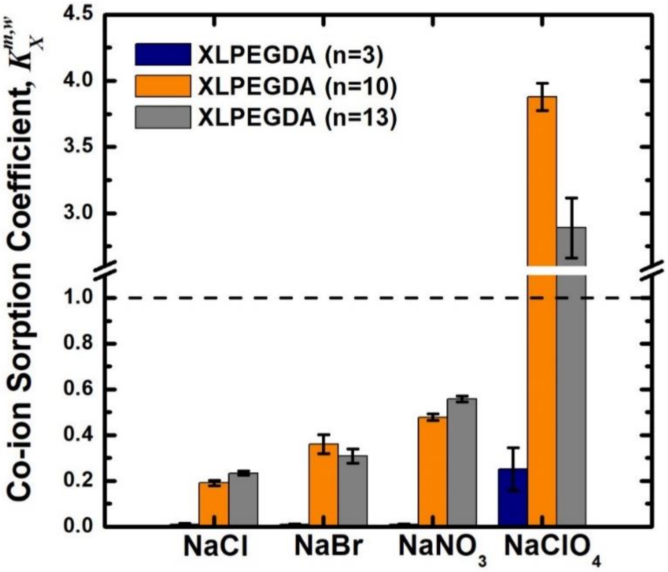

Figure 6.5. Co-ion sorption coefficient, $k_X^{m,w}$, values for XLPEGDA (n=3) (🟦), XLPEGDA (n=10) (🟧) and XLPEGDA (n=13) (⬛). Sorption coefficients were measured after samples were equilibrated in 0.1 mol/L aqueous electrolyte. Each experimental data point represents the average of four or five measurements made at room temperature, and the uncertainty was taken as one standard deviation from the mean.

For the chloride, bromide, and nitrate electrolytes, the values of $k_X^{m,w}$ are all less than unity for XLPEGDA (Figure 6.5), and this result suggests that those electrolytes are excluded from the polymer. Alternatively, for XLPEGDA with n>4 (i.e., n = 10 and 13), the perchlorate sorption coefficients are greater than unity, and this result suggests that perchlorate is more concentrated in the polymer compared to the external solution. Sorption of perchlorate in the XLPEGDA (n = 3) material is still considerably greater than the sorption of the other co-ions. This result may be due to the ability of perchlorate to complex with ethylene oxide units on other chains, but the formation of the complex may not be facilitated to the extent that is observed when n>4. These results suggest that ion-polymer complexes may form between the ethylene oxide repeat units and the perchlorate ions in the XLPEGDA materials with n>4.

The XLPEGDA results support the formation of ion-polymer complexes between sodium perchlorate and XLAMPS. The crosslinker used in XLAMPS is XLPEGDA (n = 10), so this crosslinker would provide sufficient ethylene oxide repeat units to form the complex. Ultimately, this complex may increase the perchlorate sorption in XLAMPS and contribute to a reduction in the XLAMPS apparent permselectivity measured using sodium perchlorate.

6.2.4. Co-Ion Diffusion

XLAMPS salt diffusion coefficients, D_s^m, were measured via kinetic desorption using 0.1 mol/L and 0.5 mol/L aqueous electrolyte solutions (Figure 6.6). As expected, the salt diffusion coefficients increase as the size of the co-ion decreases following the trend: $D^m_{\mathrm{NaCl}} > D^m_{\mathrm{NaBr}} > D^m_{\mathrm{NaNO_3}} > D^m_{\mathrm{NaClO_4}}$ (the hydrated co-ion radii increase in the order of Cl^-, Br^-, NO_3^-, and ClO_4^-).[54–56] Salt diffusion coefficients measured using samples initially equilibrated in 0.5 mol/L aqueous electrolyte were less than that measured using samples initially equilibrated with 0.1 mol/L aqueous electrolyte. This difference is consistent with an observed osmotic de-swelling phenomenon whereby the water content of the 0.5 mol/L equilibrated samples was less than that of the 0.1 mol/L equilibrated samples (Table 4.3).[47,50,57]

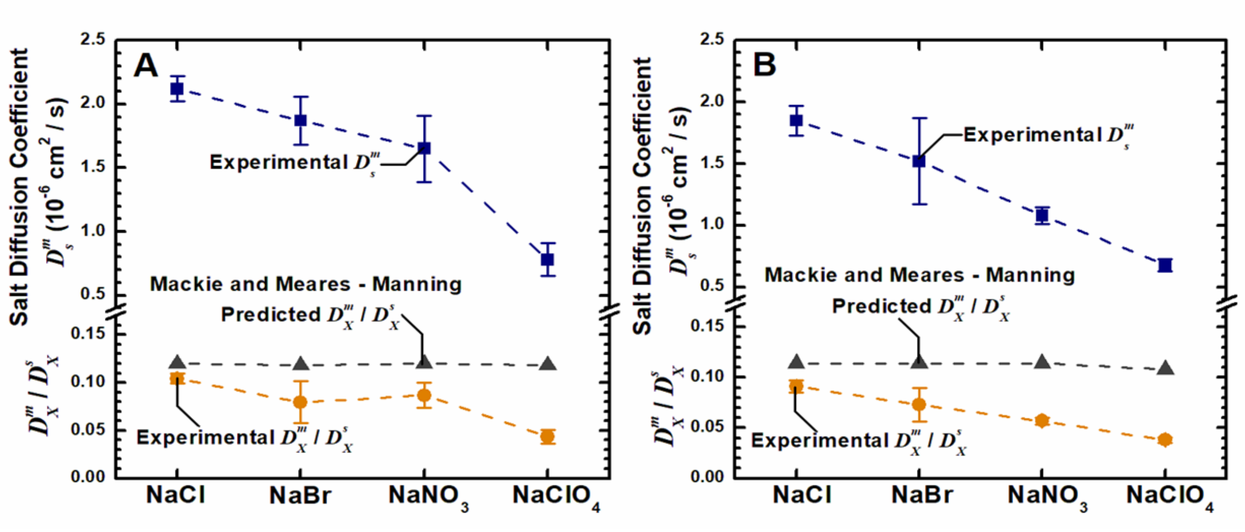

Figure 6.6. Effective XLAMPS salt diffusion coefficients, D_s^m, measured at room temperature after equilibrating samples with either (A) 0.1 mol/L or (B) 0.5 mol/L aqueous electrolyte (■). The ratio of D_X^m / D_X^s was calculated using either experimental data (●) or the combined Mackie and Meares – Manning model (▲). Each experimental data point represents the average of at least four measurements, and the uncertainty was taken as one standard deviation from the mean. The dashed lines are provided to guide the eye.

XLAMPS samples characterized using sodium chloride had the highest permselectivity and the highest salt diffusion coefficient, and samples characterized using sodium perchlorate had the lowest permselectivity and the lowest salt diffusion coefficient (Figure 6.6). These observations contradict the earlier discussion suggesting that faster co-ion (salt) diffusion is expected to result in lower permselectivity. The results, therefore, suggest that co-ion sorption properties may influence apparent permselectivity to a greater extent than the diffusion properties. For example, at both concentrations, the salt diffusion coefficient measured using sodium chloride was double that of sodium perchlorate, but the chloride sorption coefficient was about an order of magnitude lower than the perchlorate sorption coefficient.

To account for the influence of ion size on diffusivity in the membrane phase, the diffusivity measured in the membrane can be normalized by the corresponding value in bulk solution. In charged polymers, such as XLAMPS, the effective salt diffusion coefficient, D_S^m, is often approximately equivalent to the co-ion diffusion coefficient in the membrane, D_X^m. This approximation, discussed in more detail in Appendix C.8, is applicable when the concentration of sorbed counter-ions is much greater than the concentration of sorbed co-ions, and this situation is often applicable for charged membranes. Therefore, further analysis of the measured effective salt diffusion coefficient in the membrane is presented under the assumption that $D_S^m \approx D_X^m$. Correspondingly, the effective co-ion diffusion coefficient in the membrane, D_X^m, was normalized by the co-ion diffusion coefficient in bulk solution, D_X^s.

The ratio of D_X^m/D_X^s is reported in Figure 6.6. Though the magnitude of the change in diffusion coefficient properties measured using the four electrolytes is reduced compared to the raw diffusivity data, evidence of specific ion diffusivity properties still exists. Evidence of this situation is illustrated by comparing the ratio of D_X^m/D_X^s (determined using the experimental data) with calculations performed using the combined Mackie and Meares – Manning model, cf. Section 3.2.

Counter-ion condensation is not expected to occur in XLAMPS because ξ = 0.18, so Equation 20 was used to calculate the co-ion diffusion coefficients. The term $A(\xi, X)$ was evaluated using an integral approximation:

$$\frac{D_X^m}{D_X^s} \approx \left(\frac{k_w}{2-k_w}\right)^2 \left[1 - \frac{1}{3}\frac{\xi X}{2+X(1+\pi/\xi)}\right] \tag{6.1}$$

where the term in parentheses describes the influence of polymer tortuosity on D_X^m (i.e., the polymer chains act as obstacles that the co-ions must diffuse around). The square bracket term describes the influence of electrostatic effects on co-ion diffusion. In general, the first term was calculated to be in the range of 0.10 to 0.12, and the second term was calculated to be approximately 0.99 for all four co-ions. As such, the tortuosity effects appear to dominate in these materials, and electrostatic effects do not appreciably affect co-ion diffusion. Therefore, electrostatic effects likely are not responsible for co-ion specific diffusion properties.

Comparison of the value of D_X^m/D_X^s calculated using the experimental data to that determined using the Mackie and Meares – Manning model reveals evidence of co-ion specific diffusion effects in membrane phase (Figure 6.6). In general, agreement between the experimental and calculated values deteriorates as the co-ion changes from chloride to bromide, nitrate, and perchlorate. This result suggests that interactions between the co-ions and the polymer matrix act to restrict diffusivity above and beyond what would generally be expected based on ion charge and ion size.

The specific shape of the co-ion also may contribute to the observed properties. Diffusion of planar nitrate and tetrahedral perchlorate ions may be restricted to a larger extent compared to chloride and bromide ions that are spherical in shape. These shape effects may explain the stronger reduction of D_X^m/D_X^s for nitrate, as salt concentration increased from 0.1 to 0.5 mol/L, compared to the ratios for chloride and bromide. As osmotic de-swelling occurs (i.e., salt concentration increases from 0.1 to 0.5 mol/L), chain packing in the polymer may increase, and nitrate may be more vulnerable to tighter packing compared to the situation for chloride and bromide ions if nitrate interacts more strongly with the polymer.

Additionally, ion-polymer complexation between perchlorate ions and XLAMPS (Figure 6.4) may inform the larger reduction in the experimental D_X^m/D_X^s ratio for perchlorate compared to the value calculated using the Mackie and Meares – Manning model. While these complexes are not expected to be as strong as a covalent bond, they likely reduce the mobility of sodium and perchlorate ions in the polymer relative to a situation where complexation does not occur. [58] Therefore, perchlorate diffusivity in XLAMPS may be reduced via complexation to a greater extent compared to what might be expected based solely on size and shape.

6.3. Conclusions

The apparent permselectivity values of two commercial CEMs (Selemion CMV and CMI-7000s) and a crosslinked sulfonated polymer, XLAMPS, were measured using four monovalent strong electrolytes (NaCl, NaBr, $NaNO_3$ and $NaClO_4$). Co-ion specific apparent permselectivity properties were observed. Co-ion specific phenomena result from a combination of co-ion specific sorption and diffusion effects, though sorption effects appear to be more significant compared to the diffusion effects.

Three models were used to investigate the influence of electrostatic and dispersion forces (in conjunction with electroneutrality and the thermodynamic equilibrium criterion) on co-ion sorption coefficients. The Manning counter-ion condensation model showed reasonable agreement with measured chloride sorption, but the model failed to qualitatively predict the bromide and nitrate sorption coefficients. Electrostatic and dispersion forces captured some of the qualitative ion specific trends suggesting that co-ion charge density and polarizability properties contribute to ion specific sorption properties. Neither model provided quantitative agreement, but analyzing the model results revealed that dispersion energy contributions appear to contribute to ion specific properties as qualitative agreement was observed between the experimental data and the model containing the dispersion energy term. This lack of agreement was likely due to a combination of the continuum nature of these models and the sensitivity of the model to membrane dielectric constant and optical dielectric constant.

The combined Mackie and Meares – Manning counter-ion condensation model was used to analyze the influence of tortuosity and electrostatic forces on ion specific diffusion effects. The tortuosity effects on co-ion diffusion appeared to be more significant than the electrostatic effects. Diffusion of non-spherical ions may be more restricted compared to spherical ions. Finally, ion-polymer complexation involving perchlorate and ethylene oxide repeat units in XLAMPS appears to increase ion sorption and reduce ion diffusivity properties.

All of the interactions discussed in this study might be applied to guide the preparation of ion-specific selective membrane. For example, membrane static and optical dielectric constants can be adjusted to control the sorption properties of ions with difference size and polarizability. The membrane polymer tortuosity might also be adjusted to facilitate or hinder the diffusion of ions with different geometry. In addition, the ion-polymer complexation proved the possibility of preparing ion-specific selective membrane through incorporating certain complexation-forming functional groups into the membrane polymer.

6.4. References

(1) Strathmann, H.; Giorno, L.; Drioli, E. *Introduction to Membrane Science and Technology*; Wiley-VCH Weinheim, 2011; Vol. 544.

(2) Długołęcki, P.; Nymeijer, K.; Metz, S.; Wessling, M. Current Status of Ion Exchange Membranes for Power Generation from Salinity Gradients. *J. Membr. Sci.* **2008**, *319* (1–2), 214–222.

(3) McGovern, R. K.; Zubair, S. M. The Cost Effectiveness of Electrodialysis for Diverse Salinity Applications. *Desalination* **2014**, *348*, 57–65.

(4) Geise, G. M.; Lee, H.; Miller, D. J.; Freeman, B. D.; McGrath, J. E.; Paul, D. R. Water Purification by Membranes: The Role of Polymer Science. *J. Polym. Sci. Part B Polym. Phys.* **2010**, *48* (15), 1685–1718.

(5) Strathmann, H. Electrodialysis, a Mature Technology with a Multitude of New Applications. *Desalination* **2010**, *264* (3), 268–288.

(6) Tamburini, A.; Tedesco, M.; Cipollina, A.; Micale, G.; Ciofalo, M.; Papapetrou, M.; Van Baak, W.; Piacentino, A. Reverse Electrodialysis Heat Engine for Sustainable Power Production. *Appl. Energy* **2017**, *206*, 1334–1353.

(7) Veerman, J.; Saakes, M.; Metz, S. J.; Harmsen, G. J. Reverse Electrodialysis: A Validated Process Model for Design and Optimization. *Chem. Eng. J.* **2011**, *166* (1), 256–268.

(8) Kamcev, J.; Freeman, B. D. Charged Polymer Membranes for Environmental/Energy Applications. Annu. *Rev. Chem. Biomol. Eng.* **2016**, *7*, 111–133.

(9) Alotto, P.; Guarnieri, M.; Moro, F. Redox Flow Batteries for the Storage of Renewable Energy: A Review. *Renew. Sustain. Energy Rev.* **2014**, *29*, 325–335.

(10) Weber, A. Z.; Mench, M. M.; Meyers, J. P.; Ross, P. N.; Gostick, J. T.; Liu, Q. Redox Flow Batteries: A Review. *J. Appl. Electrochem.* **2011**, *41* (10), 1137.

(11) Li, X.; Zhang, H.; Mai, Z.; Zhang, H.; Vankelecom, I. Ion Exchange Membranes for Vanadium Redox Flow Battery (VRB) Applications. *Energy Env. Sci.* **2011**, *4* (4), 1147–1160.

(12) Prifti, H.; Parasuraman, A.; Winardi, S.; Lim, T. M.; Skyllas-Kazacos, M. Membranes for Redox Flow Battery Applications. *Membranes* **2012**, *2* (2), 275–306.

(13) Darling, R.; Gallagher, K.; Xie, W.; Su, L.; Brushett, F. Transport Property Requirements for Flow Battery Separators. *J. Electrochem. Soc.* **2016**, *163* (1), a5029–a5040.

(14) Richardson, S. D.; Ternes, T. A. Water Analysis: Emerging Contaminants and Current Issues. *Anal. Chem.* **2005**, *77* (12), 3807–3838.

(15) Brookes, J. D.; Carey, C. C.; Hamilton, D. P.; Ho, L.; van der Linden, L.; Renner, R.; Rigosi, A. Emerging Challenges for the Drinking Water Industry. *Environ. Sci. Technol.* **2014**, *48* (4), 2099–2101.

(16) Fuhrer, G. J. *The Quality of Our Nation's Waters: Nutrients and Pesticides*; Diane Publishing, 1999; Vol. 1225.

(17) Zhang, F.; *LaBarge*, N.; Yang, W.; Liu, J.; Logan, B. E. Enhancing Low-Grade Thermal Energy Recovery in a Thermally Regenerative Ammonia Battery Using Elevated Temperatures. *ChemSusChem* **2015**, *8* (6), 1043–1048.

(18) Zhang, F.; Liu, J.; Yang, W.; Logan, B. E. A Thermally Regenerative Ammonia-Based Battery for Efficient Harvesting of Low-Grade Thermal Energy as Electrical Power. *Energy Env. Sci* **2015**, *8* (1), 343–349.

(19) Geise, G. M.; Cassady, H. J.; Paul, D. R.; Logan, B. E.; Hickner, M. A. Specific Ion Effects on Membrane Potential and the Permselectivity of Ion Exchange Membranes. *Phys Chem Chem Phys* **2014**, *16* (39), 21673–21681.

(20) Varcoe, J. R.; Atanassov, P.; Dekel, D. R.; Herring, A. M.; Hickner, M. A.; Kohl, P. A.; Kucernak, A. R.; Mustain, W. E.; Nijmeijer, K.; Scott, K. Anion-Exchange Membranes in Electrochemical Energy Systems. *Energy Environ. Sci.* **2014**, *7* (10), 3135–3191.

(21) Nataraj, S. K.; Hosamani, K. M.; Aminabhavi, T. M. Potential Application of an Electrodialysis Pilot Plant Containing Ion-Exchange Membranes in Chromium Removal. *Desalination* **2007**, *217* (1), 181–190.

(22) Marder, L.; Sulzbach, G. O.; Bernardes, A. M.; Ferreira, J. Z. Removal of Cadmium and Cyanide from Aqueous Solutions through Electrodialysis. *J. Braz. Chem. Soc.* **2003**, *14*, 610–615.

(23) Amor, Z.; Bariou, B.; Mameri, N.; Taky, M.; Nicolas, S.; Elmidaoui, A. Fluoride Removal from Brackish Water by Electrodialysis. *Desalination* **2001**, *133* (3), 215–223.

(24) Wang, P.-Y.; Shah, I.; Huang, C. P. Preparation and Characterization of Functionalized Poly(Vinyl Chloride) Membranes for Selective Separation of Perchlorate from Water. *J. Membr. Sci.* **2015**, *476*, 561–570.

(25) Mizutani, Y. *Ion* Exchange Membranes with Preferential Permselectivity for Monovalent Ions. *J. Membr. Sci.* **1990**, *54* (3), 233–257.

(26) Sata, T. Studies on Ion Exchange Membranes with Permselectivity for Specific Ions in Electrodialysis. *J. Membr. Sci.* **1994**, *93* (2), 117–135.

(27) Nagarale, R.; Gohil, G.; Shahi, V. K. Recent Developments on Ion-Exchange Membranes and Electro-Membrane Processes. *Adv. Colloid Interface Sci.* **2006**, *119* (2–3), 97–130.

(28) Güler, E.; van Baak, W.; Saakes, M.; Nijmeijer, K. Monovalent-Ion-Selective Membranes for Reverse Electrodialysis. *J. Membr. Sci.* **2014**, *455*, 254–270.

(29) Avci, A. H.; Sarkar, P.; Tufa, R. A.; Messana, D.; Argurio, P.; Fontananova, E.; Di Profio, G.; Curcio, E. Effect of Mg^{2+} Ions on Energy Generation by Reverse Electrodialysis. *J. Membr. Sci.* **2016**, *520*, 499–506.

(30) White, N.; Misovich, M.; Yaroshchuk, A.; Bruening, M. L. Coating of Nafion Membranes with Polyelectrolyte Multilayers to Achieve High Monovalent/Divalent Cation Electrodialysis Selectivities. *ACS Appl. Mater. Interfaces* **2015**, *7* (12), 6620–6628.

(31) Cheng, C.; White, N.; Shi, H.; Robson, M.; Bruening, M. L. Cation Separations in Electrodialysis through Membranes Coated with Polyelectrolyte Multilayers. *Polymer* **2014**, *55* (6), 1397–1403.

(32) Cheng, C.; Yaroshchuk, A.; Bruening, M. L. Fundamentals of Selective Ion Transport through Multilayer Polyelectrolyte Membranes. *Langmuir* **2013**, *29* (6), 1885–1892.

(33) Inui, A.; Hama, C.; Katsuragawa, T.; Iwata, S.; Yuchi, A. Divalent/Monovalent Selectivities and Secondary Interactions of Multibasic Acids on Anion Exchange Resins. *Ind. Eng. Chem. Res.* **2013**, *52* (47), 16880–16886.

(34) Pintauro, P.; Tandon, R.; Chao, L.; Xu, W.; Evilia, R. Equilibrium Partitioning of Monovalent/Divalent Cation-Salt Mixtures in Nafion Cation-Exchange Membranes. *J. Phys. Chem.* **1995**, *99* (34), 12915–12924.

(35) Bason, S.; Freger, V. Phenomenological Analysis of Transport of Mono-and Divalent Ions in Nanofiltration. *J. Membr. Sci.* **2010**, *360* (1–2), 389–396.

(36) Cassady, H. J.; Cimino, E. C.; Kumar, M.; Hickner, M. A. Specific Ion Effects on the Permselectivity of Sulfonated Poly(Ether Sulfone) Cation Exchange Membranes. *J. Membr. Sci.* **2016**, *508*, 146–152.

(37) Li, Y.; Xu, T. Permselectivities of Monovalent Anions through Pyridine-Modified Anion-Exchange Membranes. *Sep. Purif. Technol.* **2008**, *61* (3), 430–435.

(38) Imteyaz, S. Effects of Monovalent Ions on Membrane Potential and Permselectivity: Evaluation of Fixed Charge Density of Polymer Based Zirconium Aluminophosphate Composite Membrane. *RSC Adv.* **2015**, *5* (116), 96008–96018.

(39) Robinson, R. A.; Stokes, R. H. *Electrolyte Solutions*; Courier Corporation, 2002.

(40) Manning, G. S. Limiting Laws and Counterion Condensation in Polyelectrolyte Solutions I. Colligative Properties. *J. Chem. Phys.* **1969**, *51* (3), 924–933.

(41) Manning, G. S. Limiting Laws and Counterion Condensation in Polyelectrolyte Solutions II. Self-diffusion of the Small Ions. *J. Chem. Phys.* **1969**, *51* (3), 934–938.

(42) Parsegian, A. Energy of an Ion Crossing a Low Dielectric Membrane: Solutions to Four Relevant Electrostatic Problems. *Nature* **1969**, *221* (5183), 844–846.

(43) Boström, M.; Ninham, B. Energy of an Ion Crossing a Low Dielectric Membrane: The Role of Dispersion Self-Free Energy. *Biophys. Chem.* **2005**, *114* (2–3), 95–101.

(44) Mackie, J.; Meares, P. The Diffusion of Electrolytes in a Cation-Exchange Resin Membrane I. Theoretical. *Proc. R. Soc. Lond. Ser. Math. Phys. Sci.* **1955**, *232* (1191), 498–509.

(45) Mackie, J.; Meares, P. The Diffusion of Electrolytes in a Cation-Exchange Resin Membrane. II. Experimental. *Proc. R. Soc. Lond. Ser. Math. Phys. Sci.* **1955**, *232* (1191), 510–518.

(46) Wijmans, J. G.; Baker, R. W. The Solution-Diffusion Model: A Review. *J. Membr. Sci.* **1995**, *107* (1–2), 1–21.

(47) Geise, G. M.; Falcon, L. P.; Freeman, B. D.; Paul, D. R. Sodium Chloride Sorption in Sulfonated Polymers for Membrane Applications. *J. Membr. Sci.* **2012**, *423*, 195–208.

(48) Manning, G. S. Limiting Laws and Counterion Condensation in Polyelectrolyte Solutions. 8. Mixtures of Counterions, Species Selectivity, and Valence Selectivity. *J. Phys. Chem.* **1984**, *88* (26), 6654–6661.

(49) Zhang, H.; Geise, G. M. Modeling the Water Permeability and Water/Salt Selectivity Tradeoff in Polymer Membranes. *J. Membr. Sci.* **2016**, *520*, 790–800.

(50) Geise, G. M.; Paul, D. R.; Freeman, B. D. Fundamental Water and Salt Transport Properties of Polymeric Materials. *Prog. Polym. Sci.* **2014**, *39* (1), 1–42.

(51) Andreev, Y. G.; Bruce, P. G. Polymer Electrolyte Structure and Its Implications. *Electrochimica Acta* **2000**, *45* (8–9), 1417–1423.

(52) Bruce, P. G. Structure and Electrochemistry of Polymer Electrolytes. *Electrochimica Acta* **1995**, *40* (13–14), 2077–2085.

(53) Lightfoot, P.; Mehta, M. A.; Bruce, P. G. Structure of the Poly (Ethylene Oxide)–Sodium Perchlorate Complex PEO_3–$NaClO_4$ from Powder X-Ray Diffraction Data. *J. Mater. Chem.* **1992**, *2* (4), 379–381.

(54) Marcus, Y. A Simple Empirical Model Describing the Thermodynamics of Hydration of Ions of Widely Varying Charges, Sizes, and Shapes. *Biophys. Chem.* **1994**, *51* (2–3), 111–127.

(55) Nightingale Jr, E. Phenomenological Theory of Ion Solvation. Effective Radii of Hydrated Ions. *J. Phys. Chem.* **1959**, *63* (9), 1381–1387.

(56) Ohtaki, H.; Radnai, T. Structure and Dynamics of Hydrated Ions. *Chem. Rev.* **1993**, *93* (3), 1157–1204.

(57) Kamcev, J.; Paul, D. R.; Freeman, B. D. Effect of Fixed Charge Group Concentration on Equilibrium Ion Sorption in Ion Exchange Membranes. *J. Mater. Chem. A* **2017**, *5* (9), 4638–4650.

(58) Fullerton-Shirey, S. K.; Maranas, J. K. Effect of $LiClO_4$ on the Structure and Mobility of PEO-Based Solid Polymer Electrolytes. *Macromolecules* **2009**, *42* (6), 2142–2156.

Chapter 7: Effects of Polymer Fixed Charge Group Physiochemistry on Permselectivity of and Ion Transport in AEMs

7.1. Introduction

Ion exchange membranes (IEMs) are often prepared using charged polymers, i.e., polymers having ionizable fixed charge groups incorporated into the polymer matrix.[1–3] Anion exchange membranes (AEMs) contain positively charged groups and preferentially transport anions (i.e., counter-ions) while excluding cations (i.e., co-ions). Cation exchange membranes (CEMs) contain negatively charged groups and preferentially transport cations (i.e., counter-ions) while excluding anions (i.e., co-ions).[1] Due to their selective transport ability, IEMs are often used as selective separators in diverse water purification (e.g., electrodialysis (ED) and membrane capacitive deionization (MCDI)), energy generation (e.g., reverse electrodialysis (RED)) and energy storage (e.g., redox flow battery (RFB)) applications.[4–6] Emerging separation challenges require IEMs to be exposed to aqueous electrolyte solutions containing a variety of ions different from the traditionally widely-studied sodium and chloride. For example, water deionization via ED or MCDI can be challenged with increasingly contaminated water containing ferric, chromium, cupric, cadmium, fluoride, nitrate, perchlorate and sulfate.[6–10] To achieve efficient water purification and energy production using those membrane-based technologies, the IEMs must have maximized permselectivity when exposed with specific ions.[1]

Efforts have been made in this field to tune membrane permselectivity for specific ions, and most of those focused on engineering the chemical structure of IEMs.[1,11,12] The efforts typically fall into two categories.[12–30] The first category includes membrane surface modifications, such as enhancing the degree of crosslinking on membrane surface,[25] creating a dense and neutral surface layer,[11] creating oppositely charged surface layers,[28–30] or creating a "layer-by-layer" structure.[13,14,17–19] Most efforts in this first category have been demonstrated to be effective in enhancing the membrane selectivity between ions with different valence, e.g., monovalent and divalent ions.[14,19,29] The mechanism to improve ion selectivity by the highly crosslinked or dense surface layer is based on the steric sieving effects on ions that have different size (typically hydrated radii). While the mechanism to improve ion selectivity by creating oppositely charged surface layer or "layer-by-layer" structure is based on the electrostatic sieving effects between the surface layer and ions that have different charges (i.e., valences).[11]

The second category includes modifying the fixed charge group type incorporated into the IEMs. The most commonly used anionic fixed charge group is the sulfonate group for CEMs, but research has been done to explore the effects of other anionic groups, such as carboxylic acid, phosphonic acid, boric acid, and phenolic acid on the selectivity properties and separation performance of CEMs.[25,26,31,32] For example, the study by Sata et al. concluded that CEMs having boric acid groups did not remarkably enhance the selectivity between alkaline earth metal cations and sodium ions, as compared to CEMs having sulfonic acid groups.[31] The study by Nagarale et al. suggested that CEMs with phosphoric acid groups were more effective in separating cations with identical charges as compared with CEMs with sulfonic acid groups.[26] A larger library of cationic fixed charge groups exist for AEMs, e.g., quaternary ammonium, quaternary phosphonium, quinuclidinium-based quaternary ammonium, imidazolium, pyridinium, and pentamethylguanidinium groups.[33,34] The effects of cationic fixed charge groups on the performance of AEMs have been investigated mostly in the alkaline fuel cell field,[33,35–37] so little discussion exists for aqueous based electro-membrane applications. Therefore, a study aimed at understanding the effects of cationic fixed charge group type on AEM performance in aqueous separation systems will close this knowledge gap.

In this study, we explored the effects of cationic fixed charge group type on the permselectivity of and ion transport in AEMs by examining two AEMs with trimethyl ammonium and 1,4-dimethyl imidazolium groups. Two physiochemical properties of the fixed charge group, i.e., bulkiness (quantified by Van der Waals volume[38,39]) and hydrophilicity (quantified by hydration enthalpy[40–42]) were hypothesized to be the key causes of their performance difference. Such hypothesis was formed because fixed charge group bulkiness and hydrophilicity were found to lead to the specific interactions between ions and fixed charge sites in the colloid, surfactant and ion exchange resin fields.[43–50]

Two acrylonitrile and styrene-based, crosslinked AEMs with different cationic fixed charge groups, i.e., trimethyl ammonium and 1,4-dimethyl imidazolium groups, were synthesized and used in this study. Their permselectivity, counter-ion and co-ion transport properties were characterized with electrolytes with different co-ions (i.e., lithium chloride, sodium chloride and ammonium chloride) and different counter-ions (i.e., sodium chloride, sodium bromide and sodium nitrate). Their permselectivity, counter-ion and co-ion transport properties were compared and correlated with the physiochemical properties of ions and fixed charge groups to understand the effects of fixed charge group type on the separation performance of AEMs and the mechanism behind specific interactions between different fixed charge groups and ions.

7.2. Results and Discussion

The physical and chemical properties of the two AEMs, measured in DI water, are reported in Table 4.4. The water uptake of the PVBAN-TMA[X] membrane with the trimethyl ammonium group is about 17% higher than the water uptake of PVBAN-DMI[X] with the 1,4-dimethyl imidazolium group. This result is consistent with the more negative enthalpy of hydration value for the TMA charged group compared to the DMI charged group.

Table 7.1. Estimated Van der Waals volume and hydration enthalpy values for the two fixed charge groups. The values were calculated using semi-empirical models adapted from literature.[38,40] Detailed calculation principles and procedures are presented in Appendix D.1.

Fixed Charge Group		Estimated Van der Waals Volume, V_{vdw} [Å^3]	Estimated Hydration Enthalpy, $-\Delta H_{hyd}$ [kJ/mol]
TMA[X]	Trimethyl ammonium	72	272
DMI[X]	1,4-dimethyl imidazolium	99	260

The membrane water uptake, water volume fraction and fixed charge group concentration measured using 0.5 mol/L aqueous solutions are reported in Table 4.4. Generally, the water uptake of both AEMs decreased by 20 – 55% in 0.5 mol/L aqueous electrolyte solutions compared to the situation in the DI water measurements, due to osmotic deswelling. However, the degree of deswelling (defined as $\frac{w_u \text{in DI water} - w_u \text{ in solution}}{w_u \text{in DI water}}$) varied according to fixed charge group hydrophilicity, co-ion and counter-ion type (Figure 7.1). First, the membrane with the less hydrophilic fixed charge group dehydrated more readily compared to the membrane with the more hydrophilic fixed charge group. PVBANDMI[X] generally deswelled 15% more than PVBANTMA[X] in all of the solutions. Second, both membranes dehydrate more readily when less hydrophilic counter-ions or co-ions are used. For example, both membranes deswell 3% more in ammonium chloride compared to the situation in sodium chloride, and both membranes deswell 16% more in sodium nitrate as compared to the situation in sodium chloride. The influence of counter-ion type on deswelling is more pronounced than that of the co-ion type.

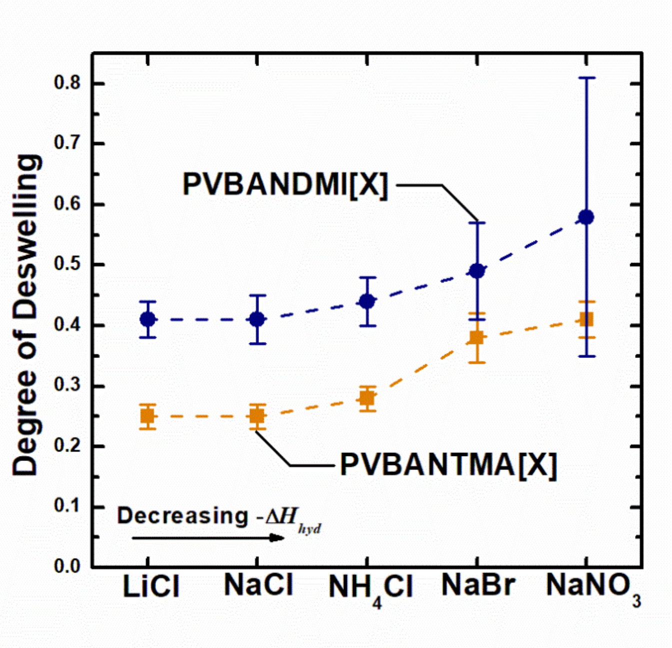

Figure 7.1. The degree of deswelling of the two AEMs measured using 0.5 mol/L aqueous solutions of different electrolytes. The $-\Delta H_{hyd}$ order of co-ions, counter-ions (Table 7.2) and fixed charge groups are: $\mathrm{Cl}^- > \mathrm{Br}^- > \mathrm{NO}_3^-$, $\mathrm{Li}^+ > \mathrm{Na}^+ > \mathrm{NH}_4^+$ and trimethyl ammonium > 1,4-dimethyl imidazolium, respectively. It is noted that the standard deviation associated with sodium nitrate is larger than other data points, presumably due to the fact that the water uptake value associated with sodium nitrate is the smallest (cf. Table 4.5), and standard propagation of uncertainty magnifies this uncertainty when the degree of deswelling is calculated.

Table 7.2. Hydration enthalpy values of the counter-ions and co-ions studied in this work. The values are based on the definition of enthalpy of hydration that it is the enthalpy change accompanying the dissolution of one mol of the ideal gaseous ions in an infinite volume of water at a temperature of 298°K and a pressure of 1 atm). Therefore, the values are calculated using the thermodynamic data associated with such process, and those thermodynamic data were obtained experimentally.[51] Ions with a higher magnitude of enthalpy are considered more hydrophilic than those ions with less negative hydration enthalpy values.

Ion	Hydration Enthalpy, $-\Delta H_{hyd}$ [kJ/mol]
Li^+	519
Na^+	409
NH_4^+	307
Cl^-	381
Br^-	347
NO_3^-	314

7.2.1. Permselectivity

The measured apparent permselectivity results were presented in Figure 7.2. Since aqueous solutions of different electrolytes that are different from 1 mol/L aqueous potassium nitrate solution (i.e., the filling solution of the electrodes used) were used in this study, the junction potential at the reference electrode/solution interface may contribute to the measured apparent permselectivity in Figure 7.2. The junction potentials can be estimated using the Henderson equation,[52] the results considering junction potential effects were presented and analyzed in Appendix D.2. Considering junction potential exaggerated the influence of co-ion type, narrowed the influence of counter-ion type, but did not create substantial difference on the influence of the fixed charge group type. More detailed discussion on junction potential is presented in Appendix D.2.

The fixed charge group, counter-ion and co-ion types influence permselectivity to a degree of different magnitude. The influence of the chemistry of the fixed charge group on permselectivity was found to be relatively small. Switching from the trimethyl ammonium (TMI) to 1,4-dimethyl imidazolium (DMI) fixed charge group led to no more than a 6% difference in permselectivity. The permselectivity values of PVBANDMI membrane were about 2 – 4 % higher than those for the PVBANTMI membrane for lithium chloride, sodium chloride, sodium bromide and sodium nitrate electrolytes. The most pronounced difference in permselectivity occurred with ammonium chloride, where the permselectivity of 1,4-dimethyl imidazolium-charged membrane was 6% higher than the trimethyl ammonium charged membrane.

Variations in the co-ion, however, can influence permselectivity to a greater extent. Up to an 18% difference in permselectivity was observed as a result of varying the co-ion. As such, the specific co-ion used influences permselectivity to a greater extent than changing the fixed charge group or the counter-ion. For both AEMs, the permselectivity decreased in the order of: NH_4Cl > NaCl > LiCl as the co-ion was changed. Such results are partially consistent with previous findings with commercially available AEMs that the ammonium permselectivity is higher than sodium chloride permselectivity.[53] Less studies exist for LiCl with AEMs in aqueous electro-membrane systems. So, an explanation of this permselectivity order as a function of co-ion type will be given in the following discussion.

Variations in counter-ions influence permselectivity up to 5%. The permselectivity order of electrolyte with different counter-ions was observed as: NaCl ≈ NaBr > $NaNO_3$. Such order was also consistent with previous findings with commercially-available and lab-prepared CEMs.[54] Explanation of this permselectivity order will be given in the following discussion as well.

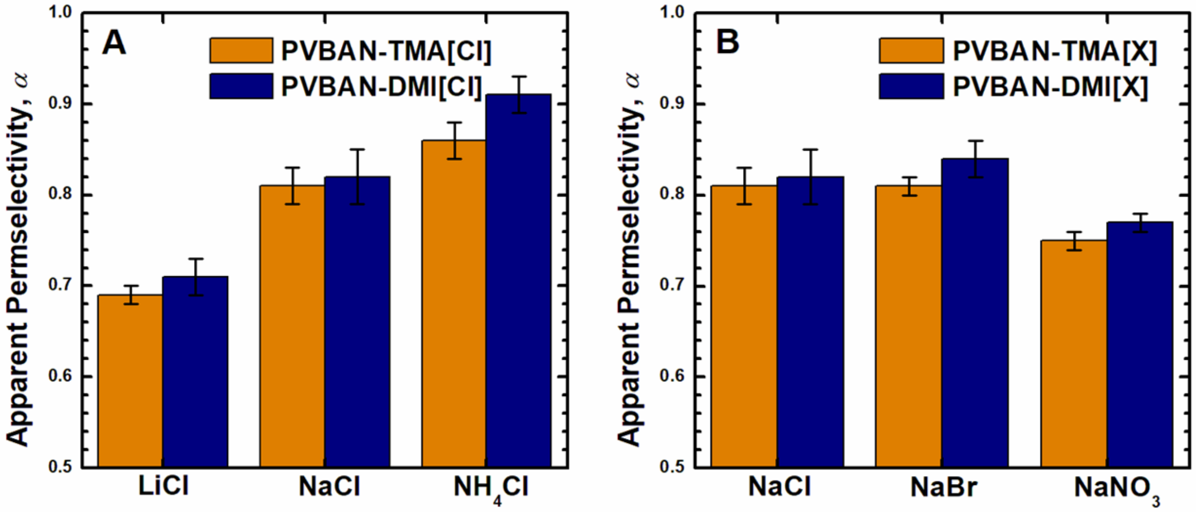

Figure 7.2. Measured membrane apparent permselectivity of the trimethyl ammonium-charged and the 1,4-dimethyl imidazolium charged AEMs characterized using 0.1 mol/L and 0.5 mol/L aqueous solutions of (A) lithium chloride, sodium chloride and ammonium chloride (i.e., different co-ions) and (B) sodium chloride, sodium bromide and sodium nitrate (i.e., different counter-ions). The measurements and calculations were conducted under/using the temperature of 25°C. The values were reported as the average and standard deviations of three samples.

The membrane permselectivity was defined using the transport numbers of counter-ion and co-ion in membrane and solution phases, respectively.[2] Based on the definitions of permselectivity and transport numbers, the permselectivity can be determined by three counter-ion and co-ion transport related factors:[55,56]

$$\alpha = 1 - \frac{k_{X/M}^{m} D_{X/M}^{m} \left(1 + \frac{1}{D_{X/M}^{s}}\right)}{k_{X/M}^{m} D_{X/M}^{m} + 1} \tag{7.1}$$

where $k_{X/M}^{m}$ is the membrane co-ion to counter-ion concentration ratio, defined as the membrane co-ion concentration normalized by counter-ion concentration, i.e., $k_{X/M}^{m} = c_X^m / c_M^m$; $D_{X/M}^{m}$ is the membrane co-ion to counter-ion diffusion ratio, defined as the membrane co-ion diffusivity normalized by counter-ion diffusivity, i.e., $D_{X/M}^{m} = D_X^m / D_M^m$. Finally, $D_{X/M}^{s}$ is the solution co-ion to counter-ion diffusion ratio, defined as the solution co-ion diffusivity normalized by counter-ion diffusivity, i.e., $D_{X/M}^{s} = D_X^s / D_M^s$.

The value of $k_{X/M}^{m}$ quantifies the extent of co-ion sorption on a per counter-ion basis (i.e. the ratio of the number of co-ions present in the polymer compared to the number of counter-ions). This quantity, for charged ion exchange materials, is expected to be less than unity due to Donnan exclusion.[57] The value of $D_{X/M}^{m}$ quantifies co-ion diffusion relative to counter-ion diffusion within the membrane. Larger $k_{X/M}^{m}$ and $D_{X/M}^{m}$ indicate that co-ion transport occurs to a larger extent as compared to counter-ion transport across the membrane, and this situation is expected to result in smaller permselectivity. The value of $D_{X/M}^{s}$ quantifies the co-ion diffusivity relative to counter-ion diffusivity in the solution phase, so larger $D_{X/M}^{s}$ values are expected to lead to larger permselectivity. The $k_{X/M}^{m}$, $D_{X/M}^{m}$ and $D_{X/M}^{s}$ values, though, influence permselectivity to different extents, among which the influence of $k_{X/M}^{m}$ is the most pronounced (Appendix D.3). For example, in the situation of an AEM measured using 0.1 mol/L and 0.5 mol/L sodium chloride solution (described in more detail in Appendix D.3), a 20% increase in $k_{X/M}^{m}$, $D_{X/M}^{m}$ and $D_{X/M}^{s}$ would be expected to cause a 5.7% reduction, 2.0% reduction and 3.2% increase in permselectivity, respectively.

To further understand the influence of changing the polymer fixed charge group on ion transport, $k_{X/M}^{m}$, $D_{X/M}^{m}$ and $D_{X/M}^{s}$ values were obtained via experiments and calculations:

$$k_{X/M}^{m} = \frac{c_X^m}{c_M^m} \tag{7.2}$$

$$c_X^m = c_s^s k_s^m \tag{7.3}$$

$$c_M^m = c_s^s k_s^m + c_A^m \tag{7.4}$$

$$D_{X/M}^{m} = \frac{D_X^m}{D_M^m} \tag{7.5}$$

$$D_s^m = \frac{D_X^m D_M^m (c_X^m + c_M^m)}{c_X^m D_X^m + c_M^m D_M^m} \tag{7.6}$$

$$\sigma_s^m = \frac{F^2}{RT} (c_M^m D_M^m + c_X^m D_X^m) \tag{7.7}$$

where c_s^s is the concentration of external solution, k_s^m is the salt sorption coefficient of membrane, c_A^m is the concentration of fixed charge group in the membrane, D_s^m is the salt diffusivity in the membrane, σ_s^m is the ionic conductivity of the membrane, F is the Faraday constant, R is the gas constant and T is the absolute temperature. The k_s^m and D_s^m values were obtained through kinetic desorption measurements. The c_A^m value was calculated using the measured *IEC* and w_u values, and σ_s^m can be measured using electrochemical impedance spectroscopy.

7.2.2. Ion Transport Breakdown: Concentration and Diffusivity Ratios

The co-ion and counter-ion transport across the membrane and in solution, was then analyzed using the calculated $k_{X/M}^{m}$, $D_{X/M}^{m}$ and $D_{X/M}^{s}$ values. Comparing the $k_{X/M}^{m}$, $D_{X/M}^{m}$ and $D_{X/M}^{s}$ values between the two membranes facilitates understanding of how changing the fixed charge group in the polymer affected transport properties from a thermodynamic or kinetic perspective.

7.2.2.1.Electrolytes with Different Co-Ions

For the electrolytes with different co-ions, i.e., lithium chloride, sodium chloride and ammonium chloride, the $k_{X/M}^{m}$ values of the 1,4-dimethyl imidazolium charged membrane are generally about 20% lower than the $k_{X/M}^{m}$ values of the trimethyl ammonium charged membrane (Figure 7.3A). This result may be due to the lower hydrophilicity of the 1,4-dimethyl imidazolium group and the resulting higher c_{A}^{m} of the 1,4-dimethyl imidazolium charged membrane (cf. Table 4.4 and 7.1). These results suggest that less hydrophilic fixed charge groups may enhance the overall co-ion exclusion performance of an AEM.

For lithium chloride and sodium chloride, the $D_{X/M}^{m}$ values of the 1,4-dimethyl imidazolium charged membrane overlap with those of the trimethyl imidazolium charged membrane. For ammonium chloride, the $D_{X/M}^{m}$ value of the 1,4-dimethyl imidazolium charged membrane is moderately lower (about 25%) than that of the trimethyl imidazolium charged membrane (Figure 7.3B). The fact that the 1,4-dimethyl imidazolium charged membrane suppressed ammonium diffusion to a much larger extent compared to the trimethyl ammonium charged membrane may be due to the larger size (quantified by Van der Waals volume) of the 1,4-dimethyl imidazolium fixed charge group as well as the tetrahedral geometry of the ammonium ion.[42,58] The tetrahedral geometry of the ammonium ion makes its diffusion more vulnerable to steric hindrance created by the polymer chains of the membrane, and the bulkier 1,4-dimethyl imidazolium group could be the source of this larger steric hindrance.[42]

Overall, the $k_{X/M}^{m}$ difference originated from fixed charge group type is about 20% for lithium chloride, sodium chloride and ammonium chloride. The $D_{X/M}^{m}$ difference originated from fixed charge group type is almost negligible for lithium chloride and sodium chloride, but about 25% for ammonium chloride. Previous discussion has shown that a 20% difference in $k_{X/M}^{m}$ or $D_{X/M}^{m}$ typically leads to about 5.7% or 2.0% difference in permselectivity, respectively. Therefore, when the AEMs are characterized using lithium chloride and sodium chloride, permselectivity difference between the two AEMs mainly comes from the difference in sorption effects. However, when the AEMs are characterized using ammonium chloride, the permselectivity difference mainly comes from the difference in diffusion effects, as a result of the size difference between the fixed charge groups as well as the tetrahedral geometry of ammonium.

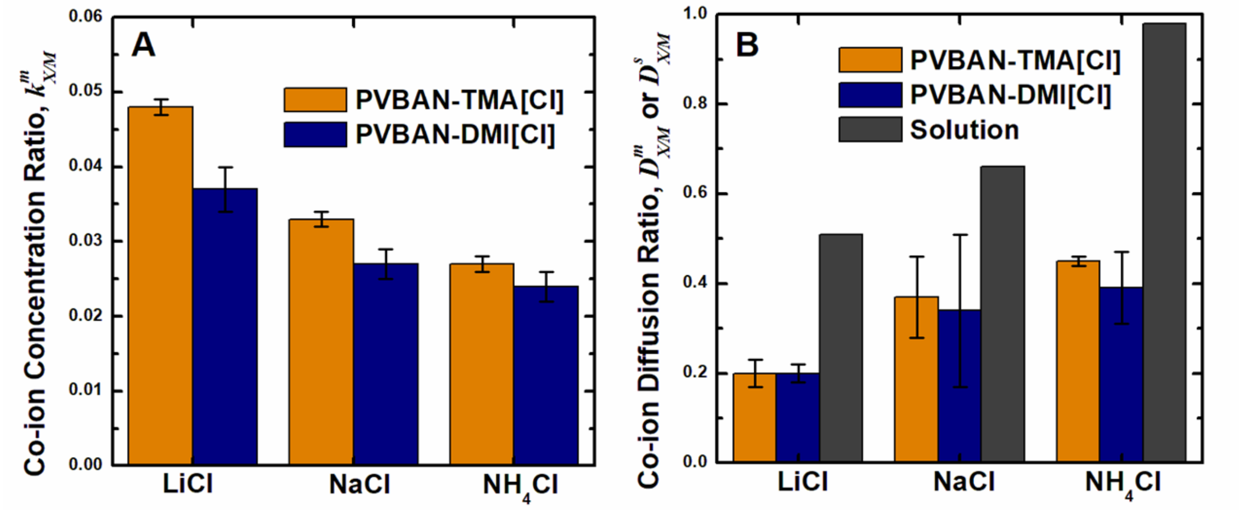

Figure 7.3. The (A) $k^m_{X/M}$ and (B) $D^m_{X/M}$ and $D^s_{X/M}$ of the two AEMs measured in 0.5 mol/L aqueous solution of lithium chloride, sodium chloride and ammonium chloride, i.e., electrolytes with different co-ions. The measurements and calculations were conducted under/using the temperature of 25°C. The values were reported as an average and standard deviation of three to four measurements.

7.2.2.2. Electrolytes with Different Counter-Ions

For the electrolytes with different counter-ions, i.e., sodium chloride, sodium bromide and sodium nitrate, the $k^m_{X/M}$ values of the 1,4-dimethyl imidazolium charged membrane were about 20 – 50% lower than those of the trimethyl ammonium charged membrane (Figure 7.4A). This result is likely also due to the lower hydrophilicity of the 1,4-dimethyl imidazolium group and the resulting higher c^m_A of the 1,4-dimethyl imidazolium charged membrane relative to the trimethyl ammonium charged membrane. The $D^m_{X/M}$ value of the 1,4-dimethyl imidazolium charged membrane overlaps with that of the 1,4-dimethyl imidazolium charged membrane for sodium chloride. While for sodium bromide and sodium nitrate, the $D^m_{X/M}$ value of the 1,4-dimethyl imidazolium charged membrane is moderately (about 25%) and dramatically (about 75%) higher than that of the trimethyl ammonium charged membrane (Figure 7.4B).

Such phenomenon is contrary to previous observations that the $D^{m}_{X/M}$ values of the 1,4-dimethyl imidazolium charged membrane are generally lower than those of the trimethyl ammonium charged membrane when electrolytes of different co-ions were used (Figure 7.3B). A hypothesis regarding the binding effects between fixed charge group and counter-ions has been proposed to explain those contrary observations and detailed explanations will be given in the next section.

Overall, the influence of fixed charge group type on $k^{m}_{X/M}$ and $D^{m}_{X/M}$ values was more pronounced (can be as high as 50% and 75%, respectively) when electrolytes with different counter-ions were used. However, the $k^{m}_{X/M}$ and $D^{m}_{X/M}$ orders show opposite directions, i.e., 1,4-dimethyl imidazolium charged membrane showed lower $k^{m}_{X/M}$ but higher $D^{m}_{X/M}$ as compared to the trimethyl ammonium charged membrane. As such the changes in sorption and diffusion, i.e., $k^{m}_{X/M}$ and $D^{m}_{X/M}$, contributions to the overall permselectivity offset each other, resulting in a situation where the nature of the fixed charge group does not appreciably influence permselectivity properties.

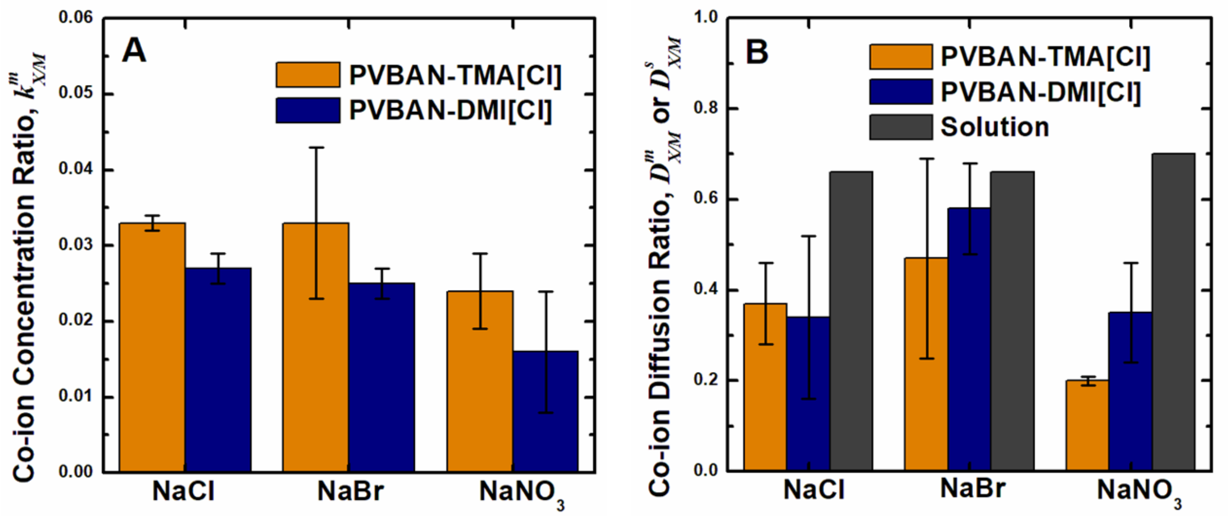

Figure 7.4. The (A) $k^{m}_{X/M}$ and (B) $D^{m}_{X/M}$ and $D^{s}_{X/M}$ values for the two AEMs measured using 0.5 mol/L aqueous solutions of sodium chloride, sodium bromide and sodium nitrate, i.e., electrolytes with different counter-ions. The measurements and calculations were conducted under/using the temperature of 25°C. The values were reported as an average and standard deviation of three to four measurements.

7.2.2.3.Reduction in Counter-Ion Diffusion Due to Specific Binding Effects

When the two AEMs were characterized using electrolytes with different co-ions, i.e., lithium chloride, sodium chloride and ammonium chloride, the $D^{m}_{X/M}$ values of the 1,4-dimethyl imidazolium membrane were generally lower than those of the trimethyl ammonium membrane. However, when electrolytes with different counter-ions were used, i.e., sodium bromide and sodium nitrate, the $D^{m}_{X/M}$ values of the 1,4-dimethyl imidazolium membrane were higher than those of the trimethyl ammonium membrane. We hypothesized that stronger binding effects between the less hydrophilic 1,4-dimethyl imidazolium fixed charge group (compared to trimethyl ammonium) and the less hydrophilic bromide and nitrate counter-ions (compared to chloride) might be the leading cause of this situation (Figure 7.5).

Such hypothesis originated from the widely recognized *Law of Matching Water Affinities* (LMWA) proposed by Collins.[59–61] The LMWA asserts that cations and anions (or ions and ion-charged sites) form stable ion pairs if their respective hydration enthalpies (considered to be a measure of "water affinities) match. Applying the LMWA to the situation in this work, it is speculated that the 1,4-dimethyl imidazolium fixed charge group, having lower $-\Delta H_{hyd}$, should form more stable pairs with bromide and nitrate (as they have lower $-\Delta H_{hyd}$, especially nitrate) compared to the trimethyl ammonium fixed charge group that has a higher $-\Delta H_{hyd}$ value. Stronger binding between the 1,4-dimethyl imidazolium group and nitrate, for example, could immobilize the nitrate counter-ions around the fixed charge groups, thus reducing the measured counter-ion diffusivity and causing a reduction in the D^{m}_{M} and an increase in $D^{m}_{X/M}$ (Equation 7.5). In the situation of the two AEMs, the 1,4-dimethyl imidazolium charged membrane might show stronger binding with bromide and nitrate, especially nitrate, as compared to the trimethyl ammonium charged membrane. Therefore, the diffusion of bromide and nitrate counter-ions might be somewhat restricted in the 1,4-dimethyl imidazolium charged membrane, as compared to the trimethyl ammonium charged membrane. Such deduction is consistent with the fact that the 1,4-dimethyl imidazolium charged membrane shows higher $D^{m}_{X/M}$ for sodium bromide (about 25% higher) and sodium nitrate (about 75% higher) as compared to the trimethyl ammonium charged membrane. The consistency might support the conclusion that stronger binding between fixed charge group and counter-ions having “matching water affinities” reduces the counter-ion diffusion in the membrane.

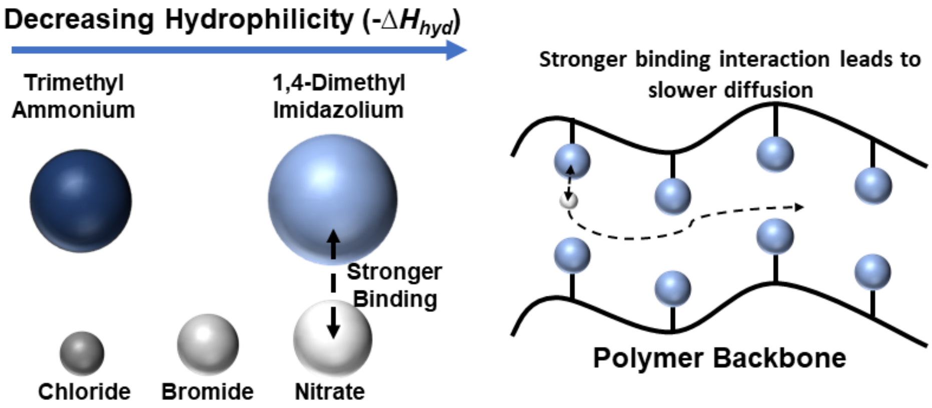

Figure 7.5. Schematic illustration of the mechanism that stronger binding between fixed charge group and counter-ion restricts the diffusion of counter-ions across the membrane.

7.3. Conclusions

Two styrene and acrylonitrile crosslinked AEMs with 1,4-dimethyl imidazolium and trimethyl ammonium fixed charge groups, respectively, were synthesized with similar *IEC* values. The water uptake, permselectivity, co-ion to counter-ion concentration and diffusivity ratios of the two AEMs were measured and compared to understand the effects of fixed charge group type on permselectivity and ion transport.

First, fixed charge group type introduced up to 6% difference in permselectivity, less pronounced than the effects of co-ion type but more pronounced than the effects of counter-ion type. The permselectivity of the 1,4-dimethyl imidazolium charged membrane was higher than the trimethyl ammonium charged membrane, and the permselectivity difference originated from both sorption and diffusion contributions to ion transport.

Second, AEMs with less hydrophilic fixed charge groups swell to a smaller extent in DI water and deswell more readily in aqueous electrolyte solutions compared to AEMs with more hydrophilic fixed charge groups. The resulting higher fixed charge group concentration of the less hydrophilic AEM makes it more effective at co-ion exclusion compared to the more hydrophilic AEM, when the *IEC* values are similar.

Overall, it was demonstrated in this work that the fixed charge group type introduced modest difference in permselectivity of AEMs, as a result of facilitated or restricted ion sorption and diffusion. AEMs with less hydrophilic fixed charge groups generally are more effective at excluding co-ions, while AEMs with bulkier fixed charge groups restrict the diffusion of non-spherical ions to a larger extent. Moreover, a hypothesis was proposed that the fixed charge group restricts the diffusion of counter-ions that have hydration enthalpy values that are closer (to the hydration enthalpy of the fixed charge group. As such, the less-hydrophilic 1,4-dimethyl imidazolium group restricts the diffusion of less-hydrophilic nitrate counter-ions. The findings from this work quantified the effects of fixed charge group type on permselectivity, counter-ion and co-ion transport, and such knowledge can be applied to engineer membrane permselectivity for a variety of electro-membrane applications.

7.4. References

(1) Kamcev, J.; Freeman, B. D. Charged Polymer Membranes for Environmental/Energy Applications. *Annu. Rev. Chem. Biomol. Eng.* **2016**, *7*, 111–133.

(2) Strathmann, H.; Giorno, L.; Drioli, E. *Introduction to Membrane Science and Technology*; Wiley-VCH Weinheim, 2011; Vol. 544.

(3) Geise, G. M.; Paul, D. R.; Freeman, B. D. Fundamental Water and Salt Transport Properties of Polymeric Materials. *Prog. Polym. Sci.* **2014**, *39* (1), 1–42.

(4) Biesheuvel, P.; Van der Wal, A. Membrane Capacitive Deionization. *J. Membr. Sci.* **2010**, *346* (2), 256–262.

(5) Prifti, H.; Parasuraman, A.; Winardi, S.; Lim, T. M.; Skyllas-Kazacos, M. Membranes for Redox Flow Battery Applications. *Membranes* **2012**, *2* (2), 275–306.

(6) Strathmann, H. Electrodialysis, a Mature Technology with a Multitude of New Applications. *Desalination* **2010**, *264* (3), 268–288.

(7) Li, H.; Zou, L.; Pan, L.; Sun, Z. Using Graphene Nano-Flakes as Electrodes to Remove Ferric Ions by Capacitive Deionization. *Sep. Purif. Technol.* **2010**, *75* (1), 8–14.

(8) Hou, C.-H.; Huang, C.-Y. A Comparative Study of Electrosorption Selectivity of Ions by Activated Carbon Electrodes in Capacitive Deionization. *Desalination* **2013**, *314*, 124–129.

(9) Marder, L.; Sulzbach, G. O.; Bernardes, A. M.; Ferreira, J. Z. Removal of Cadmium and Cyanide from Aqueous Solutions through Electrodialysis. *J. Braz. Chem. Soc.* **2003**, *14*, 610–615.

(10) Nataraj, S. K.; Hosamani, K. M.; Aminabhavi, T. M. Potential Application of an Electrodialysis Pilot Plant Containing Ion-Exchange Membranes in Chromium Removal. *Desalination* **2007**, *217* (1), 181–190.

(11) Luo, T.; Abdu, S.; Wessling, M. Selectivity of Ion Exchange Membranes: A Review. *J. Membr. Sci.* **2018**, *555*, 429–454.

(12) Khoiruddin; Ariono, D.; Subagjo; Wenten, I. G. Surface Modification of Ion-Exchange Membranes: Methods, Characteristics, and Performance. *J. Appl. Polym. Sci.* **2017**, *134* (48), 45540.

(13) Cheng, C.; White, N.; Shi, H.; Robson, M.; Bruening, M. L. Cation Separations in Electrodialysis through Membranes Coated with Polyelectrolyte Multilayers. *Polymer* **2014**, *55* (6), 1397–1403.

(14) White, N.; Misovich, M.; Yaroshchuk, A.; Bruening, M. L. Coating of Nafion Membranes with Polyelectrolyte Multilayers to Achieve High Monovalent/Divalent Cation Electrodialysis Selectivities. *ACS Appl. Mater. Interfaces* **2015**, *7* (12), 6620–6628.

(15) Tuan Le, X.; Viel, P.; Jégou, P.; Garcia, A.; Berthelot, T.; Hao Bui, T.; Palacin, S. Diazonium - Induced Anchoring Process: An Application to Improve the Monovalent Selectivity of Cation Exchange Membranes. *J. Mater. Chem.* **2010**, *20* (18), 3750–3757.

(16) Avci, A. H.; Sarkar, P.; Tufa, R. A.; Messana, D.; Argurio, P.; Fontananova, E.; Di Profio, G.; Curcio, E. Effect of Mg2+ Ions on Energy Generation by Reverse Electrodialysis. *J. Membr. Sci.* **2016**, *520*, 499–506.

(17) Stair, J. L.; Harris, J. J.; Bruening, M. L. Enhancement of the Ion-Transport Selectivity of Layered Polyelectrolyte Membranes through Cross-Linking and Hybridization. *Chem. Mater.* **2001**, *13* (8), 2641–2648.

(18) Bruening, M. L.; Sullivan, D. M. Enhancing the Ion-transport Selectivity of Multilayer Polyelectrolyte Membranes. *Chem. Eur. J.* **2002**, *8* (17), 3832–3837.

(19) Cheng, C.; Yaroshchuk, A.; Bruening, M. L. Fundamentals of Selective Ion Transport through Multilayer Polyelectrolyte Membranes. *Langmuir* **2013**, *29* (6), 1885–1892.

(20) Mizutani, Y. Ion Exchange Membranes with Preferential Permselectivity for Monovalent Ions. *J. Membr. Sci.* **1990**, *54* (3), 233–257.

(21) Farhat, T. R.; Schlenoff, J. B. Ion Transport and Equilibria in Polyelectrolyte Multilayers. *Langmuir* **2001**, *17* (4), 1184–1192.

(22) Güler, E.; van Baak, W.; Saakes, M.; Nijmeijer, K. Monovalent-Ion-Selective Membranes for Reverse Electrodialysis. *J. Membr. Sci.* **2014**, *455*, 254–270.

(23) Li, Y.; Xu, T. Permselectivities of Monovalent Anions through Pyridine-Modified Anion-Exchange Membranes. *Sep. Purif. Technol.* **2008**, *61* (3), 430–435.

(24) Nagarale, R.; Gohil, G.; Shahi, V. K. Recent Developments on Ion-Exchange Membranes and Electro-Membrane Processes. *Adv. Colloid Interface Sci.* **2006**, *119* (2–3), 97–130.

(25) Sata, T. Studies on Ion Exchange Membranes with Permselectivity for Specific Ions in Electrodialysis. *J. Membr. Sci.* **1994**, *93* (2), 117–135.

(26) Nagarale, R.; Gohil, G.; Shahi, V. K.; Rangarajan, R. Preparation and Electrochemical Characterizations of Cation-Exchange Membranes with Different Functional Groups. *Colloids Surf. Physicochem. Eng. Asp.* **2004**, *251* (1–3), 133–140.

(27) Xi, J.; Wu, Z.; Teng, X.; Zhao, Y.; Chen, L.; Qiu, X. Self-Assembled Polyelectrolyte Multilayer Modified Nafion Membrane with Suppressed Vanadium Ion Crossover for Vanadium Redox Flow Batteries. *J. Mater. Chem.* **2008**, *18* (11), 1232–1238.

(28) Sivaraman, P.; Chavan, J. G.; Thakur, A. P.; Hande, V. R.; Samui, A. B. Electrochemical Modification of Cation Exchange Membrane with Polyaniline for Improvement in Permselectivity. *Electrochimica Acta* **2007**, *52* (15), 5046–5052.

(29) Vaselbehagh, M.; Karkhanechi, H.; Takagi, R.; Matsuyama, H. Surface Modification of an Anion Exchange Membrane to Improve the Selectivity for Monovalent Anions in Electrodialysis – Experimental Verification of Theoretical Predictions. *J. Membr. Sci.* **2015**, *490*, 301–310.

(30) Farrokhzad, H.; Moghbeli, M. R.; Van Gerven, T.; Van der Bruggen, B. Surface Modification of Composite Ion Exchange Membranes by Polyaniline. *React. Funct. Polym.* **2015**, *86*, 161–167.

(31) Sata, T.; Sata, T.; Yang, W. Studies on Cation-Exchange Membranes Having Permselectivity between Cations in Electrodialysis. *J. Membr. Sci.* **2002**, *206* (1), 31–60.

(32) Sata, T. Studies on Anion Exchange Membranes Having Permselectivity for Specific Anions in Electrodialysis — Effect of Hydrophilicity of Anion Exchange Membranes on Permselectivity of Anions. *J. Membr. Sci.* **2000**, *167* (1), 1–31.

(33) Merle, G.; Wessling, M.; Nijmeijer, K. Anion Exchange Membranes for Alkaline Fuel Cells: A Review. *J. Membr. Sci.* **2011**, *377* (1–2), 1–35.

(34) Varcoe, J. R.; Atanassov, P.; Dekel, D. R.; Herring, A. M.; Hickner, M. A.; Kohl, P. A.; Kucernak, A. R.; Mustain, W. E.; Nijmeijer, K.; Scott, K. Anion-Exchange Membranes in Electrochemical Energy Systems. *Energy Environ. Sci.* **2014**, *7* (10), 3135–3191.

(35) Yan, X.; Gu, S.; He, G.; Wu, X.; Zheng, W.; Ruan, X. Quaternary Phosphonium-Functionalized Poly (Ether Ether Ketone) as Highly Conductive and Alkali-Stable Hydroxide Exchange Membrane for Fuel Cells. *J. Membr. Sci.* **2014**, *466*, 220–228.

(36) Noonan, K. J.; Hugar, K. M.; Kostalik IV, H. A.; Lobkovsky, E. B.; Abruña, H. D.; Coates, G. W. Phosphonium-Functionalized Polyethylene: A New Class of Base-Stable Alkaline Anion Exchange Membranes. *J. Am. Chem. Soc.* **2012**, *134* (44), 18161–18164.

(37) Qiu, B.; Lin, B.; Si, Z.; Qiu, L.; Chu, F.; Zhao, J.; Yan, F. Bis-Imidazolium-Based Anion-Exchange Membranes for Alkaline Fuel Cells. *J. Power Sources* **2012**, *217*, 329–335.

(38) Zhao, Y. H.; Abraham, M. H.; Zissimos, A. M. Fast Calculation of van Der Waals Volume as a Sum of Atomic and Bond Contributions and Its Application to Drug Compounds. *J. Org. Chem.* **2003**, *68* (19), 7368–7373.

(39) Bondi, A. Van Der Waals Volumes and Radii. *J. Phys. Chem.* **1964**, *68* (3), 441–451.

(40) E. Housecroft, C.; Jenkins, H. D. B. Absolute Ion Hydration Enthalpies and the Role of Volume within Hydration Thermodynamics. *RSC Adv.* **2017**, *7* (45), 27881–27894.

(41) Marcus, Y. *Ion Properties*; CRC Press, 1997.

(42) Epsztein, R.; Shaulsky, E.; Qin, M.; Elimelech, M. Activation Behavior for Ion Permeation in Ion-Exchange Membranes: Role of Ion Dehydration in Selective Transport. *J. Membr. Sci.* **2019**, *580*, 316–326.

(43) Imai, Y.; Tokiwa, Y.; Ueno, S.; Tanida, H.; Watanabe, I.; Matsubara, H.; Takiue, T.; Aratono, M. Effect of the Headgroup Structure on Counterion Binding in Adsorbed Surfactant Films Investigated by Total Reflection X-Ray Absorption Fine Structure Spectroscopy. *Bull. Chem. Soc. Jpn.* **2018**, *91* (10), 1487–1494.

(44) F. Parsons, D.; Boström, M.; Lo Nostro, P.; W. Ninham, B. Hofmeister Effects: Interplay of Hydration, Nonelectrostatic Potentials, and Ion Size. *Phys. Chem. Chem. Phys.* **2011**, *13* (27), 12352–12367.

(45) Lo Nostro, P.; Ninham, B. W. Hofmeister Phenomena: An Update on Ion Specificity in Biology. *Chem. Rev.* **2012**, *112* (4), 2286–2322.

(46) Vlachy, N.; Jagoda-Cwiklik, B.; Vácha, R.; Touraud, D.; Jungwirth, P.; Kunz, W. Hofmeister Series and Specific Interactions of Charged Headgroups with Aqueous Ions. *Adv. Colloid Interface Sci.* **2009**, *146* (1), 42–47.

(47) Collins, K. D. Ions from the Hofmeister Series and Osmolytes: Effects on Proteins in Solution and in the Crystallization Process. *Methods* **2004**, *34* (3), 300–311.

(48) Xu, L.; Li, X.; Zhai, M.; Huang, L.; Peng, J.; Li, J.; Wei, G. Ion-Specific Swelling of Poly(Styrene Sulfonic Acid) Hydrogel. *J. Phys. Chem. B* **2007**, *111* (13), 3391–3397.

(49) Schwierz, N.; Horinek, D.; Netz, R. R. Anionic and Cationic Hofmeister Effects on Hydrophobic and Hydrophilic Surfaces. *Langmuir* **2013**, *29* (8), 2602–2614.

(50) Schneider, H.-J. Binding Mechanisms in Supramolecular Complexes. *Angew. Chem. Int. Ed.* **2009**, *48* (22), 3924–3977.

(51) Smith, D. W. Ionic Hydration Enthalpies. *J. Chem. Educ.* **1977**, *54* (9), 540.

(52) Kingsbury, R. S.; Flotron, S.; Zhu, S.; Call, D. F.; Coronell, O. Junction Potentials Bias Measurements of Ion Exchange Membrane Permselectivity. *Environ. Sci. Technol.* **2018**, *52* (8), 4929–4936.

(53) Geise, G. M.; Cassady, H. J.; Paul, D. R.; Logan, B. E.; Hickner, M. A. Specific Ion Effects on Membrane Potential and the Permselectivity of Ion Exchange Membranes. *Phys Chem Chem Phys* **2014**, *16* (39), 21673–21681.

(54) Ji, Y.; Luo, H.; Geise, G. M. Specific Co-Ion Sorption and Diffusion Properties Influence Membrane Permselectivity. *J. Membr. Sci.* **2018**, *563*, 492–504.

(55) Helfferich, F. G. *Ion Exchange*; Courier Corporation, 1995.

(56) Tanaka, Y. *Ion Exchange Membranes: Fundamentals and Applications*, 2nd ed.; Elsevier: Amsterdam, 2015.

(57) Geise, G. M.; Lee, H.; Miller, D. J.; Freeman, B. D.; McGrath, J. E.; Paul, D. R. Water Purification by Membranes: The Role of Polymer Science. *J. Polym. Sci. Part B Polym. Phys.* **2010**, *48* (15), 1685–1718.

(58) Lide, D. R. *Handbook of Chemistry and Physics*; CRC Press, 2003.

(59) Salis, A.; W. Ninham, B. Models and Mechanisms of Hofmeister Effects in Electrolyte Solutions, and Colloid and Protein Systems Revisited. *Chem. Soc. Rev.* **2014**, *43* (21), 7358–7377.

(60) Collins, K. D. Charge Density-Dependent Strength of Hydration and Biological Structure. *Biophys. J.* **1997**, *72* (1), 65–76.

(61) Marcus, Y.; Hefter, G. Ion Pairing. *Chem. Rev.* **2006**, *106* (11), 4585–4621.

Chapter 8: Conclusions and Recommendations

This dissertation has provided knowledge of characterizing and optimizing the apparent permselectivity of IEMs for specific ions that are different from sodium and chloride. The ion specific permselectivity and transport behavior has been studied from the experimental, ion-specific and membrane polymer chemistry – specific perspectives. This chapter summarized the results of Chapters 5 through 7 and provided recommendations for future research.

8.1. Conclusions

In chapter 5, experiments and error propagation analysis were performed to quantify the influence of three experimental factors, i.e., temperature variations, concentration deviations and electric potential fluctuations, on apparent permselectivity measurement inaccuracy. Of the three factors considered, the influence of temperature variations was the greatest. Apparent permselectivity decreased by approximately 2% as the temperature increased from 14 to 31ºC. Second, the membrane potential fluctuations were found to contribute 0.2% to 0.5% uncertainty to membrane permselectivity measurement. Finally, the influence of solution preparation errors was found to be the smallest and contributed approximately 0.015% to 0.1% to apparent permselectivity uncertainty. In addition, thinner membrane is more sensitive to insufficient supply of fresh solution and requires a higher flow rate of fresh solution to maintain constant concentration of solutions in both chambers. None of these issues introduced uncertainty that is larger than the replicate uncertainty that came from disassembling and reassembling the measurement cell between multiple measurements on a given sample (approximately 2%). Generally, the influence of these three experimental factors on permselectivity is small and comparable to the magnitude of variability between different replicate measurements. Therefore, the uncertainty introduced by the three issues is not large enough to overwhelm the difference in permselectivity that can potentially be originated from the nature of the membrane or ion.

In chapter 6, the permselectivity of two commercially available and a lab-prepared CEMs (Selemion CMV, CMI-7000s and XLAMPS, respectively) were characterized using four monovalent strong electrolytes with different co-ions, i.e., sodium chloride, sodium bromide, sodium nitrate and sodium perchlorate. The co-ion sorption and diffusion coefficients of the XLAMPS, and the co-ion sorption coefficients of non-charged XLPEGDA were measured. Ion-specific permselectivity properties were observed for the three CEMs considered in this study, using four monovalent strong electrolytes (NaCl, NaBr, $NaNO_3$ and $NaClO_4$), and such phenomena resulted from a combination of co-ion specific sorption and diffusion effects, though sorption effects appear to be more significant than diffusion effects. Generally, increase in either co-ion sorption or diffusion coefficients cause a reduction in permselectivity. Three models were used to investigate the influence of different ion-specific parameters on ion sorption coefficient. The Manning's model showed reasonable agreement with experimental chloride sorption but failed to qualitatively predict the bromide and nitrate sorption coefficients. Electrostatic and dispersion models captured some qualitative ion specific sorption trend suggesting that co-ion charge density and polarizability contribute to ion specific sorption properties. However, none of the models provided quantitative agreement. The lack of agreement was likely due to a combination of the continuum nature of these models as the sensitivity of the model to membrane dielectric properties (i.e., dielectric constant and optical dielectric constant) that were required in the calculations. The comparison between Mackie and Meares and Manning predicted diffusion coefficients and experimental diffusion coefficients showed that polymer tortuosity effects on co-ion diffusion appeared to be more significant than the electrostatic effects. Additionally, co-ion with larger hydrated radius tends to diffuse slower, and diffusion of non-spherical ions may be more restricted compared to non-spherical ions. Finally, an ion-polymer complexation phenomenon was detected involving perchlorate and ethylene oxide repeat units in XLAMPS. Such complexation appears to increase ion sorption and reduce ion diffusion properties.

Two lab-prepared AEMs with different fixed charge group type, i.e., trimethyl ammonium and 1,4-dimethyl imidazolium, were used in Chapter 10. The permselectivity and ion transport properties of the two

AEMs were characterized using electrolytes having different co-ions, i.e., lithium chloride, sodium chloride and ammonium chloride, and electrolytes with different counter-ions, i.e., sodium chloride, sodium bromide and sodium nitrate. AEM with less hydrophilic fixed charge group was found to show lower water uptake, larger permselectivity and more effective co-ion exclusion under similar *IEC*, as compared to AEM with more hydrophilic fixed charge group. The fixed charge group type introduced up to 6% difference in permselectivity, much as pronounced as compared to the influence of co-ion type (about 18%) and of similar magnitude as compared to the influence of counter-ion type (up to 5%). The difference in permselectivity was found to result from the difference in sorption or diffusion effects. Moreover, the specific binding between counter-ion and fixed charge group with matching water affinities was hypothesized to restrict counter-ion diffusion and reduce the diffusion coefficient.

8.2. Significance

The quantification of the permselectivity measurement inaccuracy from three major experimental factors in Chapter 5, for the first time, provided reliable evidence informing the field of the expected magnitude of experimental errors for permselectivity. The results from Chapter 6 closed a knowledge gap in the field regarding how the ion specific parameters, such as ion size, polarizability and complexation-forming nature, affect ion transport within membrane phase as well as membrane permselectivity performance. The results from Chapter 7 filled another knowledge gap regarding how much permselectivity enhancement can be achieved through modifying the fixed charge group type of AEMs. Chapter 5 set the analytical foundation for Chapters 6 and 7, and the results from Chapters 6 and 7 can be applied to guide the design, engineering and optimization of novel ion specific selective membrane for a wide range of electro-membrane applications in aqueous systems.

8.3. Recommendations for Future Work

8.3.1. Continued Research on the Influence of Fixed Charge Group Type on AEM Performance with Diverse Cationic Groups

The research in the Chapter 7 of this dissertation focused on AEMs with two fixed charge groups, i.e., trimethyl ammonium and 1,4-dimethyl imidazolium. Although it has been demonstrated that the switching from trimethyl ammonium to 1,4-dimethyl imidazolium can only introduce minor enhancement (less than 6%) in permselectivity, there are a wider library of cationic groups for AEMs remained unexplored,[1–4] especially in the aqueous electro-membrane systems. A research on the influence of fixed charge group type on the separation performance of AEMs with diverse cationic groups, especially cationic groups possessing more pronounced property difference, will be beneficial to explore options on enhancing AEMs performance through modifying fixed charge group chemistry.

8.3.2. Developing Characterization Systems for Mixed Electrolytes

The results of this research were all obtained within single electrolyte systems, i.e., the aqueous solutions used in this research only contain one type of electrolytes. However, IEMs are often exposed to systems containing mixed electrolytes. For example, ions such as Na^+, Cl^-, Mg^{2+}, Br^-, and NO_3^- co-exist in sea water, and the IEMs used in RO or ED desalination processes are exposed to such mixed systems.[5–7] Moreover, in all vanadium redox flow batteries, at least seven different ions are presented in the system, i.e., V^{3+}, V^{2+}, VO^{2+}, VO_2^+, H^+, SO_4^{2-} and HSO_4^-.[8–10] The IEMs used in all vanadium redox flow battery system, will therefore be exposed to such system. Developing fundamental characterization system to understand the separation and ion transport properties of IEMs in systems having mixed electrolytes will provide more accurate guidance on optimizing those electro-membrane systems.

8.3.3. Research on Membrane Counter-ion Selectivity

The entire scope of this research is related with the permselectivity properties of IEMs, i.e., the ability of an IEM to selectively transport counter-ions but exclude co-ions. However, another important property of IEMs, the counter-ion selectivity, has not yet been explored. The counter-ion selectivity is defined as the ability of an IEM to selectively transport a certain ion from a group of ions containing charges of the same sign, e.g., K^+ from the mixed group of K^+ and Na^+. The counter-ion selectivity is as critical as permselectivity in determining the performance of many electro-membrane systems, especially the water deionization efficiency of ED[11–15] and the coulombic efficiency of RFB.[9,16,17] Additional research on understanding and optimizing the counter-ion selectivity, is therefore necessary.

8.4. References

(1) Varcoe, J. R.; Atanassov, P.; Dekel, D. R.; Herring, A. M.; Hickner, M. A.; Kohl, P. A.; Kucernak, A. R.; Mustain, W. E.; Nijmeijer, K.; Scott, K. Anion-Exchange Membranes in Electrochemical Energy Systems. *Energy Environ. Sci.* **2014**, *7* (10), 3135–3191.

(2) Merle, G.; Wessling, M.; Nijmeijer, K. Anion Exchange Membranes for Alkaline Fuel Cells: A Review. *J. Membr. Sci.* **2011**, *377* (1–2), 1–35.

(3) Yan, X.; Gu, S.; He, G.; Wu, X.; Zheng, W.; Ruan, X. Quaternary Phosphonium-Functionalized Poly (Ether Ether Ketone) as Highly Conductive and Alkali-Stable Hydroxide Exchange Membrane for Fuel Cells. *J. Membr. Sci.* **2014**, *466*, 220–228.

(4) Ran, J.; Wu, L.; Varcoe, J. R.; Ong, A. L.; Poynton, S. D.; Xu, T. Development of Imidazolium-Type Alkaline Anion Exchange Membranes for Fuel Cell Application. *J. Membr. Sci.* **2012**, *415*, 242–249.

(5) Javanmardi, J.; Moshfeghian, M. Energy Consumption and Economic Evaluation of Water Desalination by Hydrate Phenomenon. *Appl. Therm. Eng.* **2003**, *23* (7), 845–857.

(6) Han, L.; Galier, S.; Balmann, H. R. Ion Hydration Number and Electro-Osmosis during Electrodialysis of Mixed Salt Solution. *Desalination* **2015**, *373*, 38–46.

(7) Mariah, L.; Buckley, C. A.; Brouckaert, C. J.; Curcio, E.; Drioli, E.; Jaganyi, D.; Ramjugernath, D. Membrane Distillation of Concentrated Brines—Role of Water Activities in the Evaluation of Driving Force. *J. Membr. Sci.* **2006**, *280* (1), 937–947.

(8) Skyllas-Kazacos, M.; Chakrabarti, M. H.; Hajimolana, S. A.; Mjalli, F. S.; Saleem, M. Progress in Flow Battery Research and Development. *J. Electrochem. Soc.* **2011**, *158* (8), R55–R79.

(9) Weber, A. Z.; Mench, M. M.; Meyers, J. P.; Ross, P. N.; Gostick, J. T.; Liu, Q. Redox Flow Batteries: A Review. *J. Appl. Electrochem.* **2011**, *41* (10), 1137.

(10) Rychcik, M.; Skyllas-Kazacos, M. Characteristics of a New All-Vanadium Redox Flow Battery. *J. Power Sources* **1988**, *22* (1), 59–67.

(11) Rubinstein, I. Theory of Concentration Polarization Effects in Electrodialysis on Counter-Ion Selectivity of Ion-Exchange Membranes with Differing Counter-Ion Distribution Coefficients. *J. Chem. Soc. Faraday Trans.* **1990**, *86* (10), 1857–1861.

(12) Luo, T.; Abdu, S.; Wessling, M. Selectivity of Ion Exchange Membranes: A Review. *J. Membr. Sci.* **2018**, *555*, 429–454.

(13) Sata, T. Studies on Ion Exchange Membranes with Permselectivity for Specific Ions in Electrodialysis. *J. Membr. Sci.* **1994**, *93* (2), 117–135.

(14) Sata, T.; Sata, T.; Yang, W. Studies on Cation-Exchange Membranes Having Permselectivity between Cations in Electrodialysis. *J. Membr. Sci.* **2002**, *206* (1), 31–60.

(15) Tedesco, M.; Hamelers, H. V. M.; Biesheuvel, P. M. Nernst-Planck Transport Theory for (Reverse) Electrodialysis: I. Effect of Co-Ion Transport through the Membranes. *J. Membr. Sci.* **2016**, *510*, 370–381.

(16) Alotto, P.; Guarnieri, M.; Moro, F. Redox Flow Batteries for the Storage of Renewable Energy: A Review. *Renew. Sustain. Energy Rev.* **2014**, *29*, 325–335.

(17) Prifti, H.; Parasuraman, A.; Winardi, S.; Lim, T. M.; Skyllas-Kazacos, M. Membranes for Redox Flow Battery Applications. *Membranes* **2012**, *2* (2), 275–306.

Appendix A: List of Symbols

Table A.1. Nomenclature

IEC	Ion Exchange Capacity
α	Apparent Membrane Permselectivity
t_M^m	Counter-ion Transport Number in Membrane Phase
t_M^s	Counter-ion Transport Number in Solution Phase
t_X^m	Co-ion Transport Number in Membrane Phase
t_X^s	Co-ion Transport Number in Solution Phase
z_i	Valence of Ion *i*
D_i^j	Diffusivity of Ion *i* in phase *j*
M_n	Molecular Weight of Monomers and Polymers
n	Number of Repeating Units of Functional Groups of Polymer
k_X^m	Co-ion Sorption Coefficient
c_X^m	Co-ion Concentration in Membrane Phase
c_X^s	Co-ion Concentration in Solution Phase
$\gamma_\pm^s$	Averaged Ionic Activity Coefficient in Solution
$\gamma_\pm^m$	Averaged Ionic Activity Coefficient in Membrane
c_A^m	Membrane Fixed Charge Group Concentration
c_s^s	Solution Concentration
ξ	Dimensionless Parameter of Counter-ion Condensation Model
λ_B	Bjerrum Length
b	Distance Between Fixed Charge Groups on Polymer Chain
e	Elementary Charge
ε_0	Vacuum Permittivity
$\varepsilon_m(0)$	Constant Relative Permittivity of Membrane
T	Temperature
X	Ratio of Fixed Charge Group Concentration to Mobil Salt Concentration in Membrane
ΔG_i	Free Energy Change of Moving an Ion from the Solution to the Membrane Phase
ΔW_i	Born Solvation Energy
$\varepsilon_{sol}(0)$	Constant Relative Permittivity of Solution
$\alpha_m^*(i\omega_n)$	Excess Polarizability of an Ion in the Membrane
$\alpha_{sol}^*(i\omega_n)$	Excess Polarizability of an Ion in the Solution
$\varepsilon_m(i\omega_n)$	Frequency-dependent Relative Permittivity Function of the Membrane
$\varepsilon_{sol}(i\omega_n)$	Frequency-dependent Relative Permittivity Function of the Solution
a_i	Bare Ion Radius
k_w	Water Sorption Coefficient in Membrane
c_1, c_2	Numerical Parameters
ρ_p	Dry Density of Polymeric Membrane
m_1	Membrane Dry Mass in Air
m_2	Membrane Mass in Auxiliary Liquid
ρ_1	Density of Air

ρ_2	Density of Auxiliary Liquid
w_u	Membrane Water Uptake
m_{wet}	Membrane Wet Mass
m_{dry}	Membrane Dry Mass
ϕ_w	Membrane Water Volume Fraction
ρ_w	Water Density
v_E	Volume of Sodium Nitrate Used in Titration
c_E	Concentration of Sodium Nitrated Used in Titration
δ	Membrane Thickness
M_t	Concentration of Desorption Solution at Time t
M_∞	Concentration of Desorption Solution at Infinite Time
v_d	Volume of Desorption Solution
v_p	Volume of Dry Membrane Sample
E_m	Membrane Potential
R	Ideal Gas Constant
F	Faraday’s Constant
$a_\pm^{sL}$	Ion Activity of the High Concentration Solution
$a_\pm^{s0}$	Ion Activity of the Low Concentration Solution
E_x	Electrical Potential
E_{offset}	Electrode Offset Potential
c_0	Concentration of the Low Concentration Side of the Membrane
c_L	Concentration of the High Concentration Side of the Membrane
σ_{m+s}^s	Membrane Ionic Conductivity in Solution
R_{m+s}	Resistance of Membrane and Solution
R_s	Resistance of Solution
A	Membrane Area
τ	Solution Residence Time
t_{diff}	Diffusion Time Scale
V_c	Volume of the Permselectivity Measurement Chamber
f	Solution Flow Rate
$k_{X/M}^m$	Concentration Ratio of Co-ion Relative to Counter-ion in the Membrane Phase
$D_{X/M}^m$	Diffusivity Ratio of Co-ion Relative to Counter-ion in the Membrane Phase

Table A.2. Subscripts and Superscripts

X	Co-ion
M	Counter-ion
L	High Concentration Side
0	Low Concentration Side
dry	Dry Polymer
wet	Wet Polymer
$diff$	Diffusion
A	Fixed Charge Groups
m	Membrane
p	Polymer
s	Solution
w	Water
vdw	Van Der Waals
hyd	Hydration

Appendix B: Supporting Information for Chapter 5

B.1. Temperature and Concentration Dependence of Solution Phase Properties

Calculation of the apparent permselectivity via Equation 5.1 relies on solution phase transport number and thermodynamic activity properties. These parameters are both inherently temperature and concentration dependent,[1] and Table B1 reports the transport number and solution activity values that were used to calculate apparent permselectivity throughout this work. Additionally, Table B1 reports representative E_m and apparent permselectivity data for the Selemion CMV membrane. The thermodynamic activity values in Table B1 were determined from activity coefficient data reported in the literature as a function of concentration and temperature, and the solution phase transport numbers at infinite dilution were determined using data reported in the literature as a function of temperature.[1,2]

Table B.1. Solution phase transport number and thermodynamic values used in the calculation of apparent permselectivity via Equation 5.1. Representative E_m and apparent permselectivity data are shown for the Selemion CMV membrane.

Temperature (°C)	Transport Numbers at Infinite Dilution [ref]		$a_{\pm}^{s0}$ (mol/L) [ref]	$a_{\pm}^{sL}$ (mol/L) [ref]	$\frac{RT}{F}\ln\left(\frac{a_{\pm}^{s0}}{a_{\pm}^{sL}}\right)$	E_m (mV)	Apparent Permselectivity
	t_M^s	t_X^s					
14.0	0.392	0.608	0.0780	0.340	36.4	36.8±0.2	1.009±0.005
17.2	0.394	0.606	0.0779	0.341	39.6	36.6±0.2	0.992±0.005
21.0	0.395	0.605	0.0779	0.341	37.4	37.1±0.4	0.993±0.010
26.0	0.397	0.603	0.0778	0.341	38.1	37.6±0.3	0.989±0.007
31.0	0.399	0.601	0.0777	0.341	38.8	38.0±0.1	0.984±0.001

The solution phase transport numbers at infinite dilution were used to calculate apparent permselectivity via Equation 5.1, and this approach neglects the transport number dependence on solution concentration. Concentration dependent transport number data for aqueous solutions of sodium chloride at 25°C have been reported (Figure B.1a),[3,4] and these data can be used to evaluate the influence of neglecting the concentration dependence of the transport numbers on apparent permselectivity (at a fixed temperature). Neglecting the concentration dependence of the solution phase transport numbers becomes a better assumption as the apparent permselectivity of the membrane increases (Figure B.1b). Above a membrane potential of 29mV (an approximate apparent permselectivity of 0.81), the uncertainty that is contributed by this assumption is within 1%. The analysis also suggests that neglecting the concentration dependence of the solution phase transport numbers is likely not an explanation for permselectivity values that exceed unity because the influence of the concentration dependence of the solution phase transport numbers on the apparent permselectivity is smallest in the limit where membrane potential approaches the potential calculated using the Nernst equation (i.e., as the apparent permselectivity approaches unity).

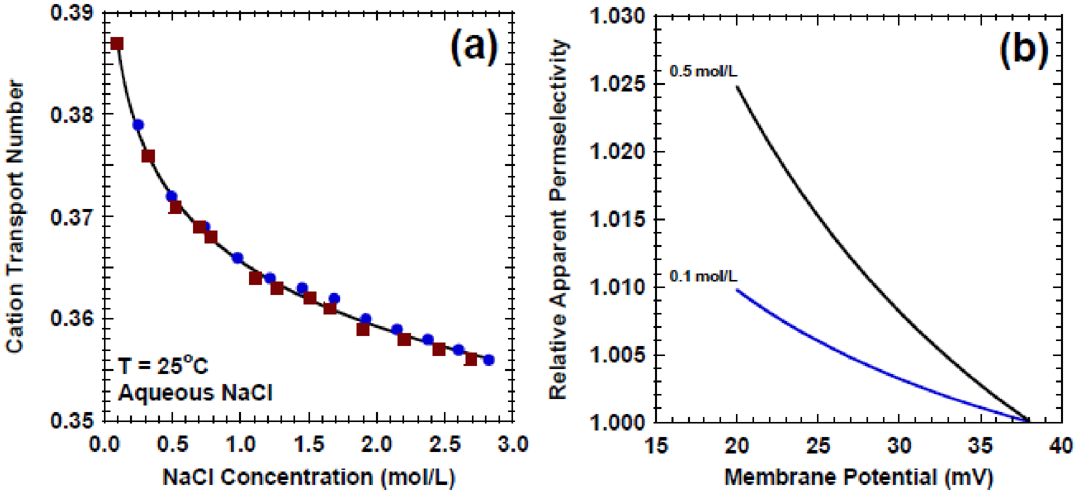

Figure B.1. (a) Sodium transport numbers measured at 25°C (data points: ■●) as a function of aqueous sodium chloride concentration (b) The influence of concentration dependence of solution phase transport numbers on apparent permselectivity calculation (via Equation 5.1) can be evaluated by defining the relative apparent permselectivity to be the apparent permselectivity value calculated at a specified salt concentration (either 0.1mol/L or 0.5mol/L) divided by the apparent permselectivity value calculated using the solution phase transport numbers at infinite dilution. The influence of the concentration dependence of the solution phase transport numbers on apparent permselectivity decreases as membrane potential increases (i.e., as apparent permselectivity increases)

B.2. Error Propagation Analysis and Sample Calculation

The contribution of uncertainty in the solution preparation process and the membrane potential measurement to the uncertainty in the apparent permselectivity were quantified using standard error propagation analysis applied to Equation 5.1.[5] The apparent permselectivity is a function of the membrane potential and solution phase thermodynamic activity values, i.e., $\alpha = f(E_m, a_\pm^{S0}, a_\pm^{SL})$. The uncertainty in the apparent permselectivity, $\Delta\alpha$, can be written as:

$$S_\alpha = \sqrt{\left(\frac{\partial f}{\partial E_m}\right)^2 \Delta E^2 + \left(\frac{\partial f}{\partial a_\pm^{s0}}\right)^2 \left(\Delta a_\pm^{s0}\right)^2 + \left(\frac{\partial f}{\partial a_\pm^{sL}}\right)^2 \left(\Delta a_\pm^{sL}\right)^2} \tag{B.1}$$

where ΔE describes the fluctuations in the measured membrane potential (cf. Figure 5.1), $\Delta a_\pm^{s0}$ is the uncertainty in the low concentration solution electrolyte activity, and $\Delta a_\pm^{sL}$ is uncertainty in the high concentration solution electrolyte activity. The Δ prefix is used throughout this discussion to represent the uncertainty in a variable. All error propagation analysis was performed relative to a base case apparent permselectivity measurement, which corresponded to the apparent permselectivity of Selemion CMV membrane at 21°C (cf. Table B.2):

Table B.2. Conditions used in the calculation.

Temperature: 21°C
High Concentration Solution: c_L = 0.5mol/L NaCl; Low Concentration Solution: c_0 = 0.1mol/L NaCl
$a_\pm^{sL}$ = 0.341; $a_\pm^{s0}$ = 0.078
t_M^s = 0.395; t_X^s = 0.605
Membrane Potential: E_m = 37.1mV
Membrane Apparent Permselectivity: α = 0.993

B.2.1. Error Propagation of the Solution Preparation Process

To calculate the data reported in Figure 5.4A, the influence of Δc_L on $\Delta\alpha$ was determined. For this analysis, $\Delta a_\pm^{s0}$ and ΔE was set equal to zero to isolate the influence of Δc_L (and, thus, $\Delta a_\pm^{sL}$) on $\Delta\alpha$. Values of $\Delta a_\pm^{sL}$ were determined from a series of Δc_L values ranging from -0.075mol/L to 0.075mol/L (i.e., up to a ±15% deviation from c_L = 0.5mol/L) under the assumption that the change in the activity coefficient over the concentration range of 0.5mol/L ± 0.075mol/L, which was calculated to be approximately 1.1%, was negligible:

$$\Delta a_{\pm}^{sL} \approx \gamma_{\pm}^{sL} \Delta c_L \tag{B.2}$$

where $\gamma_{\pm}^{sL}$ is the mean ionic activity coefficient for the high concentration solution (taken to be $\gamma_{\pm}^{sL}$ = 0.682). Finally, values of $\Delta\alpha$ were calculated using Equation B.1.

For example, consider Δc_L = 0.025mol/L; then $\Delta a_{\pm}^{sL}$ = 0.017 mol/L and $\Delta\alpha$ = 0.0277 (using Equation B.1 and B.2). Because $\Delta c_L > 0$, this example is a case where the difference in concentration between the solutions on either side of the membrane increases, so in Figure 5.4A, the values from this example are presented as 1.05 on the horizontal axis and $(\alpha+\Delta\alpha)/\alpha = 1.03$ on the vertical axis (the axes are normalized to the base case conditions described above).

The data reported in Figure 5.4B were calculated similarly. In this case, the influence of Δc_0 on $\Delta\alpha$ was determined. For this analysis, $\Delta a_{\pm}^{sL}$ and ΔE were set equal to zero to isolate the influence of Δc_0 (and, thus, $\Delta a_{\pm}^{s0}$) on $\Delta\alpha$. Values of $\Delta a_{\pm}^{s0}$ were determined from a series of Δc_0 values ranging from -0.015mol/L to 0.015mol/L (i.e., up to a ±15% deviation from c_0 = 0.1mol/L) under the assumption that the change in the activity coefficient over the concentration range of 0.1mol/L ± 0.015mol/L, which was calculated to be approximately 1.2%, was negligible:

$$\Delta a_{\pm}^{s0} \approx \gamma_{\pm}^{s0} \Delta c_0 \tag{B.3}$$

where $\gamma_{\pm}^{s0}$ is the mean ionic activity coefficient for the low concentration solution (taken to be $\gamma_{\pm}^{s0}$ = 0.779). Finally, values of $\Delta\alpha$ was calculated using Equation B.1.

For example, consider Δc_0 = 0.005mol/L, then $\Delta a_{\pm}^{s0}$ = 0.0039mol/L and $\Delta\alpha$ = 0.0277 (using Equation B.1 and B.3). Because $\Delta c_0 > 0$, this example is a case where the difference in concentration between the solutions on either side the membrane decreases, so in Figure 5.4B, the values from this example are presented as 1.05 on the horizontal axis and $(\alpha + \Delta\alpha) / \alpha = 1.03$ on the vertical axis (the axes are normalized to the base case conditions described above). In Figure 5.4B, the values from this example are represented as 1.05 on the horizontal axis and 0.972 on the vertical axis (the axes are normalized to the base case conditions described above)

The data reported in Figure 5.6 were calculated in an analogous fashion to the data reported in Figure 5.4. Similar to the examples given above, the values of ΔE and either $\Delta a_{\pm}^{sL}$ or $\Delta a_{\pm}^{s0}$ (depending on which solution was being considered) were set equal to zero to isolate the effect of salt mass deviations on either the high or low concentration solution. Calculations were performed to determine to what extent the apparent permselectivity would be affected by 0mg to 100mg sodium chloride required to prepare 1L of the 0.1mol/L or 0.5mol/L sodium chloride solutions. For example, when Δm was taken as 20mg, the corresponding values of Δc_L and Δc_0 were 0.0003mol/L. The analysis then proceeded as described above using Equation B.1, B.2 and B.3 to calculate $\Delta\alpha$ values of 0.0003 and 0.0017 for the high and low concentration solutions, respectively. Finally, the absolute values of $\Delta\alpha$ were normalized by α and reported in Figure 5.5.

B.2.2. Error Propagation of the Membrane Potential Measurement

To calculate the data reported in Figure 5.6, the influence of ΔE on $\Delta\alpha$ was determined. For this analysis, $\Delta a_{\pm}^{sL}$ and $\Delta a_{\pm}^{s0}$ were set equal to zero to isolate the influence of ΔE on $\Delta\alpha$. Values of ΔE were chosen to be in the range of -0.4mV to 0.4mV (i.e., up to a ± 1.1% deviation from $E_m = 37$mV), which was chosen to be a reasonable range based on experimentally observed fluctuations in the membrane potential measurement (cf. Figure 5.1). Finally, values of $\Delta\alpha$ were calculated using Equation B.1.

For example, when $\Delta E = 0.185$mV then $\Delta\alpha = 0.0041$ (using Equation B.1). In Figure 5.6, the values from this example are represented as 1.005 on the horizontal axis and 1.004 on the vertical axis (the axes are normalized to the base case conditions described above). Similar to the analysis described above for the data shown in Figure 5.6, values of $\Delta E > 0$ result in increases in permselectivity, while values of $\Delta E < 0$ result in decreases in permselectivity.

B.3. References

(1) Pitzer, K. S.; Peiper, J. C.; Busey, R. H. Thermodynamic Properties of Aqueous Sodium Chloride Solutions. *J Phys Chem Ref Data U. S.* **1984**, *13:1*.

(2) Robinson, R. A.; Stokes, R. H. *Electrolyte Solutions*; Courier Corporation, 2002.

(3) Braun, B. M.; Weingärtner, H. Transference Numbers of Aqueous NaCl and Na2SO4 at 25°C from EMF Measurements with Sodium-Selective Glass Electrodes. *J. Solut. Chem.* **1985**, *14* (9), 675–686.

(4) Panopoulos, D. K.; Kaneko, H.; Spiro, M. Transference Numbers of Sodium Chloride in Concentrated Aqueous Solutions and Chloride Conductances in Several Concentrated Electrolyte Solutions. *J. Solut. Chem.* **1986**, *15* (3), 243–252.

(5) Bevington, P. R.; Robinson, D. K.; Blair, J. M.; Mallinckrodt, A. J.; McKay, S. Data Reduction and Error Analysis for the Physical Sciences. *Comput. Phys.* **1993**, *7* (4), 415–416.

Appendix C: Supporting Information for Chapter 6

C.1. Discussion on the Influence of Co-Ion Sorption and Diffusion on Permselectivity

Co-ion sorption and diffusion in the membrane phase can be described using the co-ion sorption coefficient, K_X^m, and the co-ion diffusion coefficient, D_X^m, respectively. The sorption coefficient is defined generally as the ratio of the concentration of *i* in the membrane phase divided by the concentration of *i* in the solution phase, i.e., $k_i^m \equiv c_i^m / c_i^s$. Combining Equations 2.1 and 2.2 (from the main text) with the definition of k_i^m illustrates the effect of the co-ion sorption and diffusion coefficients on permeability:

$$\alpha = 1 - \frac{k_X^m D_{X/M}^m \left(1 + \frac{1}{D_{X/M}^s}\right)}{k_X^m D_{X/M}^m + k_A^m + k_X^m} \tag{C.1}$$

where $D_{X/M}^j$ is defined as the ratio of the co-ion diffusion coefficient, D_X^j, to the counter-ion diffusion coefficient, D_M^j (i.e., $D_{X/M}^j = D_X^j / D_M^j$). Additionally, the subscript *A* refers to fixed charges in the polymer.

Increases in co-ion sorption and diffusion coefficients cause a reduction in the apparent permselectivity (Figure C.1). This observation is consistent with the physical picture that both increased co-ion sorption and diffusivity are expected to enhance co-ion transport through the polymer. As such, understanding specific co-ion sorption and diffusion properties may be critical for understanding and ultimately controlling the ion specific apparent permselectivity properties of ion exchange membranes.

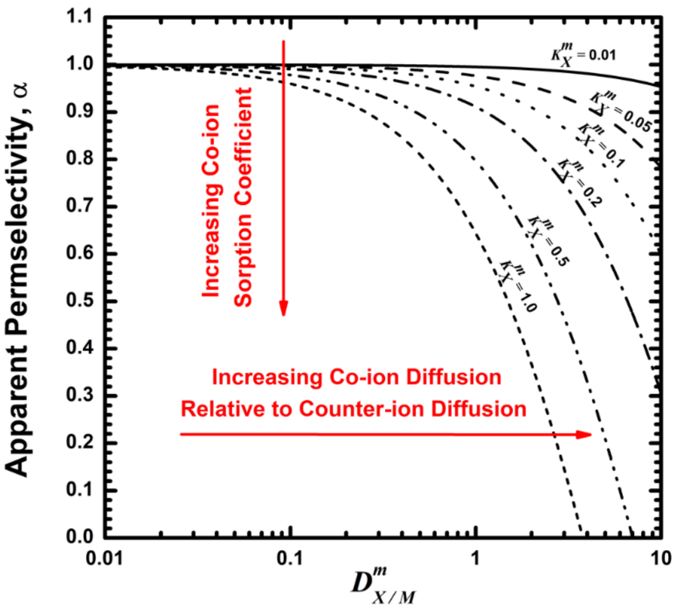

Figure C.1. Apparent permselectivity decreases with increasing K_X^m and increasing $D_{X/M}^m$ as calculated using Equation C.1. The lines of constant sorption coefficient were calculated by taking $D_{X/M}^s$ to be 0.54 (determined using sodium chloride diffusion coefficient values at infinite dilution[1]), c_A^m to be 3.0 eq/L(swollen polymer) (a typical value for CEMs[2]), and c_s^s to be 0.5 mol/L as this was one of the concentrations used in the experiments.

C.2. Membrane Permselectivity Data Analysis

Table C.1. Representative E_m and α values for XLAMPS. The measurements were made at room temperature (23±2°C), and the permselectivity, α was calculated at 23°C. The transport numbers were calculated using counter-ion and co-ion diffusion coefficients in aqueous solution at infinite dilution and 25°C.[1] The activity coefficients were calculated using Pitzer's model.[3]

Electrolyte	T (°C)	Transport Numbers at Infinite Dilution		$a_\pm^{so}$ (0.1 mol/L)	$a_\pm^{sL}$ (0.5 mol/L)	E_m (mV)	α
		t_M^S	t_x^S				
NaCl	23	0.396	0.604	0.0776	0.340	34.0±0.4	0.918±0.009
NaBr	23	0.398	0.602	0.0781	0.348	32.8±0.6	0.884±0.012
$NaNO_3$	23	0.412	0.588	0.0758	0.308	31.8±0.7	0.906±0.016
$NaClO_4$	23	0.426	0.574	0.0774	0.334	30.4±1.3	0.838±0.029

C.3. Influence of Junction Potentials on Apparent Permselectivity

The influence of electrochemical junction potentials on apparent permselectivity values has recently been reported. Due to the non-chloride nature of the electrolytes used in this study, it was not possible to eliminate the effect of the junction potentials from the measurement. The junction potentials, however, were estimated using a theoretical method based on the Henderson Equation.[4] The estimated junction potentials reduce the measured membrane potential by 2.2, 2.4, 1.6, and 1.4 mV for the sodium chloride, bromide, nitrate, and perchlorate electrolytes, respectively. As such, incorporating the estimated junction potentials into the apparent permselectivity calculation reduces the absolute value of the measured apparent permselectivity. The ion specific effects, however, are not significantly affected by incorporating the estimated junction potential values (Figure C.2).

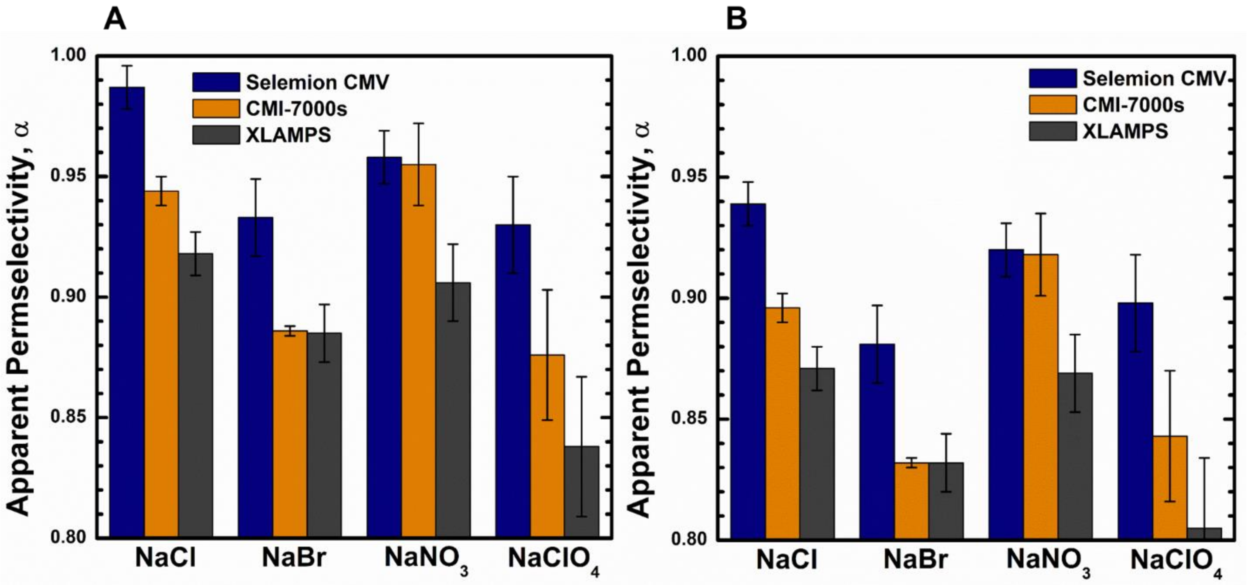

Figure C.2. Apparent permselectivity values for the three CEMs without incorporating an estimated liquid junction potential (A) and with incorporating an estimated liquid junction potential (B). The liquid junction potential was estimated using a theoretical approach based on the Henderson Equation.

C.4. Mean Ionic Activity Coefficients in the Membrane Phase

The measured equilibrium salt sorption coefficient data were combined with solution mean ionic activity values to determine the mean ionic activity coefficients for the electrolyte sorbed in the polymer $\gamma_\pm^m$ as:[5]

$$\gamma_\pm^m = (\gamma_M^m \gamma_X^m)^{1/2} = \left(\frac{\left(\gamma_\pm^s\right)^2 (c_s^s)^2}{c_M^m c_X^m}\right)^{1/2} \tag{C.2}$$

where γ_i^j and c_i^j are the activity coefficient and concentration, respectively, of ion, i, in phase j, $\gamma_\pm^s$ is the mean ionic activity coefficient of the electrolyte in solution (calculated using the Pitzer model), *M* refers to the counter-ion, *X* refers to the co-ion, *m* refers to the membrane phase, *s* refers to the solution phase, and *m,w* denotes the membrane phase concentration on the volume of sorbed water basis. The co-ion concentration in the membrane phase was measured experimentally, and the counter-ion concentration in the membrane phase was determined using the measured co-ion concentration and the fixed charge concentration in the polymer, c_A^m, which was determined from the ion exchange capacity, *IEC*, of the material as:[6,7]

$$c_M^m = c_A^m + c_X^m = \left(\frac{\mathrm{IEC}}{w_u}\rho_w\right) + c_X^m \tag{C.3}$$

The measured values of c_X^m and the calculated values of c_M^m, $\gamma_\pm^s$, and $\gamma_\pm^m$ are reported in Table C.2 for both of the external electrolyte solution concentrations (0.1 and 0.5 mol/L) used in this study.

Table C.2. Concentrations of co-ions and counter-ions in the XLAMPS membrane phase, solution phase mean ionic activity coefficients, and membrane phase mean ionic activity coefficients for the four electrolytes and two external solution concentrations (0.1 and 0.5 mol/L) used in this study.

Electrolytes	Membrane Phase Co-ion Concentration, c_X^m (mol/L (water))		Membrane Phase Counter-ion Concentration, c_M^m (mol/L (water))		Solution Phase Mean Ionic Activity Coefficient, $\gamma_\pm^s$		Membrane Phase Mean Ionic Activity Coefficient, $\gamma_\pm^m$	
	0.1 mol/L	0.5 mol/L	0.1 mol/L	0.5 mol/L	0.1 mol/L	0.5 mol/L	0.1 mol/L	0.5 mol/L
NaCl	0.004	0.080	1.364	1.440	0.776	0.680	1.051	1.002
NaBr	0.010	0.151	1.370	1.511	0.781	0.696	0.664	0.728
$NaNO_3$	0.012	0.153	1.372	1.513	0.758	0.616	0.594	0.641
$NaClO_4$	0.046	0.546	1.406	1.906	0.774	0.668	0.305	0.327

C.5. Estimation of the Manning's Parameter for XLAMPS

The dimensionless parameter, ξ, was needed to use Manning's counter-ion condensation theory. To calculate ξ for XLAMPS, the dielectric constant of the hydrated membrane, $\varepsilon_m(0)$, and the distance between fixed charge groups on the polymer chain, *b*, were needed (Equation 3.4 in the main text). The value of $\varepsilon_m(0)$, i.e., the constant relative permittivity of the hydrated polymer, was taken to be 40 using an empirical method that relates polymer water content with polymer dielectric constant.[8] The distance between fixed charges, *b*, was estimated based on the composition and the structure of the polymer.

XLAMPS is a crosslinked network, and fixed charge groups (on the AMPS monomer) can be located on different nodes of the network (Figure C.3). The fixed charge groups are connected by the crosslinker. For each fixed charge group, the adjacent fixed charge group can be attached on node A, B or C (Figure C.3). The likelihood of forming these three configurations was assumed to be equivalent as information to the contrary is not presently available. The final length of the repeat unit, *L*, was taken to be the average of these three configurations.

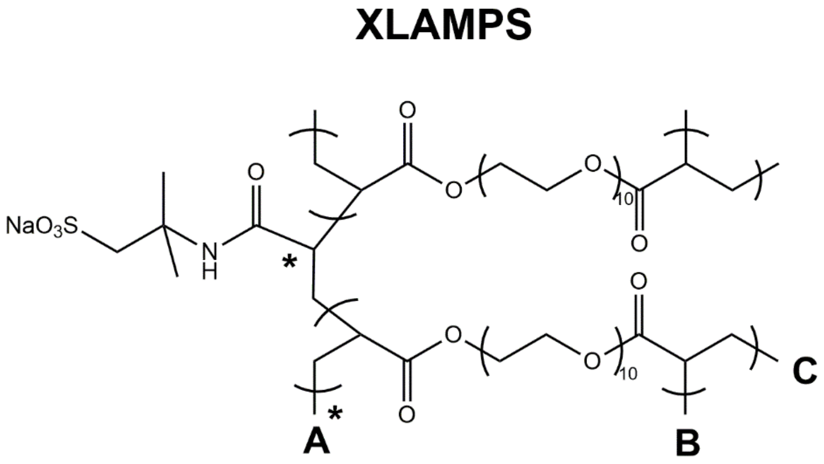

Figure C.3. Schematic illustration of the XLAMPS network structure.

In configuration A, there are four C-C covalent bonds between the two charged AMPS groups. Manning's theory assumes that the polymer is an infinitely long line charge, which requires the charged groups to be projected onto the polymer backbone (i.e., the two starred positions in Figure C.3) for the purpose of the calculation. In this situation, the length L is equal to the straight-line distance between the two starred positions, and it can be calculated using the number of C-C bonds, the C-C covalent bond length, *l*, and the bond angle, θ:

$$L = nl\sin\frac{\theta}{2} \tag{C.4}$$

where l is 1.53 Å, θ is 109.5^o for sp3 hybridized C-C covalent bond,[9] and b was calculated to be 5.0 Å for configuration A.

The estimation methods used for configuration B and C were the same as that use for configuration A. In configurations B and C, C-O and C=O bonds are also involved. The C-O bond length is 1.42 Å,[9] and the bond angle for the sp3 hybridized C-O covalent bond is 109.5^o. The sp2 hybridized C=O bond angel is 120^o.

The depiction of XLAMPS in Figure C.3 does not reflect the specific chemical composition of the material. In XLAMPS, the molar ratio of uncharged crosslinker, PEGDA (n=10), and charged monomer, AMPS, was determined to be 1.3, i.e., the network contains 1.3 uncharged crosslinker molecules per charged monomer. Assuming that AMPS and PEGDA are evenly distributed in the final XLAMPS material, there are an average of 2.3 crosslinker molecules between each charged group. The value of b was calculated as the product of number of crosslinker molecules between fixed charge groups (i.e., 2.3) and the length, L, i.e. b = 2.3L. The calculated values of L and b are presented in Table C.3.

Table C.3. Estimation of b and ξ. The bond lengths were obtained from the literature.[9]

Configuration Types	Bond Type				L (Å)	Average L (Å)	b (Å)	ξ
	θ = 109.5^o l = 1.53Å	θ = 109.5^o l = 1.42Å	θ = 120^o l = 1.53Å	θ = 120^o l = 1.42Å				
n in Configuration A	4	0	0	0	5.0			
n in Configuration B	22	13	2	2	47.7	33.8	77.4	0.18
n in Configuration C	22	14	2	2	48.8			

C.6. Modeling Parameters

To calculate the electrostatic energy using Born model, the ion radius, a_i, static dielectric constant of the membrane, $\varepsilon_m(0)$, and static dielectric constant of the solution, $\varepsilon_{sol}(0)$, must be evaluated. The ion radius, a_i, was taken as the bare ionic radius.[1] The static dielectric constant, $\varepsilon_m(0)$, of XLAMPS was taken as 40, using an empirical water volume fraction-based relationship based on measurements made using Nafion®.[8,10] The static dielectric constants of the electrolyte solutions (Table C.5) were obtained from the literature.

Table C.4. Static dielectric constant, $\varepsilon_{sol}(0)$, values at 20°C for the solutions used in this study.[11,12]

Solutions	NaCl		NaBr		$NaNO_3$		$NaClO_4$	
	0.1M	0.5M	0.1M	0.5M	0.1M	0.5M	0.1M	0.5M
$\varepsilon_{sol}(0)$	76	72	75	70	77	73	71	66

To calculate the dispersion energy, ΔD_i, the frequency-dependent relative permittivity for the solution, $\varepsilon_{sol}(i\omega_n)$, frequency-dependent excess ionic polarizability in the membrane and solution, $\alpha_m^*(i\omega_n)$ and $\alpha_{sol}^*(i\omega_n)$, respectively, and the frequency-dependent membrane relative permittivity, $\varepsilon_m(i\omega_n)$, must be known for frequencies greater than 1.23×10^{14} Hz.[13–16]

The function $\varepsilon_{sol}(i\omega_n)$ of all solutions were taken as that for water, $\varepsilon(i\omega_n)$,[17] due to the lack of available data for electrolyte solutions at different concentrations. This approximation therefore potentially neglects ion-specific properties of the external solution.

The frequency-dependent excess ionic polarizability in the membrane, $\alpha_m^*(i\omega_n)$, and in solution, $\alpha_{sol}^*(i\omega_n)$, were both modeled as the ionic excess polarizability in water, $\alpha^*(i\omega_n)$. This approximation was made due to the lack of ionic polarizability data measured in different solvents or polymers.[13] The function $\alpha^*(i\omega_n)$ can be evaluated using a single oscillator model with a single co-ion specific adsorption frequency, ω_I, using the London approximation:[13]

$$\alpha^*(i\omega_n) = \frac{\alpha^*(0)}{1+\omega_n^2/\omega_I^2} \tag{C.5}$$

where $\alpha^*(0)$ is the static ionic excess polarizability, ω_I is the ionic single adsorption frequency that can be calculated from the first ionization potential of the co-ion.[1] The bare ionic radii, a_i, used to calculate electrostatic and dispersion energy values and the $\alpha^*(0)$ and ω_I values used to calculate the dispersion energy are given in Table C.6.

Table C.5. Ion properties used to calculate the electrostatic and dispersion energy values

Ions	a_i (Å)[1]	$\alpha^*(0)$ (Å^3)[18]	ω_I (10^{16} Hz)[18]
Cl^-	1.81	3.40	1.97
Br^-	1.96	4.63	1.79
NO_3^-	1.79	4.92	1.58
ClO_4^-	2.20	5.14	2.13

The frequency-dependent membrane relative permittivity, $\varepsilon_m(i\omega_n)$, was modeled using a single oscillator model, which is a typical approach for hydrocarbon films:[19]

$$\varepsilon_m(i\omega_n) = 1 + \frac{\varepsilon_m^*(0)}{1+\left(\omega_n/_{10^{16}}\right)} \tag{C.6}$$

where 10^{16} is a typical approximation of the adsorption frequency for hydrocarbon membranes,[19] and $\varepsilon_m^*(0)$ is the relative permittivity of the membrane in the optical frequency range (i.e., optical dielectric constant). The value of $\varepsilon_m^*(0)$ can be determined using the refractive index *n* of the membrane:[19]

$$\varepsilon_m^*(0) = n^2 \tag{C.7}$$

The refractive index *n* in the optical frequency range can be calculated from measured reflectivity values, $\mathcal{R}$, using the formula:[20]

$$n = \frac{1+\sqrt{\mathcal{R}}}{1-\sqrt{\mathcal{R}}} \tag{C.8}$$

The reflectivity of a film-shaped sample in the optical frequency range was obtained using UV-vis spectroscopy. A Lambda 950s UV/Vis/NIR with an integrating sphere (Perkin Elmer) was used to measure the XLAMPS reflection spectrum. Samples for these measurements were equilibrated with DI water and cut into circular coupons with a diameter of 1.9 cm. Samples were removed from DI water, wiped quickly to remove surface water, and loaded into the instrument to collect four independent spectra. The spectra were measured over a wavelength range of 400 nm to 700 nm, and the scanning speed was 4.44 nm/s. The reflectivity was taken as the average value within this wavelength range, and *n* and $\varepsilon_m^*(0)$ were calculated as described above. The reported value of $\varepsilon_m^*(0)$ was an average of three measurements, and the uncertainty was taken as one standard deviation from the mean. The *n* and $\varepsilon_m^*(0)$ from the three measurements were presented in detail in next section.

C.7. UV-Vis Spectroscopy for XLAMPS

A Lambda 950s UV/Vis/NIR with an integrating sphere (Perkin Elmer) was used to measure the XLAMPS reflection spectrum. Samples for these measurements were equilibrated with DI water and cut into circular coupons with a diameter of 1.9 cm. Samples were removed from DI water, wiped quickly to remove surface water, and loaded into the instrument to collect four independent spectra. The spectra were measured over a wavelength range of 400 nm to 700 nm, and the scanning speed was 4.44 nm/s. The reflectivity was taken as the average value within this wavelength range, and *n* and $\varepsilon_m^*(0)$ were calculated as described in the main text. The reported value of $\varepsilon_m^*(0)$ was an average of three measurements, and the uncertainty was taken as one standard deviation from the mean. The refractive index *n* and optical dielectric constant, $\varepsilon_m^*(0)$, of XLAMPS were measured and the data from the three measurements are shown in Figure C.4.

The values of $\varepsilon_m^*(0)$ were determined by averaging over the measurements made at wavelengths ranging from 400 to 700 nm. The values from each measurement (i.e., first, second and third) were 3.1±0.1, 2.83±0.04 and 3.0±0.1, respectively. The values were averaged and standard error propagation was used to arrive at the value of $\varepsilon_m^*(0) = 3.0\pm0.1$.

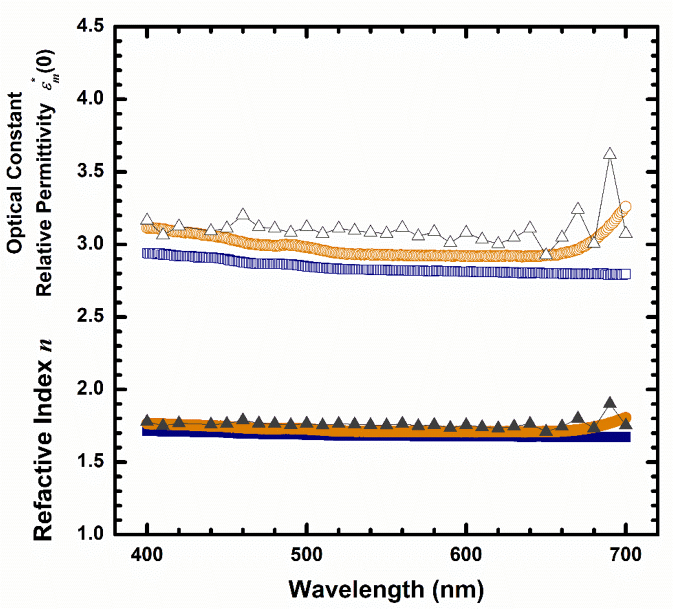

Figure C.4. Refractive index, n, for the first (▲), second (■), and third measurements (●), and optical relative permittivity, $\varepsilon_m^*(0)$, for the first (△), second (□), and third measurements (○). The first measurement was conducted in a different instrument than the second and third measurements.

C.8. Discussion of the Diffusion Assumption

The measured effective salt diffusion coefficient in XLAMPS, D_S^m, is related to the individual counter-ion and co-ion diffusion coefficients, D_M^m and D_X^m respectively, using the Nernst-Planck equation and a charge balance that reflects the charged nature of this cation exchange material:[6]

$$D_S^m = \frac{D_M^m D_X^m (c_M^m + c_X^m)}{D_M^m c_M^m + D_X^m c_X^m} \tag{C.9}$$

When the concentration of counter-ions (cations) in the polymer is much greater than the concentration of co-ions in the polymer (i.e., $c_M^m \gg c_X^m$), the effective salt diffusion coefficient in the membrane phase approaches that of the co-ion, i.e., $D_S^m \approx D_X^m$.[21] In many circumstances of practical interest, this approximation is reasonable for cation exchange materials since the concentration of counter-ions in the polymer often exceeds that of the co-ions by a substantial factor.

In the XLAMPS materials, the concentrations of counter-ions in the membrane, c_M^m, are at least one order of magnitude greater than the concentration of co-ions in the membrane, c_X^m, for sodium chloride, bromide, and nitrate (Table C.6). These results suggest that $c_M^m \gg c_X^m$ is a good assumption for XLAMPS exposed to these three electrolytes at the two concentrations considered.

Table C.6. The values of c_M^m/c_X^m for XLAMPS in equilibrium with either 0.1 or 0.5 mol/L aqueous solution of the four electrolytes considered.

Electrolyte	$c_M^{m,p}/c_X^{m,p}$	
	0.1 mol/L	0.5 mol/L
NaCl	407	18
NaBr	136	10
$NaNO_3$	115	10
$NaClO_4$	31	4

C.9. References

(1) Marcus, Y. *Ion Properties*; CRC Press, 1997.

(2) Xu, T. Ion Exchange Membranes: State of Their Development and Perspective. *J. Membr. Sci.* 2005, *263* (1–2), 1–29.

(3) Pitzer, K. S.; Mayorga, G. Thermodynamics of Electrolytes.: II. Activity and Osmotic Coefficients for Strong Electrolytes with One or Both Ions Univalent. In *Molecular Structure And Statistical Thermodynamics: Selected Papers of Kenneth S Pitzer*; World Scientific, 1993; pp 396–404.

(4) Kingsbury, R. S.; Flotron, S.; Zhu, S.; Call, D. F.; Coronell, O. Junction Potentials Bias Measurements of Ion Exchange Membrane Permselectivity. *Environ. Sci. Technol.* 2018, *52* (8), 4929–4936.

(5) Kamcev, J.; Paul, D. R.; Freeman, B. D. Effect of Fixed Charge Group Concentration on Equilibrium Ion Sorption in Ion Exchange Membranes. *J. Mater. Chem. A* 2017, *5* (9), 4638–4650.

(6) Geise, G. M.; Lee, H.; Miller, D. J.; Freeman, B. D.; McGrath, J. E.; Paul, D. R. Water Purification by Membranes: The Role of Polymer Science. *J. Polym. Sci. Part B Polym. Phys.* 2010, *48* (15), 1685–1718.

(7) Kamcev, J.; Freeman, B. D. Charged Polymer Membranes for Environmental/Energy Applications. *Annu. Rev. Chem. Biomol. Eng.* 2016, *7*, 111–133.

(8) Zhang, H.; Geise, G. M. Modeling the Water Permeability and Water/Salt Selectivity Tradeoff in Polymer Membranes. *J. Membr. Sci.* 2016, *520*, 790–800.

(9) Lide, D. R. *Handbook of Chemistry and Physics*; CRC Press, 2003.

(10) Kamcev, J.; Galizia, M.; Benedetti, F. M.; Jang, E.-S.; Paul, D. R.; Freeman, B. D.; Manning, G. S. Partitioning of Mobile Ions between Ion Exchange Polymers and Aqueous Salt Solutions: Importance of Counter-Ion Condensation. *Phys. Chem. Chem. Phys.* 2016, *18* (8), 6021–6031.

(11) Buchner, R.; Hefter, G. T.; May, P. M. Dielectric Relaxation of Aqueous NaCl Solutions. *J. Phys. Chem. A* 1999, *103* (1), 1–9.

(12) Wachter, W.; Kunz, W.; Buchner, R.; Hefter, G. Is There an Anionic Hofmeister Effect on Water Dynamics? Dielectric Spectroscopy of Aqueous Solutions of NaBr, NaI, NaNO3, NaClO4, and NaSCN. *J. Phys. Chem. A* 2005, *109* (39), 8675–8683.

(13) Boström, M.; Ninham, B. Energy of an Ion Crossing a Low Dielectric Membrane: The Role of Dispersion Self-Free Energy. *Biophys. Chem.* 2005, *114* (2–3), 95–101.

(14) Boström, M.; Ninham, B. Dispersion Self-Free Energies and Interaction Free Energies of Finite-Sized Ions in Salt Solutions. *Langmuir* 2004, *20* (18), 7569–7574.

(15) Parsons, D. F.; Ninham, B. W. Importance of Accurate Dynamic Polarizabilities for the Ionic Dispersion Interactions of Alkali Halides. *Langmuir* 2009, *26* (3), 1816–1823.

(16) Duignan, T. T.; Parsons, D. F.; Ninham, B. W. A Continuum Model of Solvation Energies Including Electrostatic, Dispersion, and Cavity Contributions. *J. Phys. Chem. B* 2013, *117* (32), 9421–9429.

(17) Dagastine, R. R.; Prieve, D. C.; White, L. R. The Dielectric Function for Water and Its Application to van Der Waals Forces. *J. Colloid Interface Sci.* 2000, *231* (2), 351–358.

(18) Kunz, W.; Belloni, L.; Bernard, O.; Ninham, B. W. Osmotic Coefficients and Surface Tensions of Aqueous Electrolyte Solutions: Role of Dispersion Forces. *J. Phys. Chem. B* 2004, *108* (7), 2398–2404.

(19) Mahanty, J.; Ninham, B. W. *Dispersion Forces*; Academic Press, 1976; Vol. 1.

(20) Born, M.; Wolf, E. Principles of Optics, 7th (Expanded) Edition. *U. K. Press Synd. Univ. Camb.* 1999, *461*.

(21) Kamcev, J.; Paul, D. R.; Manning, G. S.; Freeman, B. D. Ion Diffusion Coefficients in Ion Exchange Membranes: Significance of Counterion Condensation. *Macromolecules* 2018, *51* (15), 5519–5529.

Appendix D: Supporting Information for Chapter 7

D.1. Estimating Van der Waals Volume

The van der Waals volume of fixed charge groups were estimated using an empirical method adapted from the literature.[1] According to this method, the van der Waals volume of an organic molecule can be calculated by considering contributions from the atoms, bond and ring structure composing the molecule. Therefore, the van der Waals volume (Å^3/molecule) can be calculated from this following formula:

$$V_{vdw} = \sum \text{all atom contributions} - 5.92N_B - 14.7R_A - 3.8R_{NA} \quad \text{(D.1)}$$

where the $\sum \text{all atom contributions}$ is the sum of van der Waals volume of all atoms included in a molecule, N_B is the total number of bonds regardless of bond type, R_A is the number of aromatic rings, and R_{NA} is the total number of non-aromatic rings.

The "all atom contributions" terms indicates the sum of the individual van der Waals volume of atoms included in a molecule and such values are available in the literature.[1] To estimate the van der Waals volume of trimethyl ammonium and 1,4-dimethyl imidazolium groups, the total number, bonds and rings in the two groups are counted and used in the calculation. The calculation procedures can be illustrated using Table D.1:

Table D.1. Estimation of van der Waals volume of the two fixed charge groups. The "H", "C" and "N" in the Component column indicates hydrogen, carbon and nitrogen atom, respectively. The Contribution column was calculated using the number of components and the contribution from a single component. The contribution of a single component, i.e., atom, bond or ring was obtained from literature.[1]

Trimethyl Ammonium			1,4-Dimethyl Imidazolium		
Component	Number	Contribution (Å^3)	Component	Number	Contribution (Å^3)
H	9	65.2	H	8	57.9
C	3	61.7	C	5	102.9
N	1	15.6	N	2	31.2
Bonds	12	-71.0	Bonds	15	-88.8
Aromatic Rings	0	0	Aromatic Rings	0	0
Non-aromatic Rings	0	0	Non-aromatic Rings	1	-3.8
V_{vdw}		71.5	V_{vdw}		99.4

D.2. Influence of Junction Potential on Apparent Permselectivity

The junction potential can be estimated using the Henderson Equation,[2] as discussed in Appendix C.3 already. The calculation of junction potential will be skipped here. The membrane apparent permselectivity results considering junction potential are presented in Figure D.1:

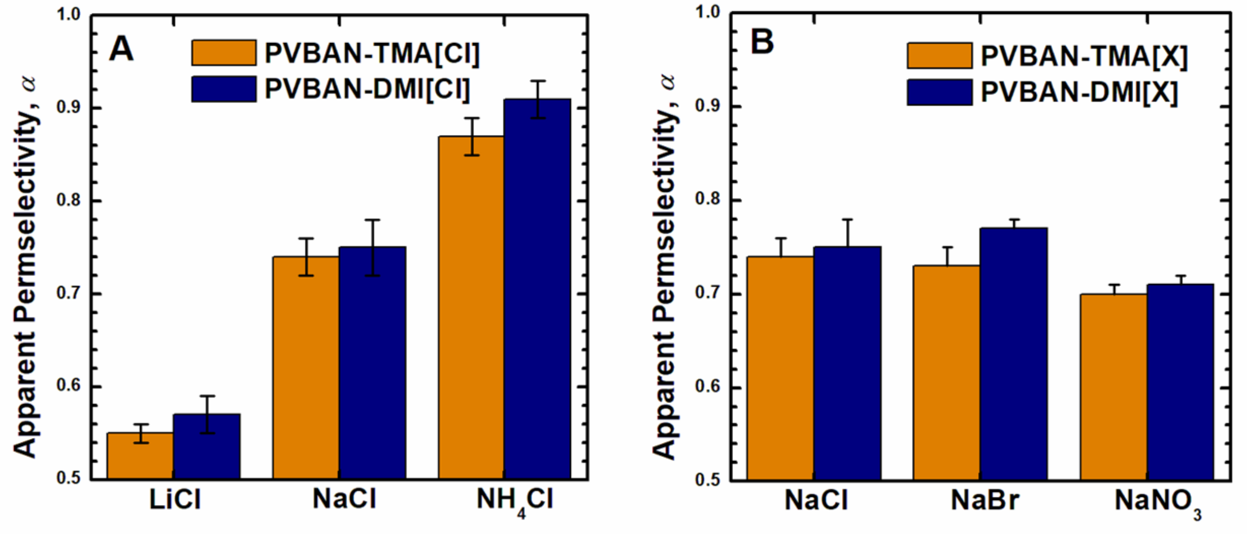

Figure D.1. Apparent permselectivity of the two AEMs measured using 0.5 mol/L aqueous solutions of (A) lithium chloride, sodium chloride and ammonium chloride (i.e., different co-ions) and (B) sodium chloride, sodium bromide and sodium nitrate (i.e., different counter-ions) under 25°C. The membrane junction potentials were calculated using the Henderson Equation and incorporated in the results.

Figure D.1 can be compared with Figure 7.2 to draw conclusions on the effects of junction potential on apparent permselectivity of the two AEMs. First of all, junction potential correction reduced membrane permselectivity values for both membranes and all electrolytes considered relative to their values in the absence of the correction. Second, including the junction potential correction enlarged the difference in the permselectivity values of both membranes measured using electrolytes with a common counter-ions, i.e., lithium chloride, sodium chloride and ammonium chloride. Third, junction potential correction affected the difference in permselectivity for both membranes measured using electrolytes with a common co-ion, i.e., sodium chloride, sodium bromide and sodium nitrate to a lesser extent than what permselectivity was measured using electrolytes with a common counter-ion.

D.3. Magnitude of Influence of Concentration and Diffusion Ratios on Permselectivity

The $k_{X/M}^{m}$, $D_{X/M}^{m}$ and $D_{X/M}^{s}$ values associated with different electrolyte solutions all affect membrane permselectivity, but the influence of each term on permselectivity is different. The subsequent analysis was done to determine the magnitude of the effect resulting from each factor:

- Calculations were done based on Equation 1.
- The base scenario:
    - c_A^m = 3 mol/L (water sorbed)
    - $k_{X/M}^{m}$ = 0.162 (calculated using ideal Donnan exclusion with external solution concentration = 0.5 mol/L)
    - $D_{X/M}^{s} = 0.66$ (calculated using the ion diffusivity of sodium and chloride in aqueous solution of infinite dilution)
    - $D_{X/M}^{m} = 0.66$ (assuming the sodium and chloride diffusion was suppressed to the same extent in membrane)
- Starting from the base scenario, we calculated the relative change in permselectivity as $k_{X/M}^{m}$, $D_{X/M}^{m}$ or $D_{X/M}^{s}$ were varied.
- Results were presented in Figure D.2. Compared with the base scenario:
    - Permselectivity reduced by 5.7% when $k_{X/M}^{m}$ increased by 20%
    - Permselectivity reduced by 1.9% when $D_{X/M}^{m}$ increased by 20%
    - Permselectivity increased by 3.2%when $D_{X/M}^{m}$ increased by 20%
    - Changes in $k_{X/M}^{m}$ have the most pronounced effect on permselectivity.

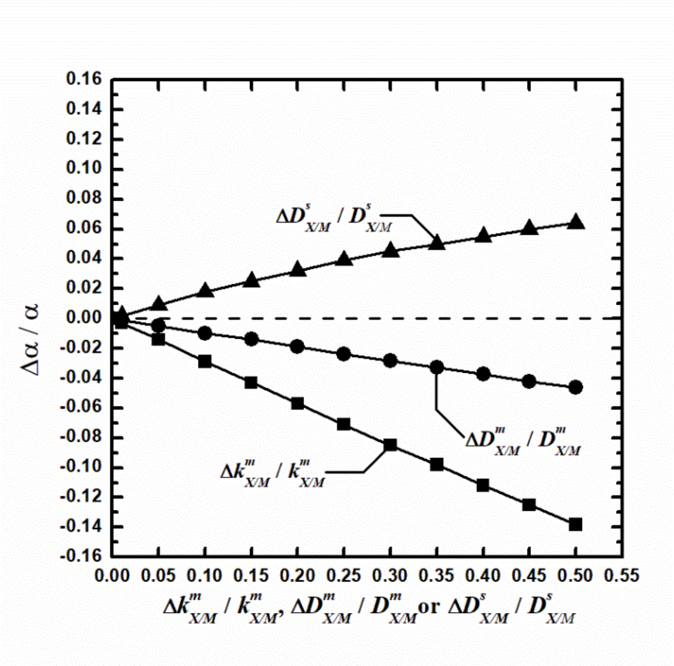

Figure D.2. Membrane permselectivity decreases with increasing $k^{m}_{X/M}$ or $D^{m}_{X/M}$ but increases with increasing $D^{s}_{X/M}$, according to Equation 7.1.

D.4. References

(1) Zhao, Y. H.; Abraham, M. H.; Zissimos, A. M. Fast Calculation of van Der Waals Volume as a Sum of Atomic and Bond Contributions and Its Application to Drug Compounds. *J. Org. Chem.* **2003**, *68* (19), 7368–7373.

(2) Kingsbury, R. S.; Flotron, S.; Zhu, S.; Call, D. F.; Coronell, O. Junction Potentials Bias Measurements of Ion Exchange Membrane Permselectivity. *Environ. Sci. Technol.* **2018**, *52* (8), 4929–4936.

Vita

Yuanyuan Ji graduated from Linchuan No.1 High School (Fuzhou, China) in 2010. Subsequently, Yuanyuan attended Tianjin University, where she majored in Chemical Engineering and double majored in Finance from Nankai University. After earning a Bachelor of Science degree in Chemical Engineering from Tianjin University in 2014, Yuanyuan enrolled at the University of Virginia to pursue a Ph.D. in Chemical Engineering under the guidance of Prof. Geoffrey M. Geise. Yuanyuan earned her Master of Science degree in Chemical Engineering in July of 2017 and her Doctor of Philosophy degree in Chemical Engineering in December of 2019.

Permanent email address: yuanyuanji92@gmail.com

This dissertation was typed by Yuanyuan Ji